Chapter 4

Synthesis and Evaluation of NH_2 and SH linker Free Benzothiazole-Triazole Compounds: Insights into Antimicrobial efficacy

4.1 Introduction

Benzothiazole, a compound that combines benzene and thiazole rings, has attracted the interest of researchers across different fields due to its wide range of chemical and biological properties. Benzothiazole derivatives have the potential to serve as a multi-purpose agent, demonstrating anticancer,[217] anti-inflammatory,[218] antiviral,[219] antidiabetic,[220] antimalarial,[221] and antileishmanial activity.[222] Their intrinsic luminescent properties make them highly attractive for material science applications, such as organic light-emitting diodes (OLEDs).[223] There are a variety of benzothiazole-based drugs available for clinical applications, including riluzole (amyotrophic lateral sclerosis),[224] ethoxzolamide (Mycobacterium tuberculosis),[225] frentizole (immunosuppressive),[226] and pramipexole (antiparkinsonian).[227] Numerous methods have been established for synthesizing benzothiazole. The conventional approach to produce benzothiazole derivatives includes a condensation reaction between 2-amino thiophenol and acyl chloride, acids, ketones, or aldehydes.[228]

The chemical stability and multifunctionality of 1,2,4-Triazole's five-membered ring structure, featuring three nitrogen atoms, have significance in medicinal chemistry. To synthesize 1,2,4-triazole derivatives, nitrogen atoms can be sourced from raw materials like amidines, amidrazones, aryl diazoniums, and hydrazone.[229] The pharmacological activity of these compounds is well-known and encompasses various effects such as antifungal,[230] anticancer,[231] antituberculosis,[232] antiviral,[232] antihypertensive,[233] and anti-inflammatory[234] properties.

Benzothiazole-linked triazole compounds have the potential to yield multifunctional molecules with versatile properties that can be utilized in drug discovery.[235] Moreover, N-acyl hydrazones exhibit a wide range of biological activities, including antimicrobial, antitumor, and anti-inflammatory properties. Incorporating an N-acyl hydrazone-like

structure into a target compound could have potential biological effects.[236] The production of benzothiazole tethered triazole can be achieved through several synthesis methods, including the reaction of 2-amino benzothiazole and 2-mercapto benzothiazole with certain linkers like NH_2 or SH groups, or by click reactions.[237,238,239,240,241,242] The identification of a research gap has led to the conclusion that there are few compounds which have a direct association between benzothiazole and triazole without the presence of a linker or click reactions.

Antimicrobial resistance (AMR) is widely recognized as a major global threat to public health and development.[243] In 2019, bacterial AMR directly caused 1.27 million deaths and contributed to 4.95 million additional fatalities. Misuse and overuse of antimicrobials in humans, animals, and plants develop drug-resistant pathogens. The 2022 Global Antimicrobial Resistance and Use Surveillance System (GLASS) has raised concerns on high rates of third-generation cephalosporin-resistant *E. coli* (42%) and methicillin-resistant *S. aureus* (35%) in 76 countries.[244] The World Health Organization (WHO) took a crucial step in 2017 by issuing a document that outlined a list of 12 families of antibiotic-resistant bacteria, known as "priority pathogens". This collection represents the most critical threat to human health. *Ac. baumannii*, *P. aeruginosa*, and *Enterobacteriaceae* are the top three bacteria on the critical list due to their resistance to carbapenems. Bacteria such as *E. faecium*, *S. aureus*, *H. pylori*, *Campylobacter spp*., *N. gonorrhoeae* and *Salmonellae* fall under the high-risk category. These bacteria cause serious conditions like skin infections, severe gastroenteritis, and STDs, posing treatment challenges. Lastly, the group labelled as a medium risk includes *S. pneumoniae*, *H. influenzae*, and *Shigella species*. Although not as threatening as others, these bacteria still pose health concerns.[245]

Besides the problem of bacterial resistance, fungal infections are becoming a major concern for public health. WHO introduced the first fungal priority pathogens list (WHO FPPL) in 2022, following the model of the bacterial priority pathogens list (WHO BPPL). The list comprised 19 fungal pathogens, and they were classified into three priority groups (critical, high, and medium) based on their rankings. The 'Critical' group, which encompasses pathogens such as *C. neoformans*, *C. auris*, *A. fumigatus*, and *C. albicans*, is noteworthy.

These fungi represent a significant threat because of their high health complications, lethality, and the increasing resistance to current antifungal treatments.[246]

To discover new compounds that exhibit potential therapeutic activity, our focus was on synthesizing a hybrid molecule that incorporates the benzothiazole moiety that is directly attached to triazole as our primary goal, then evaluate their pharmacological properties. The therapeutics properties of benzothiazoles are widely recognized and encompass antimicrobial and anticancer activities.[247] Similarly, triazoles are renowned for their diverse biological roles, particularly as antifungal and antibacterial agents.[248] By combining these two pharmacophores, we aim to utilize the synergistic potential of their bioactive properties to combat the growing challenge of microbial and fungal resistance. A comprehensive analysis was performed on the synthesized compounds to establish their structural integrity and purity. ^{1}H NMR and ^{13}C NMR spectroscopy provided detailed insights into the molecules, confirming their structures and purity of compounds. Mass spectrometry was employed to ascertain the molecular weights, while Infrared (IR) spectroscopy was utilized to identify functional groups and confirm molecular architecture. In the initial phase of our in vitro studies, we first conducted a zone of inhibition assay. Subsequently, Minimum Inhibitory Concentration (MIC) tests as part of our in vitro assays were carried out. The zone of inhibition analysis provided a starting point, and the MIC test showed that the compounds 8g, 8k and 8m shows antimicrobial activity comparable to chloramphenicol while compounds 8d, 8e, 8j and 8m could inhibit *C. albicans* better than standard griseofulvin. Together, these results suggest these compounds could be effective new agents in the fight against microbial and fungal resistance. The process of molecular docking was utilized to examine the specific receptor's interactions with compounds. The pharmacokinetic and medicinal chemistry properties of the synthesized compounds were determined using ADMET prediction, leading to the final outcomes.

4.2 Result and discussion

4.2.1 Chemistry

The process of preparing the titled compounds **8a-m** involves a series of steps, which are depicted in Scheme 1. The compound Ethyl benzothiazole-2-carboxylate **3** was prepared

by refluxing 2-amino thiophenol and diethyl oxalate. Benzothiazole-2-carbohydrazide **4** was obtained by refluxing the ester group in benzothiazole with hydrazine hydrate (99%) in ethanol, leading to its conversion to carbohydrazide. The potassium dithiocarbazinate salt **5** was prepared by reaction of carbohydrazide **4** with methanolic potassium hydroxide, followed by the addition of carbon disulfide at room temperature. A reflux reaction of potassium dithiocarbazinate salt **5** and hydrazine hydrate (99%) in water yielded a benzothiazole-tethered triazole molecule. Various aldehydes were employed to further derivatized compound **6**, resulting in the formation of titled compound (E)-5-(benzo[d]thiazol-2-yl)-4-(benzylideneamino)-4H-1,2,4-triazole-3-thiol **8a**-**m**.

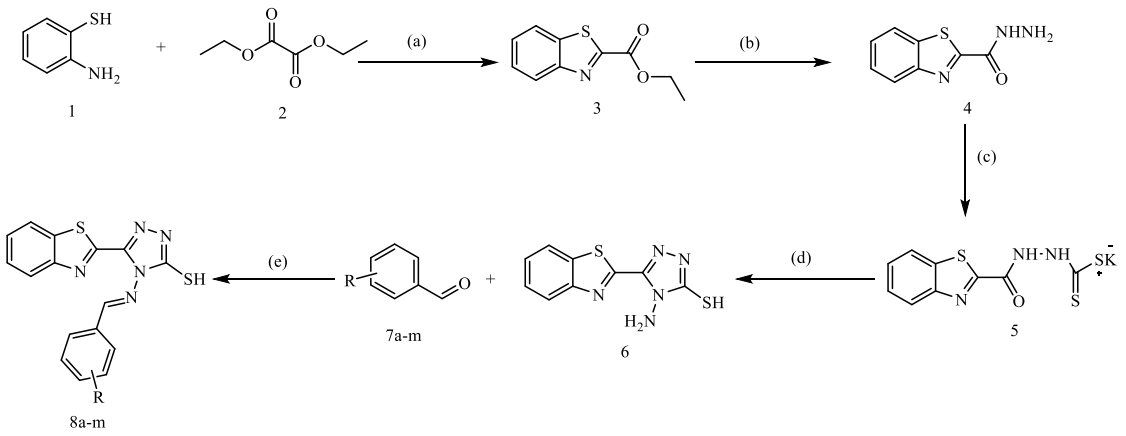

Scheme 1: Synthetic pathway of hybrid molecules 8a-m

Reagents and conditions: (a) reflux; (b) $NH_2NH_2.H_2O$, EtOH, reflux; (c) CS_2, KOH, MeOH, RT; (d) $NH_2NH_2.H_2O$, H_2O, reflux; (e) NaOH, MeOH, RT

Initially, the use of acetic acid in methanol at reflux temperature did not yield the desired Schiff base, prompting further reaction optimization. As a result, it was necessary to re-evaluate and systematically optimize the reaction conditions. We aimed to increase both the yield and efficiency of the Schiff base formation. To determine the optimal conditions, we conducted experiments using different acids, bases, and solvents, as shown in Table 1. The use of NaOH in methanol proved to be an effective technique for synthesizing Schiff base. This method increased efficiency, enabling reactions to finish in 2-3 h. The addition of NaOH results in a homogeneous mixture of reactants, which helps to facilitate the

process. As the reaction progressed, the appearance of precipitates indicated the Schiff base had formed successfully. Easy filtration of the precipitates simplified product isolation.

Table 1: Optimization of reaction conditions

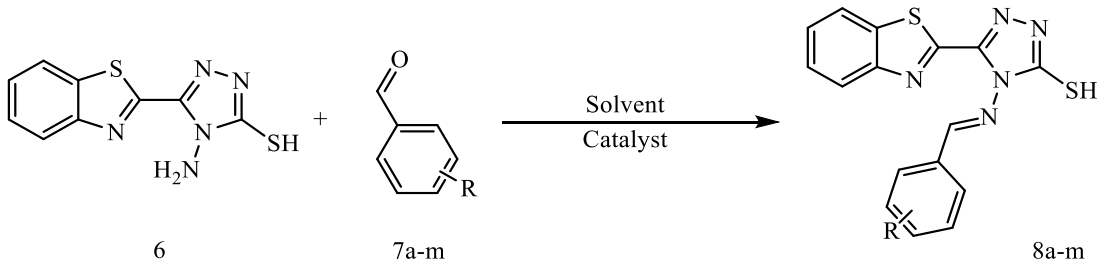

6 7a-m 8a-m

Entry [a]	Catalyst	Solvent	Reaction conditions	Reaction time (hr)	Yield (%) [e]
1[b]	gl. Acetic acid	MeOH	Reflux	18 h	No product
2[b]	gl. Acetic acid	EtOH	Reflux	18 h	No product
3[b]	HCl	MeOH	Reflux	18 h	Trace
4[b]	HCl	EtOH	Reflux	18 h	Trace
5[b]	H_2SO_4	MeOH	Reflux	12 h	17
6[b]	H_2SO_4	EtOH	Reflux	12 h	15
7[b]	H_2SO_4	DMF	Reflux	12 h	14
8[c]	KOH	MeOH	RT	6 h	71
9[d]	KOH	EtOH	RT	6 h	68
10[d]	NaOH	MeOH	RT	2-3 h	96
11[d]	NaOH	EtOH	RT	2-3 h	92
12[d]	NaOH	DMF	RT	2-3 h	90

[a] The reaction was conducted using 1.0 equivalent of compound 6 with 1.1 equivalent of aromatic aldehydes derivatives 7a-m. [b] the range of 0.3 to 1.0 equivalents was employed for the catalyst [c]

the amount of catalyst used ranges from 0.5-1.0 equivalents [d] 1.0 equivalents of catalyst was used [e] isolated yield by filtration of precipitates obtained by cooling reaction mixture at rt

Various spectroscopic techniques were employed to analyse the structural and compositional characteristics of the 13 synthesized compounds. ^{1}H NMR spectroscopy was employed to explore proton environments in hydrogen-containing functional groups. The thiol group proton in most compounds exhibited chemical shifts in the narrow range of 14.64-14.75 ppm, indicative of the strong deshielding effect typically associated with the sulfur atom's electronegativity. Notably, the thiol proton signal was not observed in compounds 8b, 8d, and 8i. The rapid thiol proton exchange with deuterium can cause this anomaly, particularly in compounds with active hydrogen atoms like thiols, leading to broadening beyond detection. The derivative 8c with a hydroxy group in the second position showed unexpected behaviour. At 14.64 ppm, the OH proton was observed, whereas the thiol proton experienced an upfield shift of 10.71 ppm. The unusual change in chemical shift for the thiol proton can be attributed to intramolecular hydrogen bonding between the thiol and hydroxy groups. The thiol proton undergoes an upfield shift, most likely because of the shielding effect induced by hydrogen bonding. Chemical shifts between 9.70 and 11.09 ppm were observed for the CH=N group in the Schiff base moiety. The variation is due to the change in electron density around the imine nitrogen caused by the substituents on the aromatic rings. This affects the chemical shift of the adjacent hydrogen. The aromatic proton chemical shifts shown range between 7.01 to 8.74 ppm. This range showcases diverse electronic configurations in aromatic compounds substitution and their interaction with Schiff bases. A peculiar downfield shift of the ring protons was observed at 8.74 ppm in derivative 8h, where the nitro group was at the meta position of the aromatic ring. In contrast to 8g, where the nitro group is ortho to the aromatic ring protons, the proton signals were more typical and less shifted. The nitro group at the meta position causes a pronounced downfield shift in the meta-substituted nitro derivative, influencing the electron density of nearby aromatic protons. This results in a higher deshielding and a downfield shift. The ortho-substituted nitro derivative may have normal proton shifts because of spatial arrangement and steric effects, offsetting the electron-withdrawing impact of the nitro group.

The ^{13}C NMR characterization displayed diverse electronic environments in the derivatives. Thiol group-linked carbon atoms exhibited chemical shifts at 167.45-153.38 ppm for derivatives 8a-m. Additionally, the carbon atoms in the Schiff base exhibited chemical shifts within a narrower range of 144.01-152.95 ppm. The observed range indicates a stable electronic atmosphere influenced by the nitrogen double bond, with minor deviations potentially caused by various substituents on the aromatic system or structural variations in the derivatives. The C_2 atom of benzothiazole rings, which is bonded to nitrogen, sulfur, and the carbon of the triazole ring, exhibited chemical shifts ranging from 152.66 to 163.49 ppm. In this area, molecules showcase complex electronic interplay, with every atom affecting the carbon's electronic environment. The shifts in this range suggest structural variations among the derivatives. This is due to the influence of each atom's electronegativity and bonding on the electron density surrounding the central carbon.

FT-IR spectra effectively confirmed the validity of the chemical bonds and groups. The presence of C–H stretching of alkanes across different derivatives was confirmed by characteristic peaks observed in the spectra, ranging from 2901 to 3001 cm^{-1}. The imine group's C=N stretching vibrations were observed within the range of 1589 to 1658 cm^{-1}, serving as a fundamental indication of the Schiff base structure within our compounds. By detecting C–N stretching frequencies within the range of 1257 to 1311 cm^{-1}, we could validate the bonding arrangements in the various derivatives. Mass spectrometry confirmed the molecular structures, besides NMR and IR analysis. Positive and negative ion modes in MS analysis consistently confirmed the expected molecular weights.

4.2.2 In vitro antimicrobial activity evaluation and Structure Activity Relationship study (SAR)

A variety of pathogenic strains were tested to evaluate the antimicrobial activity of the novel synthesized benzothiazole tethered triazole hybrids 8a-8m. The included bacteria encompassed both Gram-positive species, such as *Staphylococcus aureus* and *Streptococcus pyogenes*, and Gram-negative species like *Escherichia coli*, *Pseudomonas aeruginosa*, and *Acinetobacter baumannii*. Antifungal efficacy of these compounds was tested against yeast *Candida albicans*, and mold strains *Aspergillus niger* and *Aspergillus*

clavatus. The primary aim of this comprehensive testing was to assess the susceptibility of microbial strains to our novel benzothiazole tethered triazole hybrids. Antimicrobial activity was assessed using the agar well diffusion method **(Table 2)** and the broth micro-dilution method **(Table 3)**. The effectiveness of these compounds was then compared to standard antimicrobial agents like chloramphenicol and ampicillin to inhibit bacterial growth and griseofulvin to inhibit fungal growth. **Figure 1** illustrates the comprehensive findings of the structural activity relationship analysis conducted for the compounds.

The zone of inhibition (ZOI) results revealed Compound 8g had the strongest activity against *E. coli*, with a measurement of 15 mm. It showed significant antimicrobial potential, although less effective than ampicillin (19 mm) or chloramphenicol (23 mm). Compound 8e showed significant activity against *P. aeruginosa* with a 14 mm ZOI, followed by 8k. Compounds 8k and 8i showed the highest ZOI of 14 mm against *Ac baumannii*. Compounds 8a and 8k were highly effective against *S. aureus*, producing a 14 mm zone of inhibition comparable to standard antibiotics. *S. pyogenes* was susceptible to compounds 8d, 8h, 8k, and 8m, with a ZOI of 13 mm, indicating their potential efficacy against this strain. The highest ZOI against *C. albicans* was 12 mm with a 55% inhibition area (AI), suggesting moderate antifungal potential. The effectiveness against *A. niger* and *A. clavatus* was reduced, with ZOI values below 12 mm. This suggests a decrease in effectiveness against these fungal strains. The agar well diffusion assay served as a primary screening method for evaluating the antimicrobial activity of our synthesized compounds. To achieve a precise and quantitative assessment of the compound's efficacy, we subsequently employed the minimum inhibitory concentration analysis. MIC enables accurate assessment of antimicrobial properties.

The standard antibiotics Ampicillin and Chloramphenicol displayed MIC of 30 µg/mL and 50 µg/mL, respectively, against *E. coli*. Notable activity was found in three derivatives: 8c (*o*-OH), 8e (2,4-F), and 8m (thiophene substitution). All three exhibited an MIC 62.5 µg/mL. The positioning of nitro groups on the aromatic ring significantly influenced activity levels. Compound 8g with *o*-NO_2 group showed MIC 50 µg/mL against *E. coli*, similar to chloramphenicol. However, the *m*-NO_2 group reduced its activity. The nitro group's strong electron withdrawing ability reduces activity by delocalizing negative

charge over oxygen atoms. Placing this group on ortho or para in the aromatic ring enhances electrophilicity and improves interaction with bacterial targets. The resonance effect is weaker in the meta position, potentially leading to lower antibacterial activity.

Table 2: Antimicrobial activity of hybrid compounds 8a-m and standard drugs by Agar well diffusion method

Compounds	Zone of inhibition in mm (100 µg/mL)															
	Gram-negative bacteria						Gram-positive bacteria				Fungus					
	E. coli		*P. aeruginosa*		*Ac. baumannii*		*S. aureus*		*S. pyogenes*		*C. albicans*		*A. niger*		*A. clavatus*	
	ZOI (mm)	AI (%) [a]	ZOI (mm)	AI (%) [b]	ZOI (mm)	AI (%) [a]	ZOI (mm)	AI (%) [a]	ZOI (mm)	AI (%) [a]	ZOI (mm)	AI (%) [c]	ZOI (mm)	AI (%) [c]	ZOI (mm)	AI (%) [c]
8a	13	68	11	57	13	76	14	87	12	66	9	41	10	45	8	36
8b	11	57	11	57	12	70	11	68	12	66	10	45	10	45	8	36
8c	13	68	13	68	13	76	12	75	12	66	11	50	9	41	9	41
8d	14	73	12	63	12	70	12	75	13	72	11	50	11	50	10	45
8e	14	73	14	73	13	76	11	68	12	66	11	50	11	50	11	50

Chloramphenicol	Ampicillin	8m	8l	8k	8j	8i	8h	8g	8f
23	19	13	11	13	13	13	12	15	13
-	100	68	57	68	68	68	63	78	68
19	-	12	12	14	12	12	12	13	11
100	-	63	63	73	63	63	63	68	57
23	17	12	13	14	12	14	12	10	12
-	100	70	76	82	70	82	70	58	70
20	16	13	11	12	13	14	11	12	13
-	100	81	68	75	81	87	68	75	81
20	18	13	12	13	11	12	13	12	11
-	100	72	66	72	61	66	72	66	61
-	-	10	11	11	10	10	12	12	12
-	-	45	50	50	45	45	55	55	55
-	-	12	10	9	11	11	10	10	12
-	-	55	45	41	50	50	45	45	55
-	-	11	10	8	11	10	9	9	12
-	-	50	45	36	50	45	41	41	55

Griseofulvin	-	-	-	-	-	-	-	-	-	-	22	100	22	100	22	100

AI= Activity index; [a] activity index was measured by comparing standard drug ampicillin; [b] activity index was measured using standard chloramphenicol; [c] standard used for activity index was griseofulvin

Two of synthesized compounds 8k (3-Br) and 8m (thiophene) displayed exceptional antimicrobial performance on *P. aeruginosa*, with an MIC 50 µg/mL equivalent to standard chloramphenicol. While, compound 8d (4-Br) derivative showed diminished activity with an MIC 100 µg/mL. This reinforces the importance of substitution patterns on the aromatic ring for antibacterial efficacy. The MIC of Compound 8e (2,4-F) was 62.5 µg/mL, only slightly higher than the two compounds aforementioned. The antibacterial activity of compounds 8a, 8d, and 8k against *Ac. baumannii* was significant, with an MIC of 62.5 µg/mL. This result implies that bromine substitutions might augment the antimicrobial effectiveness of these compounds. The synthesized compounds showed selective effectiveness against Gram-positive strains. Among the compounds tested, only 8h had an MIC of 62.5 µg/mL against *S. pyogenes*. Compounds 8a and 8j showed equal MIC (62.5 µg/mL) values against *S. aureus*. The observed pattern shows stronger antibacterial effects on Gram-negative bacteria.

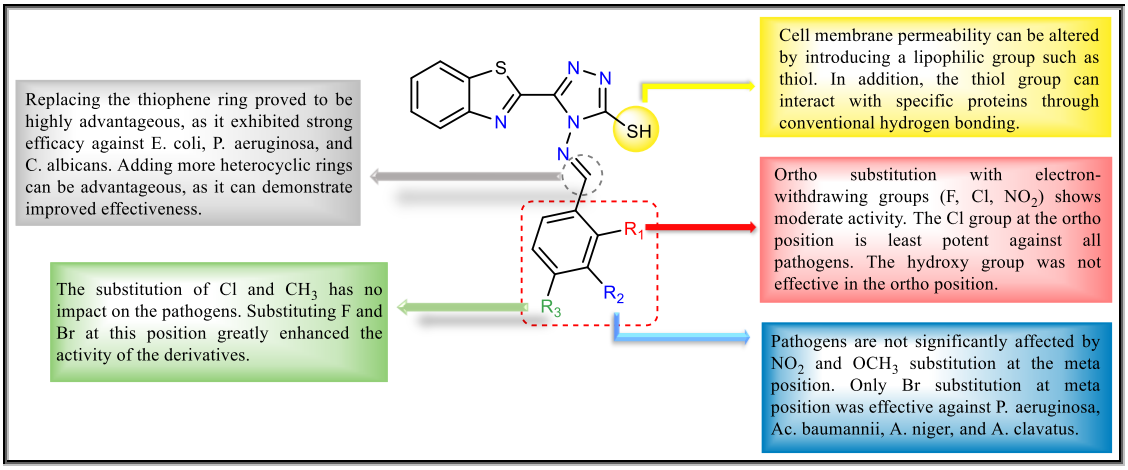

Figure 1: Overview of Structure activity relationship study of the synthesized compounds benzothiazole tethered triazole

The antifungal activity showed an efficacious effect on *C. albicans*. Nine out of thirteen compounds showed significant antifungal activity, highlighting the importance of specific structural changes. The presence of 4-bromo, 2,4-difluoro, 4-fluoro, and thiophene substitutions in compounds 8d, 8e, 8j, and 8m respectively resulted in noteworthy antifungal activity, as indicated by MIC values of 250 µg/mL. This suggests that the electronic and steric properties of these substituents contribute to their potent antifungal capability. The synthesized compounds were more potent against *C. albicans* with a lower MIC value compared to griseofulvin (500 µg/mL). The derivatives 8b (4-Cl), 8f (3,4-OCH_3), 8g (2-NO_2), 8h (3-NO_2), and 8l (4-CH_3) also exhibited strong potency, with MIC values of 500 µg/mL. These derivatives have similar antifungal potential as griseofulvin, despite being less effective than the previous group. Along with *C. albicans*, we also investigated the antifungal activity against *A. niger* and *A. clavatus*. However, there were distinct differences in the results obtained from these fungal strains. The compounds were not effective against *A. niger* and *A. clavatus*.

Table 3: Minimum inhibitory concentration (MIC, µg/mL) of hybrid heterocycles 8a-m and standard drugs against gram-positive, gram-negative bacteria and fungus

Compounds	Minimum inhibitory concentration (µg/mL)							
	Gram-negative bacteria			Gram-positive bacteria		Fungus		
	E. coli MTCC443	*P. aeruginosa*	*Ac. baumannii*	*S. aureus* MTCC96	*S. pyogenes*	*C. albicans* MTCC227	*A. niger* MTCC282	*A. clavatus* MTCC132
8a	200	125	**62.5**	**62.5**	100	1000	500	500
8b	125	100	125	100	100	**500**	500	500

8m	8l	8k	8j	8i	8h	8g	8f	8e	8d	8c
62.5	200	125	200	125	100	**50**	200	**62.5**	100	**62.5**
50	100	**50**	125	250	200	200	125	**62.5**	100	100
100	100	**62.5**	125	200	200	250	250	100	**62.5**	100
200	100	100	**62.5**	100	125	125	100	200	100	100
200	100	100	200	100	**62.5**	250	125	200	125	200
250	**500**	1000	**250**	1000	**500**	**500**	**500**	**250**	**250**	1000
>1000	500	**250**	1000	500	1000	1000	500	>1000	500	1000
>1000	500	**250**	1000	500	1000	1000	500	>1000	500	1000

Ampicillin	30	-	30	40	25	-	-	-
Chloramphenicol	50	50	50	50	50	-	-	-
Griseofulvin	-	-	-	-	-	500	100	100

Based on the results of the in vitro activity, we proceeded with in silico molecular docking studies on the chosen antibacterial and antifungal compounds. This computational approach allowed us to explore the molecular interactions between our compounds and specific target proteins associated with the microbial pathogens of interest.

4.2.3 Molecular docking studies

Following promising MIC test outcomes, we conducted in silico molecular docking analyses and Table 4 displays the key interactions. The aim was to investigate synthesized compounds interaction with essential proteins in microorganisms. Penicillin-Binding Protein (PBPs) (R1) from *E. coli* was chosen due to its pivotal role in bacterial cell wall synthesis and tailoring.[249] The dipeptide terminus in PBPs is crucial for cross-linking and strengthening the bacterial cell wall. Inhibiting PBPs disrupts cell wall synthesis, resulting in bacterial cell lysis and death.[250,251,252] DNA gyrase (R2), a type II topoisomerase, is crucial for DNA replication, transcription, and repair in bacteria. It plays a vital role in bacterial DNA replication by introducing negative supercoil into DNA.[253] Targeting DNA gyrase in *P. aeruginosa* can potentially eliminate the pathogen.[254] Secreted aspartic proteases (Saps) (R3) are involved in breaking down host cell membranes and tissues, making it easier for fungi to invade and cause infection.[255,256] Targeting R3 aims to assess compound impact on *C. albicans* invasion, reduce virulence, and explore interactions.[257]

The binding energy of chloramphenicol in R1 was -6.5 kcal/mol. It formed conventional hydrogen bonds with His216, Ser44, and Ser87, and also had a carbon-hydrogen bond with Asn112 (3.98 Å) and a pi-donor hydrogen bond with Ser110 (3.62 Å). However, the interaction between Ser87 (1.94 Å) and carbonyl group was unfavourable. In comparison, 8g demonstrated a superior binding affinity (-7.6 kcal/mol) and established two hydrogen bonds with Ser87 via the Schiff base (N=CH part) and nitro group, as shown in **Figure 2**. The residue Ser44 also showed dual H-bonds with the nitro group at distance 2.95 Å and 2.87 Å. The involvement of pi interactions, like a pi-donor hydrogen bond and a pi-cation bond, emphasizes the importance of a strong binding conformation.

Table 4: Molecular docking interaction between selected receptor with ligands and docking scores

Receptor	Ligand	Binding energy (kcal/mol)	Hydrogen bonding residues	Distance of H-bonds (Å)	Other interacting residues
R1 (*E. coli*)	Chloramphenicol	-6.5	HIS216, SER44, SER87	2.13, 2.70, 2.86	SER110, SN1A12
	8g	-7.6	SER87, SER44	3.36, 2.87	ASN112, SER110, ARG198
R2 (*P. aeruginosa*)	Chloramphenicol	-6.5	SER49, THR167, ARG78	2.90, 2.83, 3.04	ASP75, GLU52
	8k	-7.4	ARG78	3.55	GLU52, ASN48, ILE80, ASP51, VAL122, VAL169, ILE196
	8m	-7.2	ARG78	3.65	GLU52, ASP51, ILE80, ASN48, ILE96, VAL122, VAL169

R3 (*C. albicans*)	Griseofulvin	-6.6	-	-	TYR84, THR22, GLY220
	8d	-7.5	THR222	3.01	TYR225, GLY85, TYR84
	8e	-8.1	THR222	3.08	ALA303, TYR225, THR221, ASP32, GLY34, ASP218, TYR84
	8j	-7.6	THR222	3.15	TYR225, THR22, TYR84, ASP218, ASP32
	8m	-6.7	THR222	3.15	TYR225, TYR84

(A)

(B)

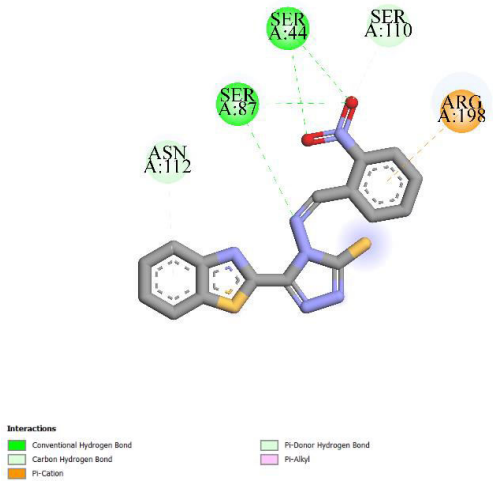

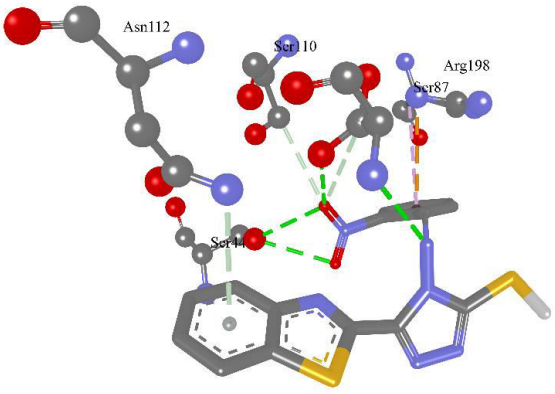

(C)

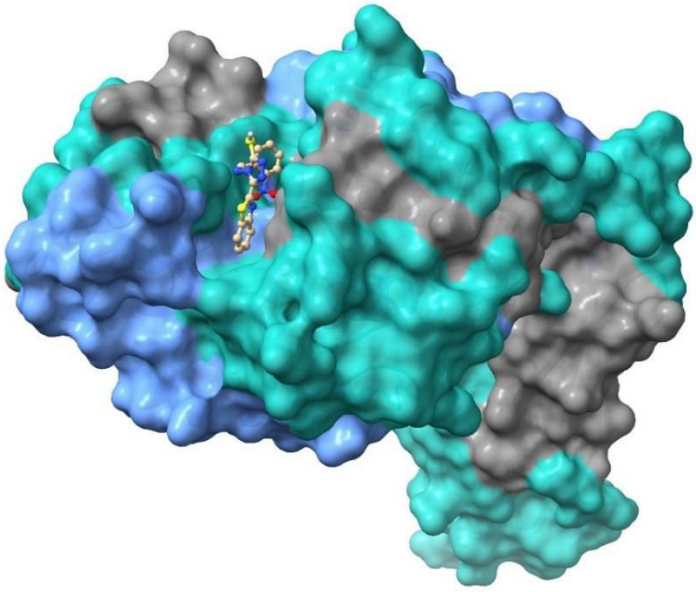

Figure 2: (A) Docked compound 8g interactions with protein residues in 2D (B) Compound 8g interactions with protein residues in 3D (c) Representation of compound 8g within the binding pocket of protein R1

The binding energy of chloramphenicol in R2 was -6.5 kcal/mol, forming crucial hydrogen bonds. Compound 8k exhibited significant binding with a docking energy of -7.4 kcal/mol, indicating a greater affinity for the R2 protein compared to chloramphenicol. Residue Arg78 and 8k form a hydrogen bond at 3.55 Å with a thiol group, along with a pi-anion bond with Glu52 at 3.94 Å, as shown in **Figure 3**.

(A)

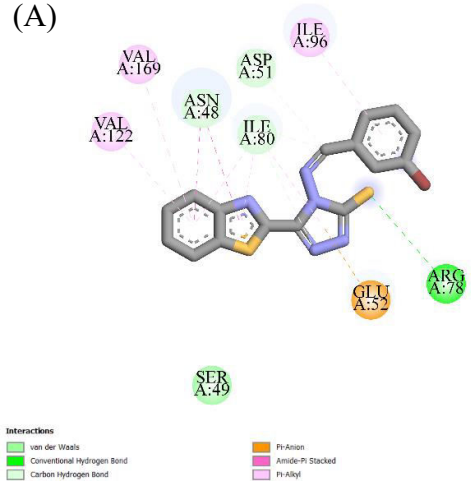

(B)

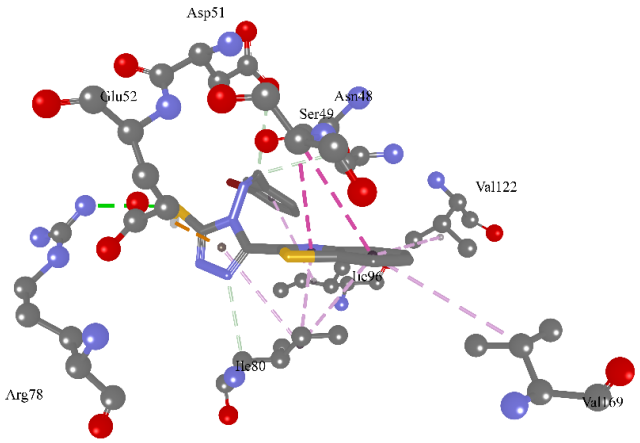

(C)

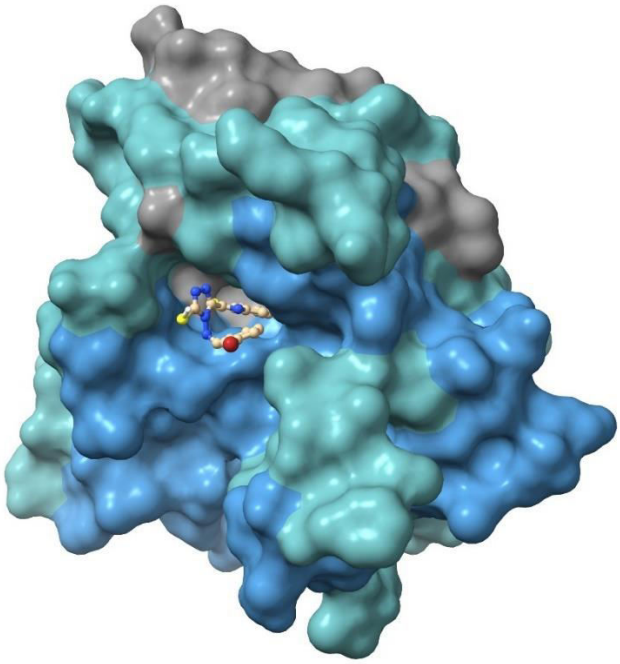

Figure 3. (A) 2D representation of docked ligand 8k with residues of protein (B) Compound 8k interaction with target protein in 3D (C) Docked compound 8k inside the pocket of protein R2

Carbon-hydrogen bonds in Asn48, Ile80, and Asp51 enhanced compound interactions. Residue Asn48 formed three C–H bonds with 8k, involving the Schiff base, benzothiazole, and thiazole rings. The amide pi-stacked bond and pi-alkyl interactions contribute to strong binding and inhibitory potential of compound 8k. The binding energy of -7.2 kcal/mol and previous MIC assay results suggest a favourable interaction between compound 8m and R2.

The R3 target protein, involved in *C. albicans* pathogenicity, was used to dock griseofulvin and four synthesized compounds (8d, 8e, 8j, and 8m) with MIC activity of 250 µg/mL. Griseofulvin exhibited a binding energy of -6.6 kcal/mol, primarily binding through a carbon–hydrogen bond. Its methoxy group interacted with Thr222 (3.69 Å) and Gly220 (3.45 Å), demonstrating a basic binding mechanism. The most potent compound among the tested was 8e, with a binding energy of -8.1 kcal/mol. It showed diverse interactions with R3, including hydrogen bonds, pi-alkyl, pi-donor hydrogen, carbon-hydrogen, pi-sigma, pi-pi stacked bonds, and notably, halogen (fluorine) interactions,

which are shown in Fig. 4. Residue Thr222 and triazole ring of 8e form a conventional hydrogen bond at 3.08 Å. The presence of pi interactions was extensive, as evidenced by the interaction of Ala303 (5.47 Å), Tyr225 (3.68 Å), and Thr221 (4.00 Å) suggesting a deliberate positioning of 8e within the binding site. The presence of a halogen bond in 8e influences its binding dynamics. This bond forms between the fluorine atom and the residues Asp32, Gly34, and Asp218. Fluorine interacts with Asp32 at distances of 3.14 Å and 3.37 Å, contributing to the complex's stability and affinity. While not as impactful as 8e, Compound 8j, 8m, and 8d still displayed reasonable interactions, revealing the influence of substitutions on binding affinity and specificity. These derivatives still showed good binding energy and interaction profile compared to griseofulvin, indicating its potential as an effective inhibitor.

(A) (B)

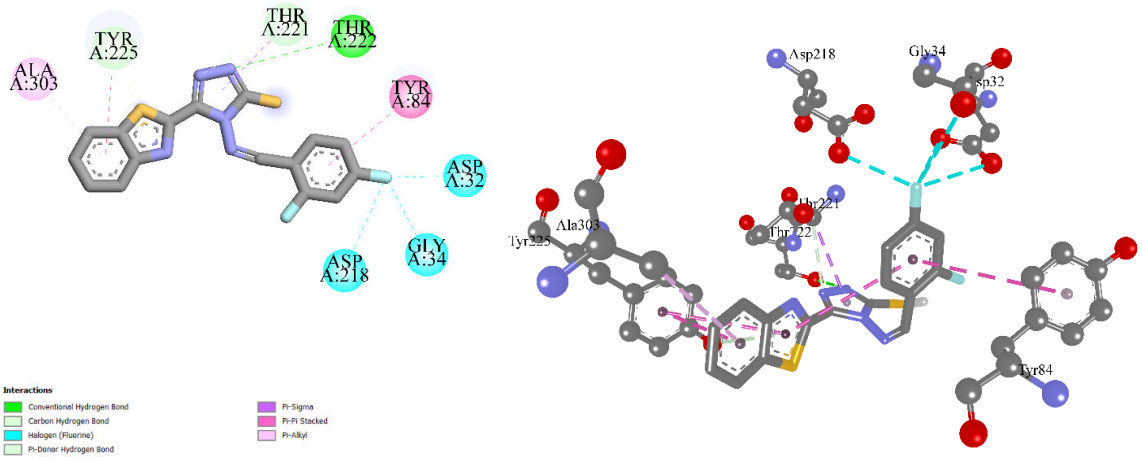

(C)

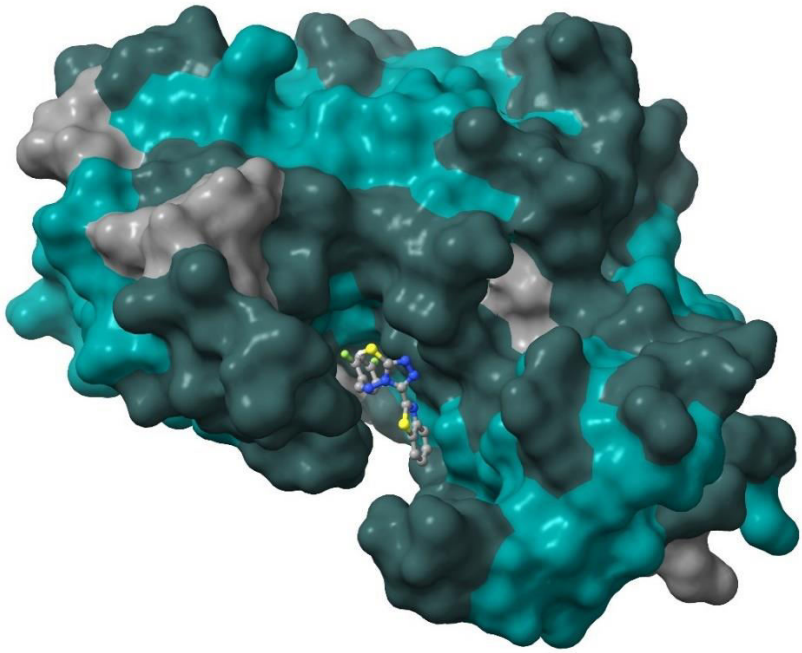

Figure 4: (A) Key interactions for compound 8e with protein residues in 2D (B) Interacting residues of protein with compound 8e in 3D (C) illustration of docked compound 8e inside the R3 protein pocket

Each interaction contributes uniquely to the overall binding affinity, presenting multiple opportunities for further optimization. This analysis provided insight into the interaction mechanisms of synthesized compounds, including 8g, 8e, and 8k, with targeted proteins. It also established a strong correlation between docking results and MIC values. In docking simulations, these compounds displayed stronger binding affinities and specific interaction patterns, which corresponded to their higher efficacy, as indicated by lower MIC values. Compounds 8g, 8e, and 8k displayed diverse interactions, suggesting their potential as antibacterial and antifungal agents. To validate the docking method, the co-crystallized ligands were redocked into their corresponding protein targets, and the docked conformations were then compared to the original crystal structures. The validation results showed RMSD values (Fig. 5) of 1.12 Å for R1, 0.317 Å for R2, and 1.026 Å for R3, indicating accurate prediction of ligand binding modes.

(A) (B)

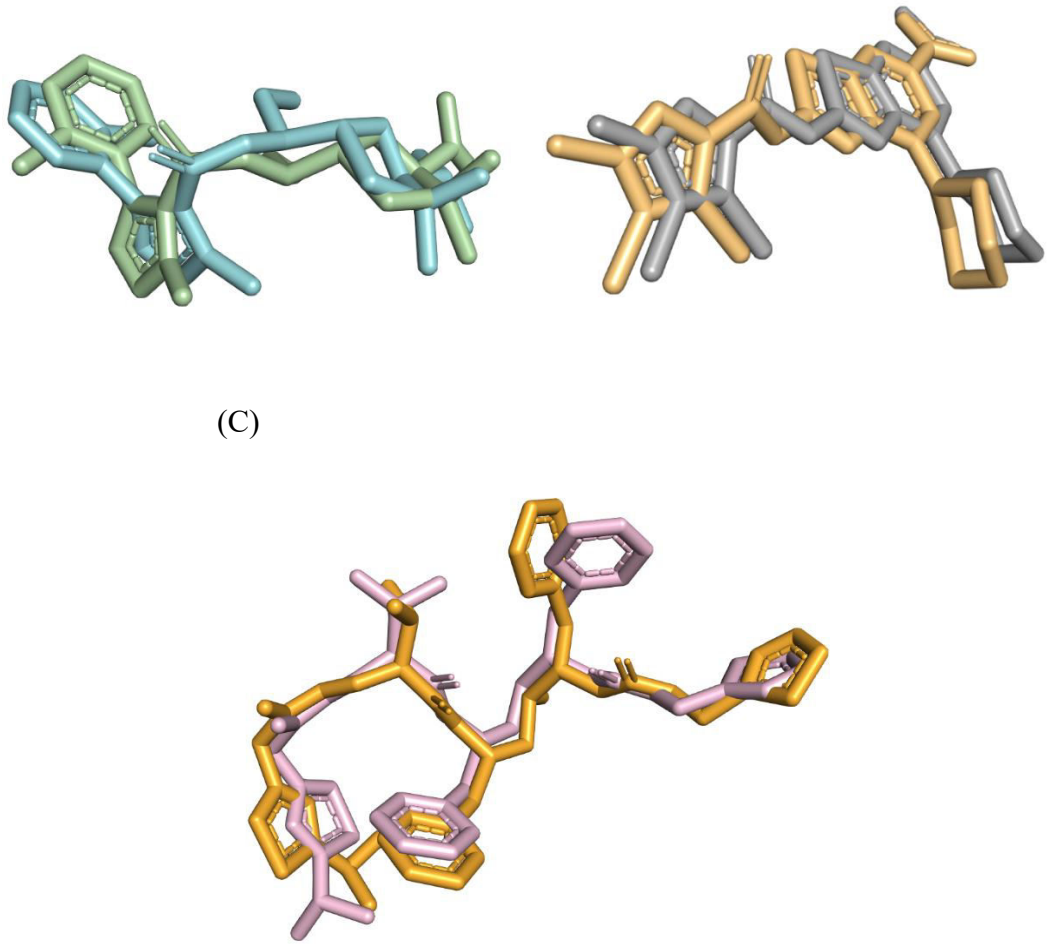

(C)

Figure 5: Superimpositions of the co-crystallized ligands with docked ligands (A) Co-crystalized ligand (light green) of protein R1 with docked ligand (cyan) (B) Native ligand (orange) of Protein R2 with docked ligand (purple) (C) superimposed native ligand (golden) of protein R3 on the docked ligand (grey)

4.2.4 In silico Pharmacokinetic properties of selected compounds

The compounds 8d, 8e, 8g, 8j, 8k, and 8m display a uniform number of hydrogen acceptors upon physiochemical profiling. This aligns with their robust Total Polar Surface Area (TPSA), indicating a high potential for specific molecular interactions. The compounds have a wide range of log P values, but a relatively narrow range of log D values, indicating a balance between neutral and ionized forms at physiological pH. All compounds satisfy

Lipinski's Rule of Five and meet the Golden Triangle criteria. Most compounds have low GI absorption, except 8j, which has high GI absorption due to slight better Caco-2 permeability. The distribution profiles have high plasma protein binding (PPB) and variable volumes of distribution (VD), with no compound expected to penetrate the blood-brain barrier (BBB). Metabolically, their potential to inhibit cytochrome P450 enzymes varies, affecting drug-drug interactions and biotransformation. CL (clearance) and T1/2 (half-life) metrics demonstrate diverse rates of elimination. Toxicity evaluations present a low risk, although the high skin sensitization prediction for 8m warrants further investigation. The boiled egg graph shows the relationship between WLOGP and TPSA in **Figure 6**.

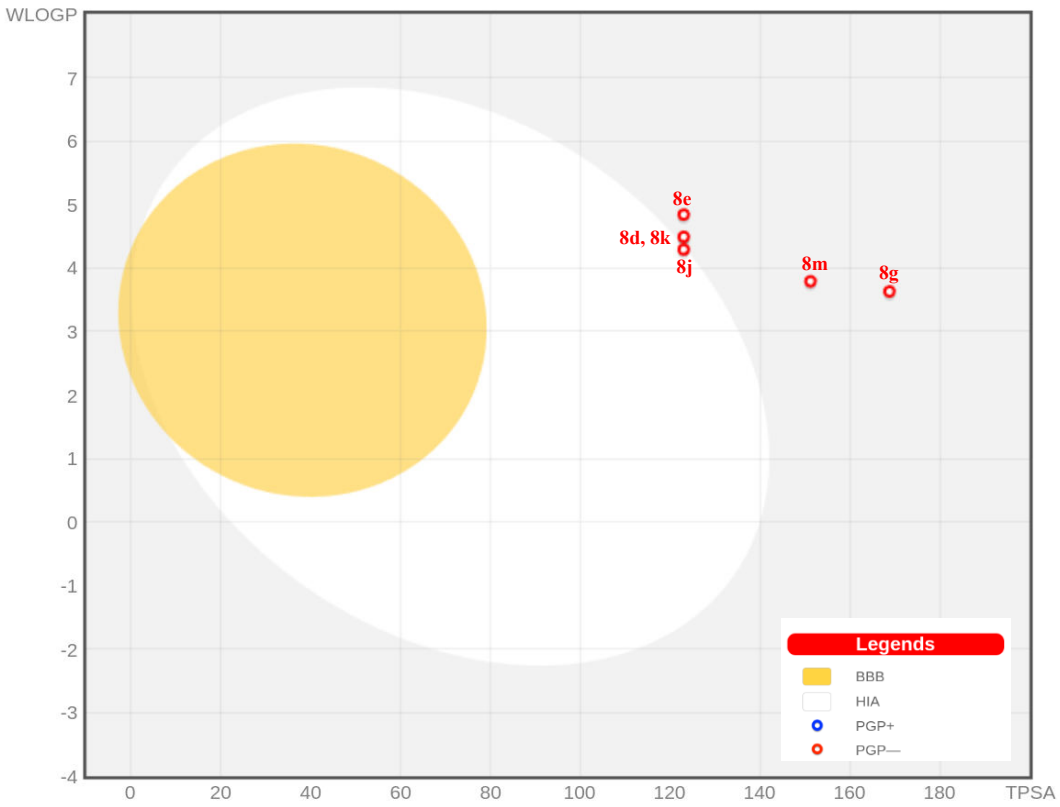

Figure 6: Boiled egg representation of the active compounds

The visual indicates no compounds fall within the yellow egg yolk area, which represents good permeability across both the gastrointestinal tract and blood-brain barrier. Compounds 8g and 8m positioned outside the yolk area but within the white area suggest

they may be P-glycoprotein (PGP) substrates, with 8g potentially being a non-substrate (PGP−) and 8m potentially being a substrate (PGP+). The evaluated compounds show promising drug-like characteristics, with acceptable ADMET profiles. Compound 8j, with higher GI absorption and low toxicity, and compound 8g, with PGP non-substrate potential, have advantages for further drug development.

Table 5: ADMET profile of the active compounds

Properties	8d	8e	8g	8j	8k	8m
Physiochemical properties						
nHA	5	5	8	5	5	5
nHD	0	0	0	0	0	0
TPSA	123	123	168.82	123	123	151.24
logS	-6.788	-6.633	-6.209	-6.337	-6.749	-6.093
logP	5.479	4.984	4.558	4.812	5.39	4.558
logD	3.695	4.006	3.875	3.859	3.674	3.733
Medicinal chemistry						
SAscore	2.58	2.684	2.678	2.532	2.626	2.769
Lipinski Rule	Accepted	Accepted	Accepted	Accepted	Accepted	Accepted
Golden Triangle	Accepted	Accepted	Accepted	Accepted	Accepted	Accepted
Absorption						
Caco-2 Permeability	-4.882	-4.84	-4.892	-4.884	-4.907	-4.686
MDCK Permeability	1.5×10^{-5}	1.9×10^{-5}	1.07×10^{-4}	1.7×10^{-5}	1.5×10^{-5}	2.5×10^{-5}
GI absorption	Low	Low	Low	High	Low	Low
Distribution						
PPB	97.68 %	97.73 %	97.62 %	97.15 %	97.66 %	97.58 %
VD	1.347	0.737	0.414	0.922	1.287	0.888
BBB Penetration	No	No	No	No	No	No
Metabolism						
CYP1A2 inhibitor	Yes	Yes	No	Yes	Yes	Yes
CYP2C19 inhibitor	No	No	Yes	No	No	Yes
CYP2C9 inhibitor	Yes	Yes	Yes	Yes	Yes	Yes
Excretion						

CL	3.507	5.394	5.066	5.428	3.751	5.138
T 1/2	0.025	0.016	0.042	0.022	0.033	0.044
Toxicity						
H-HT	0.234	0.783	0.55	0.54	0.288	0.121
Rat Oral Acute Toxicity	0.011	0.019	0.009	0.011	0.01	0.005
FDAMDD	0.087	0.664	0.064	0.239	0.138	0.066
Skin Sensitization	0.218	0.221	0.337	0.224	0.217	0.467
Eye Corrosion	0.003	0.003	0.003	0.003	0.003	0.003

Note: nHA= no. of H-bond acceptor, nHB= no. of H-bond donor, TPSA= total polar surface area, SAscore= synthetic accessibility score, MDCK permeability= Madin-Darby Canine Kidney cells, GI absorption= Gastrointestinal absorption, PPB= plasma protein binding, VD= volume distribution, CL= clearance, $T_{½}$= half-life, H-HT= Human Hepatotoxicity, FDAMDD= FDA Maximum Daily Dose

4.3 Experimental

4.3.1 Materials and methods

All chemicals and reagents used in this research were of analytical grade and used without further purification, ensuring accurate experimental results. To ensure quality and consistency, we procured the chemicals directly from reputable suppliers. The 2-aminothiophenol (Cas no: 137-07-5) and diethyl oxalate (Cas no: 95-92-1) were purchased from the Spectrochem. Carbon disulfide (Cas no: 75-15-0) and hydrazine hydrate (99%) (Cas no: 7803-57-8) were of analytical grade obtained from the CDH (Central Drug House). We sourced both potassium hydroxide (Cas no: 1310-58-3) and sodium hydroxide (Cas no: 1310-73-2) from Molychem for our reactions. For thin-layer chromatography, we used Silica Gel 60 F_{254} TLC Aluminum Sheets (Merck KGaA, Darmstadt Germany) and visualized the spots under UV light at 254 nm and 365 nm. ^{1}H NMR spectra (400 MHz) and ^{13}C NMR spectra (101 MHz) were recorded on AvanceNeo Ascend spectrometer in DMSO-d_6 solvent. The expression of chemical shifts is in δ ppm, measured relative to Tetramethyl silane (TMS) as an internal standard. The mass spectral analysis, a Waters ACQUITY QDa spectrometer was utilized, operating with a direct inlet method. A Shimadzu FTIR-8400 spectrometer was used to record the Fourier Transform Infrared (FT-

IR) spectrum. The potassium bromide (KBr) pellet method was employed to prepare the samples for infrared spectroscopy. The melting points were recorded on an electrothermal device from Tempo instruments using open capillaries and are uncorrected.

→ **General procedure for synthesis of benzothiazole-2-carboxylate (3)**

The mixture of diethyl oxalate (20 mmol) and 2-aminothiophenol (10 mmol) was refluxed for 5 h. After confirming the completion of the reaction using TLC in ethyl acetate and n-hexane (2:1), the mixture was cooled to room temperature and stirred with 50 mL of methanol for 30 min. This mixture was poured into the solution of HCl (20 mL) and water (80 mL) with vigorous stirring. The white coloured solid was obtained which was separated by vacuum filtration, dried, and recrystallized from methanol, resulting in a 94% yield of benzothiazole-2-carboxylate.

→ **General procedure for synthesis of benzothiazole-2-carbohydrazide (4)**

Benzothiazole-2-carboxylate (10 mmol) was dissolved in 50 mL of absolute ethanol. To this solution, hydrazine hydrate (99%) was added dropwise and the mixture was refluxed for 6 h. The completion of the reaction was verified through the TLC in solvent system ethyl acetate and n-hexane (2:1). Reaction mixture was cooled down to room temperature, vacuum filtered, washed with water and dried overnight to get the yellow coloured benzothiazole-2-carbohydrazide in 86% yield.

→ **Synthesis of potassium 2-(benzo[d]thiazole-2-carbonyl) hydrazine-1-carbodithioate salt (5)**

Benzothiazole-2-carbohydrazide (10 mmol) was dissolved in a methanolic solution of KOH (15 mmol) and stirred at room temperature. A dropwise addition of carbon disulfide (15 mmol) was made to the mixture, which was then stirred for 18 h. Once the reactants were fully consumed as indicated by TLC, the mixture underwent vacuum filtration and was washed multiple times with diethyl ether. The product was dried at 80°C in the oven for 3 h. The resulting yellow colored potassium 2-(benzo[d]thiazole-2-carbonyl) hydrazine-1-carbodithioate salt, with a yield of 92%, was directly used in the subsequent step without further purification.

→ **Synthesis of 4-amino-5-(benzo[d]thiazol-2-yl)-4H-1,2,4-triazole-3-thiol (6)**

The potassium dithiocarbazinate salt (5) (10 mmol) was dissolved in water, followed by the dropwise addition of hydrazine hydrate 99% (20 mmol) to the solution. The resulting mixture was then refluxed at 90°C. As the reaction progressed, hydrogen sulfide gas was generated and its presence was confirmed through a test using lead acetate solution (the lead acetate-soaked filter paper to undergo a color change from white to black). The reaction mixture was cooled to room temperature after the complete evolution of hydrogen sulfide gas, and the workup was performed using a 20% HCl solution in water. Precipitates with a slight yellow color were observed, which were then vacuum filtered, oven dried at 100°C, and washed with hot ethanol. This process resulted in the formation of pure white 4-amino-5-(benzo[d]thiazol-2-yl)-4H-1,2,4-triazole-3-thiol. White solid; yield: 90%; mp 221–223°C; ^{1}H NMR (400 MHz, DMSO-d_6), ppm: 6.19 (s, 2H, NH_2), 7.61 (dddd, J_1 = 22.4 Hz, J_2 = 8.4 Hz, J_3 = 7.2 Hz, J_4 = 1.3 Hz, 2H, Ar–H), 8.14–8.21 (d, 1H, Ar–H), 8.22–8.29 (d, 1H, Ar–H), 14.38 (s, 1H, SH); ^{13}C NMR (101 MHz, DMSO-d_6), ppm: 122.91 (Ar–C), 124.05, 127.14, 127.52, 135.15, 144.94 (C–C), 152.49, 152.55 (C–C), 167.36 (C–SH); ESI-MS: *m/z* 249.90 $[M + H]^+$.

→ **General procedure for synthesis of (E)-5-(benzo[d]thiazol-2-yl)-4-(benzylideneamino)-4H-1,2,4-triazole-3-thiol derivatives (8a-m)**

4-amino-5-(benzo[d]thiazol-2-yl)-4H-1,2,4-triazole-3-thiol (10 mmol) was added to the 20 mL of methanol and sonicated for 5 min. NaOH (10 mmol) was added to this suspension and stirred at room temperature until complete dissolution of all reactants. After 30 min, aromatic aldehyde (11 mmol) was added to the solution and stirred at room temperature. The precipitates that formed in the reaction mixture were filtered under vacuum, washed with water, and left to dry overnight at room temperature. A wash with hot ethanol was carried out subsequently to achieve pure derivatives (8a-m) of (E)-5-(benzo[d]thiazol-2-yl)-4-(benzylideneamino)-4H-1,2,4-triazole-3-thiol.

(E)-5-(benzo[d]thiazol-2-yl)-4-(benzylideneamino)-4H-1,2,4-triazole-3-thiol (8a)

Light yellow solid; yield: 96%; mp 173–175°C; FT-IR ν_{max}, cm^{-1}: 2901 (C–H alkane stre.), 1643 (C=N stre.), 1280 (C–N stre.); ^{1}H NMR (400 MHz, DMSO-d_6), ppm: 7.55–7.69 (m, 4H, Ar–H), 7.71 (dd, J_1 = 8.5, J_2 = 5.9 Hz, 1H, Ar–H), 8.04–8.06 (m, 2H, Ar–H), 8.11 (d, J = 7.8 Hz, 1H, Ar–H), 8.26 (d, J = 7.8 Hz, 1H, Ar–H), 9.87 (s, 1H, HC=N), 14.70 (s, 1H,

SH); ^{13}C NMR (101 MHz, DMSO-d_6), ppm: 123.04 (Ar–C), 123.40, 124.25, 127.28, 129.64, 129.86, 132.30, 135.51, 135.61, 151.99 (HC=N), 152.67, 153.40 (C–C), 167.45 (C–SH); ESI-MS: *m/z* 338.1 [*M* + H]$^+$; Calculated, %: $C_{16}H_{11}N_5S_2$; C, 56.95; H, 3.29; N, 20.76; Found, %: C, 56.90; H, 3.25; N, 20.73.

(E)-5-(benzo[d]thiazol-2-yl)-4-((4-chlorobenzylidene)amino)-4H-1,2,4-triazole-3-thiol (8b)

Yellow solid; yield: 94%; mp 216–218°C; FT-IR ν_{max}, cm^{-1}: 2901 (C–H alkane stre.), 1658 (C=N stre.), 1273 (C–N stre.); ^{1}H NMR (400 MHz, DMSO-d_6), ppm: 7.46–7.49 (m, 1H, Ar–H), 7.52–7.61 (m, 1H, Ar–H), 7.64–7.66 (m, 2H, Ar–H), 8.01–8.06 (m, 3H, Ar–H), 8.15–8.17 (m, 1H, Ar–H), 10.28 (s, 1H, HC=N); ^{13}C NMR (101 MHz, DMSO-d_6), ppm: 122.67 (Ar–C), 123.76, 126.46, 127.24, 129.85, 130.82, 135.15, 137.39, 152.95 (HC=N), 153.33, 161.53 (C–C), 164.57 (C–SH); ESI-MS: *m/z* 370.3 [*M* – H]$^-$; Calculated, %: $C_{16}H_{10}ClN_5S_2$; C, 51.68; H, 2.71; N, 18.83; Found, %: C, 51.62; H, 2.69; N, 18.80.

(E)-2-(((3-(benzo[d]thiazol-2-yl)-5-mercapto-4H-1,2,4-triazol-4-yl)imino) methyl) phenol (8c)

White solid; yield: 93%; mp 228–230°C; FT-IR ν_{max}, cm^{-1}: 2901 (C–H alkane stre.), 1612 (C=N stre.), 1273 (C–N stre.); ^{1}H NMR (400 MHz, DMSO-d_6), ppm: 7.01–7.08 (m, 2H, Ar–H), 7.48–7.62 (m, 3H, Ar–H), 7.96–7.97 (dd, J_1 = 7.8 Hz, J_2 = 1.8 Hz, 1H, Ar–H), 8.09–8.11 (d, J = 8.1 Hz, 1H, Ar–H), 8.21–8.23 (m, 1H, Ar–H), 10.23 (s, 1H, HC=N), 10.71 (s, 1H, SH), 14.65 (s, 1H, OH); ^{13}C NMR (101 MHz, DMSO-d_6), ppm: 117.40 (Ar–C), 118.32, 120.30, 122.95, 124.17, 127.27, 127.60, 129.25, 135.13, 135.26, 152.37, 152.70 (HC=N), 159.23 (C–OH), 163.18 (C–SH), 163.30 (C–C); ESI-MS: *m/z* 352.2 [*M* – H]$^-$; Calculated, %: $C_{16}H_{11}N_5OS_2$; C, 54.38; H, 3.14; N, 19.82; Found, %: C, 54.36; H, 3.13; N, 19.80.

(E)-5-(benzo[d]thiazol-2-yl)-4-((4-bromobenzylidene)amino)-4H-1,2,4-triazole-3-thiol (8d)

Yellow solid; yield: 90%; mp 212–215°C; FT-IR ν_{max}, cm^{-1}: 2901 (C–H alkane stre.), 1589 (C=N stre.), 1280 (C–N stre.); ^{1}H NMR (400 MHz, DMSO-d_6), ppm: 7.54 (dt, J_1 = 20.3 Hz, J_2 = 7.2 Hz, 2H, Ar–H), 7.77–7.82 (m, 2H, Ar–H), 7.94 (dd, J_1 = 8.6 Hz, J_2 = 2.6 Hz,

2H, Ar–H), 8.06 (d, *J* = 8.0 Hz, 1H, Ar–H), 8.18 (d, *J* = 8.0 Hz, 1H, Ar–H), 9.95 (s, 1H, HC=N); ^{13}C NMR (101 MHz, DMSO-*d*$_6$), ppm: 122.84 (Ar–C), 124.17, 127.13, 127.24, 127.54, 131.26, 131.62, 132.88, 135.41, 144.10, 151.98 (HC=N), 152.65, 163.46 (C–C), 165.01 (C–SH); ESI-MS: *m/z* 416.4 [*M* – H]$^-$; Calculated, %: $C_{16}H_{10}BrN_5S_2$; C, 46.16; H, 2.42; N, 16.82; Found, %: C, 46.14; H, 2.39; N, 16.81.

(E)-5-(benzo[d]thiazol-2-yl)-4-((2,4-difluorobenzylidene)amino)-4H-1,2,4-triazole-3-thiol (8e)

Yellow solid; yield: 87%; mp 228–230°C; FT-IR ν_{max}, cm^{-1}: 2978 (C–H alkane stre.), 1612 (C=N stre.), 1280 (C–N stre.); ^{1}H NMR (400 MHz, DMSO-*d*$_6$), ppm: 7.35–7.40 (td, J_1 = 8.5, J_2 = 2.5 Hz, 1H, Ar–H), 7.51–7.57 (m, 1H, Ar–H), 7.58–7.67 (m, 2H, Ar–H), 8.10–8.34 (m, 3H, Ar–H), 10.24 (s, 1H, HC=N), 14.73 (s, 1H, SH); ^{13}C NMR (101 MHz, DMSO-*d*$_6$), ppm: 105.66 (Ar–C), 113.95, 117.04, 122.94, 124.25, 127.27, 127.63, 130.24, 135.46, 144.13 (HC=N), 152.49 (C–C), 158.20–158.24 (m, C–F), 161.63–167.39 (m, C–F), 163.24 (C–SH); ESI-MS: *m/z* 372.3 [*M* – H]$^-$; Calculated, %: $C_{16}H_9F_2N_5S_2$; C, 51.47; H, 2.43; N, 18.76; Found, %: C, 51.42; H, 2.40; N, 18.73.

(E)-5-(benzo[d]thiazol-2-yl)-4-((3,4-dimethoxybenzylidene)amino)-4H-1,2,4-triazole-3-thiol (8f)

Yellow solid; yield: 89%; mp 190–192°C; FT-IR ν_{max}, cm^{-1}: 3001 (C–H alkane stre.), 1627 (C=N stre.), 1311 (C–N stre.); ^{1}H NMR (400 MHz, DMSO-*d*$_6$), ppm: 3.89 (s, 6H, 2*OCH_3), 7.17–7.19 (d, J_1 = 8.4 Hz, 1H, Ar–H), 7.52–7.54 (m, 1H, Ar–H), 7.54–7.56 (m, 1H, Ar–H), 7.57–7.62 (m, 1H, Ar–H), 7.64–7.65 (d, *J* = 1.9 Hz, 1H, Ar–H), 8.09–8.11 (d, *J* = 8.0 Hz, 1H, Ar–H), 8.18–8.25 (m, 1H, Ar–H), 9.70 (s, 1H, HC=N), 14.64 (s, 1H, SH); ^{13}C NMR (101 MHz, DMSO-*d*$_6$), ppm: 56.05 (3–OCH_3), 56.29 (4–OCH_3), 110.16 (Ar–C), 112.11, 122.94, 124.20, 124.82, 125.39, 127.20, 127.64, 135.53, 144.09, 149.71 (C–OCH_3), 151.90 (HC=N), 152.61, 153.38 (C–OCH_3), 153.67 (C–C), 166.75 (C–SH); ESI-MS: *m/z* 396.4 [*M* – H]$^-$; Calculated, %: $C_{18}H_{15}N_5O_2S_2$; C, 54.39; H, 3.80; N, 17.62; Found, %: C, 54.35; H, 3.77; N, 17.60.

(E)-5-(benzo[d]thiazol-2-yl)-4-((2-nitrobenzylidene)amino)-4H-1,2,4-triazole-3-thiol (8g)

Yellowish orange solid; yield: 87%; mp 192–194°C; FT-IR ν_{max}, cm^{-1}: 2908 (C–H alkane stre.), 1604 (C=N stre.), 1257 (C–N stre.); ^{1}H NMR (400 MHz, DMSO-d_6), ppm: 7.54–7.66 (m, 2H, Ar–H), 7.90–7.94 (td, J_1 = 7.8 Hz, J_2 =1.5 Hz, 1H, Ar–H), 8.01–8.04 (t, J = 7.6 Hz, 1H, Ar–H), 8.11–8.13 (d, J = 8.0 Hz, 1H, Ar–H), 8.18–8.26 (t, J = 7.3 Hz, 2H, Ar–H), 8.38–8.41 (m, 1H, Ar–H), 10.65 (s, 1H, HC=N), 14.74 (s, 1H, SH); ^{13}C NMR (101 MHz, DMSO-d_6), ppm: 122.98 (Ar–C), 124.26, 125.55, 127.18, 127.26, 127.55, 127.61, 129.91, 133.79, 134.92, 135.36, 144.24 (HC=N), 149.32, 152.74 (C–NO_2), 160.83 (C–C), 163.57 (C–SH); ESI-MS: *m/z* 381.3 [M – H]$^-$; Calculated, %: $C_{16}H_{10}N_6O_2S_2$; C, 50.25; H, 2.64; N, 21.98; Found, %: C, 50.24; H, 2.62; N, 21.95.

(E)-5-(benzo[d]thiazol-2-yl)-4-((3-nitrobenzylidene)amino)-4H-1,2,4-triazole-3-thiol (8h)

Light yellow solid; yield: 89%; mp 230–232°C; FT-IR ν_{max}, cm^{-1}: 2939 (C–H alkane stre.), 1604 (C=N stre.), 1273 (C–N stre.); ^{1}H NMR (400 MHz, DMSO-d_6), ppm: 7.48–7.60 (tq, J_1 = 15.1 Hz, J_2 = 7.4 Hz, 2H, Ar–H), 7.83–7.87 (t, J = 8.0 Hz, 1H, Ar–H), 8.03–8.05 (d, J = 8.0 Hz, 1H, Ar–H), 8.13–8.15 (d, J = 8.2 Hz, 1H, Ar–H), 8.37–8.43 (m, 2H, Ar–H), 8.75 (s, 1H, CH–NO_2), 10.18 (s, 1H, HC=N), 14.70 (s, 1H, SH); ^{13}C NMR (101 MHz, DMSO-d_6), ppm: 122.76 (Ar–C), 123.71, 124.23, 127.26, 127.38, 127.55, 131.39, 134.05, 135.12, 135.26, 148.68 (C–NO_2), 151.70 (HC=N), 152.65, 163.08 (C–SH), 163.41 (SC–C); ESI-MS: *m/z* 381.3 [M – H]$^-$; Calculated, %: $C_{16}H_{10}N_6O_2S_2$; C, 50.25; H, 2.64; N, 21.98; Found, %: C, 50.22; H, 2.61; N, 21.94.

(E)-5-(benzo[d]thiazol-2-yl)-4-((2-chlorobenzylidene)amino)-4H-1,2,4-triazole-3-thiol (8i)

Dark yellow solid; yield: 91%; mp 213–215°C; FT-IR ν_{max}, cm^{-1}: 2993 (C–H alkane stre.), 1635 (C=N stre.), 1280 (C–N stre.); ^{1}H NMR (400 MHz, DMSO-d_6), ppm: 7.47 (t, J = 7.6

Hz, 1H, Ar–H), 7.53–7.65 (m, 4H, Ar–H), 8.08 (d, *J* = 8.1 Hz, 1H, Ar–H), 8.17 (d, *J* = 7.8 Hz, 1H, Ar–H), 8.37 (dd, J_1 = 6.9 Hz, J_2 = 2.1 Hz, 1H, Ar–H), 11.09 (s, 1H, CH=N); ^{13}C NMR (101 MHz, DMSO-d_6), ppm: 122.67 (Ar–C), 123.69, 126.32, 127.19, 128.49, 130.69, 131.22, 133.91, 135.18, 135.45, 145.13 (HC=N), 152.97, 156.26 (C–C), 164.64 (C–SH); ESI-MS: *m/z* 370.4 [*M* – H]$^-$; Calculated, %: $C_{16}H_{10}ClN_5S_2$; C, 51.68; H, 2.71; N, 18.83; Found, %: C, 51.63; H, 2.68; N, 18.79.

(E)-5-(benzo[d]thiazol-2-yl)-4-((4-fluorobenzylidene)amino)-4H-1,2,4-triazole-3-thiol (8j)

Light yellow solid; yield: 90%; mp 211–213°C; FT-IR ν_{max}, cm^{-1}: 2908 (C–H alkane stre.), 1597 (C=N stre.), 1257 (C–N stre.); ^{1}H NMR (400 MHz, DMSO-d_6), ppm: 7.45–7.50 (t, *J* = 8.7 Hz, 2H, Ar–H), 7.53–7.65 (tq, J_1 = 14.7 Hz, J_2 = 7.2 Hz, 2H, Ar–H), 8.08–8.14 (m, 3H, Ar–H), 8.17–8.25 (m, 2H, Ar–H), 9.86 (s, 1H, HC=N), 14.68 (s, 1H, SH); ^{13}C NMR (101 MHz, DMSO-d_6), ppm: 116.99 (Ar–C), 117.21, 122.96, 123.34, 124.24, 127.26, 127.63, 128.96, 132.19, 132.28, 135.44, 144.03 (HC=N), 151.95, 152.66 (C–C), 153.38 (C–SH), 166.14 (C–F); ESI-MS: *m/z* 354.3 [*M* – H]$^-$; Calculated, %: $C_{16}H_{10}FN_5S_2$; C, 54.07; H, 2.84; N, 19.71; Found, %: C, 54.06; H, 2.82; N, 19.67.

(E)-5-(benzo[d]thiazol-2-yl)-4-((3-bromobenzylidene)amino)-4H-1,2,4-triazole-3-thiol (8k)

White solid; yield: 93%; mp 214–216°C; FT-IR ν_{max}, cm^{-1}: 2939 (C–H alkane stre.), 1589 (C=N stre.), 1273 (C–N stre.); ^{1}H NMR (400 MHz, DMSO-d_6), ppm: 7.54–7.66 (m, 3H, Ar–H), 7.87–7.90 (m, 1H, Ar–H), 8.05–8.07 (d, *J* = 7.8 Hz, 1H, Ar–H), 8.09–8.11 (m, 1H, Ar–H), 8.20 (t, *J* = 1.9 Hz, 1H, Ar–H), 8.23–8.26 (m, 1H, Ar–H), 9.89 (s, 1H, HC=N), 14.73 (s, 1H, SH); ^{13}C NMR (101 MHz, DMSO-d_6), ppm: 122.96 (Ar–C), 123.02, 123.37, 124.26, 127.34, 127.69, 128.39, 131.89, 132.02, 134.64, 135.37, 136.11, 144.01 (HC=N), 152.70, 163.50 (C–C), 165.64 (C–SH); ESI-MS: *m/z* 416.2 [*M* – H]$^-$; Calculated, %: $C_{16}H_{10}BrN_5S_2$; C, 46.16; H, 2.42; N, 16.82; Found, %: C, 46.12; H, 2.39; N, 16.78.

(E)-5-(benzo[d]thiazol-2-yl)-4-((4-methylbenzylidene)amino)-4H-1,2,4-triazole-3-thiol (8l)

Light yellow; yield: 96%; mp 206–208°C; FT-IR ν_{max}, cm^{-1}: 1604 (C=N stre.), 1273 (C–N stre.); ^{1}H NMR (400 MHz, DMSO-d_6), ppm: 2.44 (s, 3H, CH_3), 7.43–7.45 (d, J = 7.9 Hz, 2H, Ar–H), 7.53–7.64 (m, 2H, Ar–H), 7.92–7.94 (d, J = 7.9 Hz, 2H, Ar–H), 8.09–8.11 (m, 1H, Ar–H), 8.23–8.26 (dt, J_1 = 7.8 Hz, J_2 = 2.5 Hz, 1H, Ar–H), 9.78 (s, 1H, HC=N), 14.67 (s, 1H, SH); ^{13}C NMR (101 MHz, DMSO-d_6), ppm: 21.84 (CH_3), 122.98 (Ar–C), 124.16, 124.22, 127.23, 129.66, 130.43, 135.52, 135.61, 144.06, 151.95 (HC=N), 152.64, 163.36 (C–C), 167.39 (C–SH); ESI-MS: *m/z* 350.3 [M – H]$^-$; Calculated, %: $C_{17}H_{13}N_5S_2$; C, 58.10; H, 3.73; N, 19.93; Found, %: C, 58.9; H, 3.72; N, 19.90.

(E)-5-(benzo[d]thiazol-2-yl)-4-((thiophen-2-ylmethylene)amino)-4H-1,2,4-triazole-3-thiol (8m)

Light yellow solid; yield: 84%; mp 197–199°C; FT-IR ν_{max}, cm^{-1}: 2924 (C–H alkane stre.), 1651 (C=N stre.), 1273 (C–N stre.); ^{1}H NMR (400 MHz, DMSO-d_6), ppm: 7.34–7.36 (t, J = 4.4 Hz, 1H, Ar–H), 7.55–7.67 (m, 2H, Ar–H), 7.93 (d, J = 3.7 Hz, 1H, Ar–H), 8.08–8.13 (dd, J_1 = 14.1 Hz, J_2 = 6.5 Hz, 2H, Ar–H), 8.25–8.27 (d, J = 7.9 Hz, 1H, Ar–H), 10.03 (s, 1H, HC=N), 14.66 (s, 1H, SH); ^{13}C NMR (101 MHz, DMSO-d_6), ppm: 122.94 (Ar–H), 123.40, 124.25, 127.29, 127.68, 129.31, 134.61, 135.62, 137.21, 144.02 (HC=N), 152.62, 161.11 (C–C), 163.36 (C–SH); ; ESI-MS: *m/z* 342.4 [M – H]$^-$; Calculated, %: $C_{14}H_9N_5S_3$; C, 48.96; H, 2.64; N, 20.39; Found, %: C, 48.93; H, 2.63; N, 20.35.

4.3.2 In vitro antimicrobial and antifungal assay

The evaluation of antimicrobial and antifungal efficacy was conducted in our experiment using a two-step approach. To evaluate the zone of inhibition, the first step involved implementing the Minimal Bactericidal Concentration by agar well diffusion method. Subsequently, the Broth Dilution Method was utilized to determine the Minimum Inhibitory Concentration (MIC). This method offers a comprehensive analysis of the antimicrobial properties of the compounds.

Agar Well Diffusion method

To evaluate the antibacterial and antifungal properties of the synthesized compounds, we utilized the agar cup method in this study. In our study, we utilized a range of standard microbial strains, including *Escherichia coli* (MTCC–442), *Pseudomonas aeruginosa* (MTCC–441), *Staphylococcus aureus* (MTCC–96), *Streptococcus Pyogenes* (MTCC–443), *Acinetobacter baumannii* (MTCC–12890), *Candida albicans* (MTCC–227), *Aspergillus Niger* (MTCC–282), and *Aspergillus clavatus* (MTCC–1323). These strains were acquired from the Institute of Microbial Technology located in Chandigarh. The nutrient medium of choice for cultivating and diluting drug suspensions was Mueller Hinton Broth. The size of the inoculum for the test strain was precisely adjusted to 10^8 CFU/mL by evaluating turbidity. The desired drug concentrations were achieved by using DMSO as a diluent. To conduct the study, concentrations of 5, 25, 50, 100, and 250 µg/mL were employed for standard drugs such as chloramphenicol, ampicillin, and griseofulvin, as well as synthesized compounds (reference drugs). In conducting the zone of inhibition assay, we first liquefied a suitable medium, which was then inoculated with a known quantity of each microbial suspension to ensure the formation of clearly defined zones of inhibition. A uniform layer of 2-5 mm thickness was formed by pouring the inoculated medium into Petri dishes. These dishes were then stored under conditions that prevented any significant growth or death of the microorganisms and ensured that the surface of the medium was dry when used. In order to carry out the testing, we prepared solutions of the reference substance and the antibiotics being investigated in DMSO. These solutions were subsequently applied directly onto cavities that were formed on the agar surface. In order to maintain consistency, it was ensured that the same amount of solution was applied in each case. To prevent any potential interaction between the more concentrated solutions, a statistically appropriate design was used to arrange a series of doses in a geometric progression for both the reference and test substances on each dish.

The temperature for incubating the bacterial cultures was meticulously adjusted to 37°C, whereas the fungal cultures were incubated at a slightly lower temperature of 27°C. Both cultures underwent an incubation period lasting approximately 18 hr. To improve the regression slope and maintain consistency in solution application time, a diffusion period of 1-4 hr was employed prior to incubation, at room temperature. Post-incubation, the

diameters or areas of the circular inhibition zones were measured with precision, and the potency of the antibiotics was calculated using appropriate statistical methods. The required precision was ensured by conducting each assay with an adequate number of replications per dose. In some cases, the assay was repeated, and the results were combined statistically to ascertain whether the potency of the antibiotic being examined met the minimum required standards.

Minimal Inhibition Concentrations

After the initial analysis of the zone of inhibition, we evaluated the antibacterial and antifungal efficacy of the synthesized drugs through the micro broth dilution method. To maintain sterility, the glassware was sterilized prior to testing. The synthesized compounds were evaluated against a range of standard bacterial and fungal strains, including *E. coli* (MTCC–443), *P. aeruginosa* (MTCC–1688), *S. aureus* (MTCC–96), *S. pyogenes* (MTCC–442), *A. baumannii* (MTCC–12890), *C. albicans* (MTCC–227), *A. niger* (MTCC–282), and *A. clavatus* (MTCC–1323). All the microbial cultures utilized in this research were gained from the esteemed Microbial Type Culture Collection situated at the Institute of Microbial Technology in Chandigarh. Mueller Hinton Broth served as the nutrient medium for the bacterial cultures, facilitating the growth and dilution of the compound suspension, while Sabouraud Dextrose Broth was specifically used to provide nutrition for the fungal strains. In order to maintain uniformity, the inoculum size for each test strain was standardized to 10^8 CFU/mL through turbidity comparisons. To attain the desired drug concentrations for testing, DMSO was employed as the diluent. A serial dilution was performed in order to facilitate the primary and secondary screening procedures. At the beginning of the screening process, a stock solution for each synthesized drug was made, with a concentration of 2000 µg/mL. From this stock, dilutions of 1000 µg/mL, 500 µg/mL, and 250 µg/mL were prepared and tested. The drugs that exhibited activity in this phase underwent additional evaluation in the secondary screening process. This involved subjecting them to dilutions of various concentrations, specifically 200 µg/mL, 100 µg/mL, 50 µg/mL, 25 µg/mL, 12.5 µg/mL, and 6.250 µg/mL. Along with each set of tests, a control tube was included which did not have any antibiotic present. This control tube was subcultured before inoculation by spreading a loopful evenly over a suitable medium and

incubated at 37°C for overnight. The lowest concentration that inhibited visible growth of the organism compared to the control was used to determine the MIC.[258] Tubes that did not exhibit visible growth, similar to the controlled tube, underwent subculturing and were incubated once again in order to compare the growth quantity to the original inoculum. The reading of results was conducted meticulously, with the highest dilution showing at least 99% inhibition being considered as the MIC. This determination depended crucially on the inoculum size, which was standardized across all tests. As part of the quality control process, the MIC of a control organism was determined to ensure accuracy. Additionally, a second set of dilutions was inoculated with an organism of known sensitivity to validate the testing procedures.

4.3.3 Molecular modeling

The interactions between newly synthesized compounds and three different target proteins were examined using molecular docking in this study. The selected molecules were subjected to molecular docking individually with penicillin-binding protein (R1) from *E. coli*, DNA gyrase (R2) from P. aeruginosa, and secreted aspartic protease (R3) from C. albicans, in order to evaluate their interactions. Crystal structures of protein (R_1 | PDB id: 3MZD | X-ray Diffraction | 1.90 Å; R_2 | PDB id: 8BN6 | X-ray Diffraction | 1.60 Å; R_3 | PDB id: 3Q70 | X-ray Diffraction | 1.40 Å) were directly obtained from the RCSB Protein Data Bank. The water molecules and heteroatoms were removed from the receptor using UCSF Chimera 1.17.3 and the co-crystallized ligand was separated and saved for the method validation.[210] Protein preparation for molecular docking was conducted using the UCSF Chimera's Dock Prep tool. Incomplete side chains were reconstructed using the Dunbrack 2010 rotamer library, ensuring structural completeness.[211] Hydrogens were added to facilitate accurate modeling of interactions, and Gasteiger charges were assigned for precise electrostatic calculations in the docking process. The ligands used in the molecular docking were minimized using UCSF Chimera by steepest descent method to ensure their lowest energy conformations, enhancing the accuracy of the docking. The particular site where the co-crystallized ligand was located was chosen for molecular docking because it represents a biologically relevant and experimentally validated binding region. Docking was performed using AutoDock Vina 1.5.7 integrated as an extension tool

in the UCSF Chimera.[165,259] The docking parameters: number of binding modes was limited to 10, exhaustiveness of the search was set to 8, and the maximum energy difference was constrained to 3 kcal/mol to focus on the most energetically favorable interactions. The top-ranked poses resulting from the docking were analyzed and visualized using BIOVIA Discovery Studio Visualizer 2024, providing detailed insights into the ligand-protein interactions.[213] To validate our docking approach, we re-docked the co-crystallized ligand with the receptor. The output ligand's position was then superimposed on the native ligand, and the deviation was measured to assess the accuracy of the docking simulation.

4.3.4 In silico drug likeness analysis

To evaluate drug-likeness and ADME properties, we employed SwissADME and gave particular attention to key factors, including solubility, permeability, and adherence to Lipinski's 'Rule of Five'. The 'Boiled Egg' model was employed to forecast gastrointestinal absorption and blood-brain barrier penetration.[260] To assess toxicity, the ADMETlab 2.0 web server was employed, giving estimates of potential toxicities.[261] By evaluating the pharmacokinetic profiles and safety, this thorough analysis played a crucial role in efficiently identifying potential drug candidates.

4.4 Conclusion

In conclusion, our research introduces novel benzothiazole-tethered triazole compounds that were deliberately designed to exclude traditional linkers like NH_2 and SH. The successful synthesis and subsequent characterization of these compounds were achieved through the utilization of various analytical methods, including ^{1}H NMR, ^{13}C NMR, mass spectrometry, and IR spectroscopy. When compounds were subjected to in vitro testing, it was found to possess an excellent antimicrobial activity against *E. coli*, P. aeruginosa, and C. albicans. Notably, this activity was equivalent to, or even greater than, that of standard drugs. Their effectiveness against Gram-positive bacteria, such as S. aureus and S. pyogenes, was observed to be at a moderate level. Moreover, the results from molecular docking correlated with the rates of microbial inhibition, and the ADMET analysis demonstrated encouraging characteristics for subsequent studies on drug safety and efficacy. These results strongly suggest that benzothiazole incorporating triazole

compounds has valuable potential as innovative antimicrobial agents, and thus, they should be further explored and enhanced.

4.5 Spectral data

- **Spectral data of compound 8a**

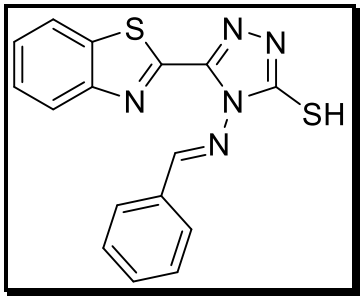

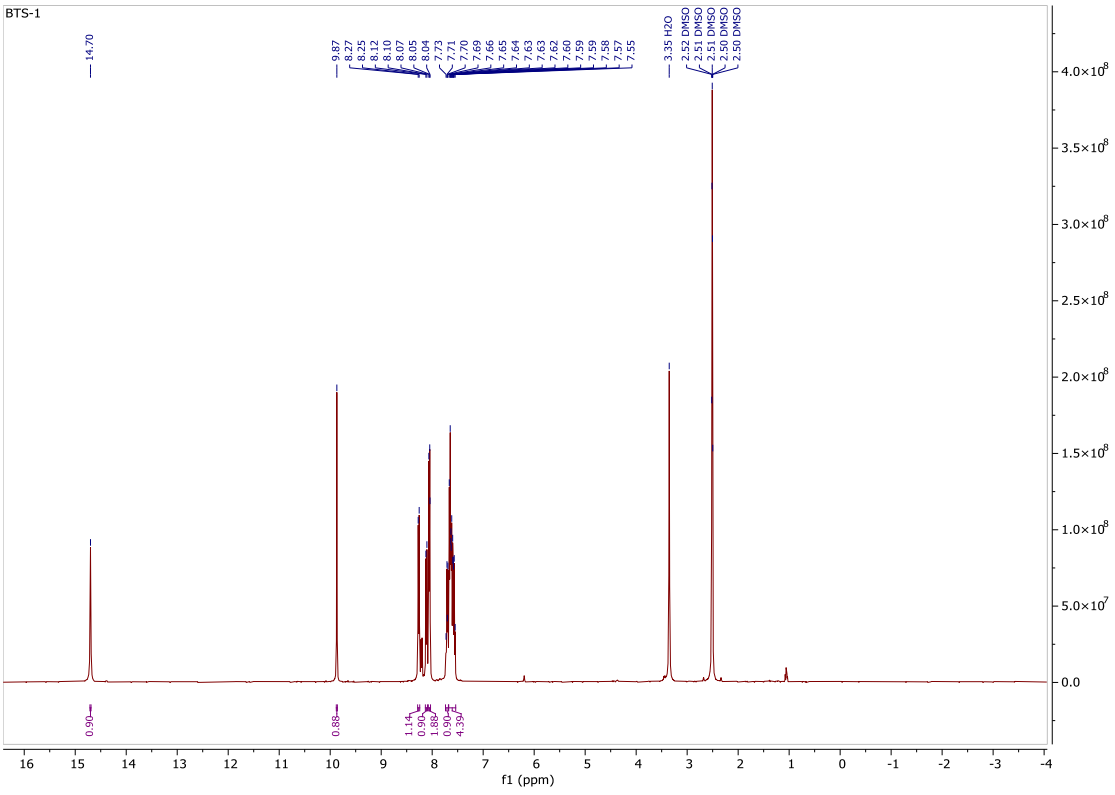

Figure 7: Representative ^{1}H NMR spectrum of compound 8a

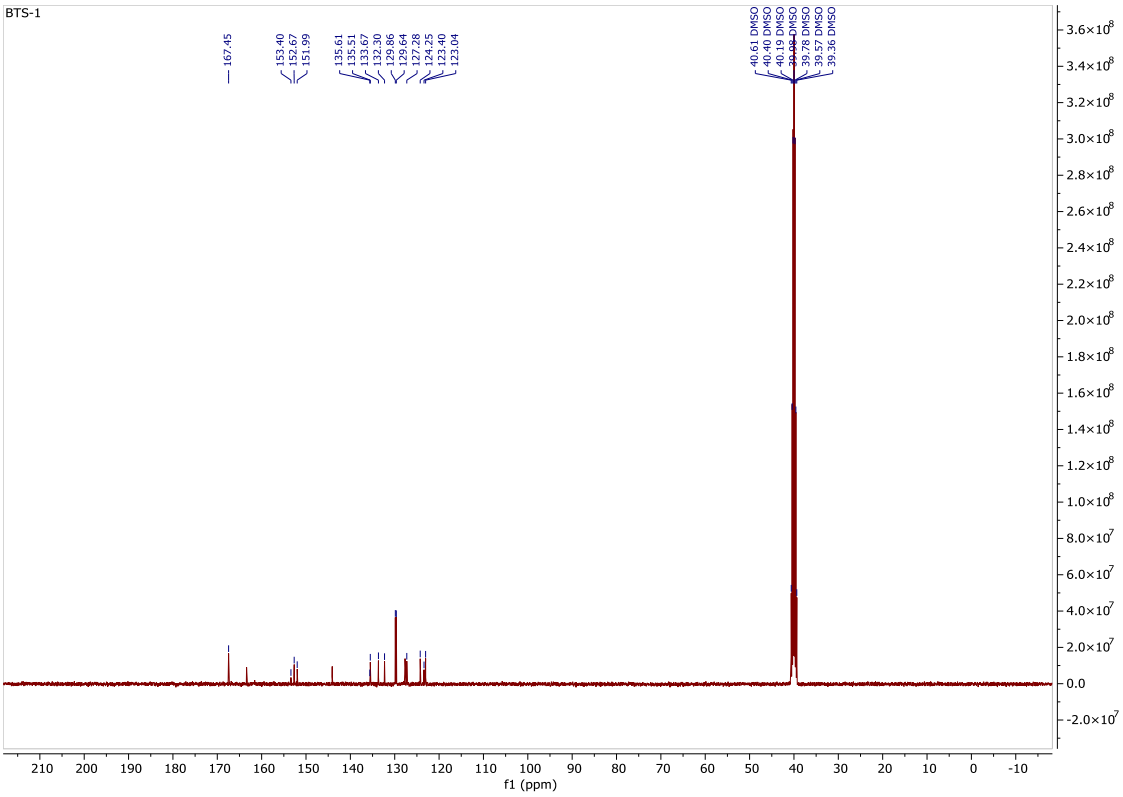

Figure 8: Representative ^{13}C NMR spectrum of compound 8a

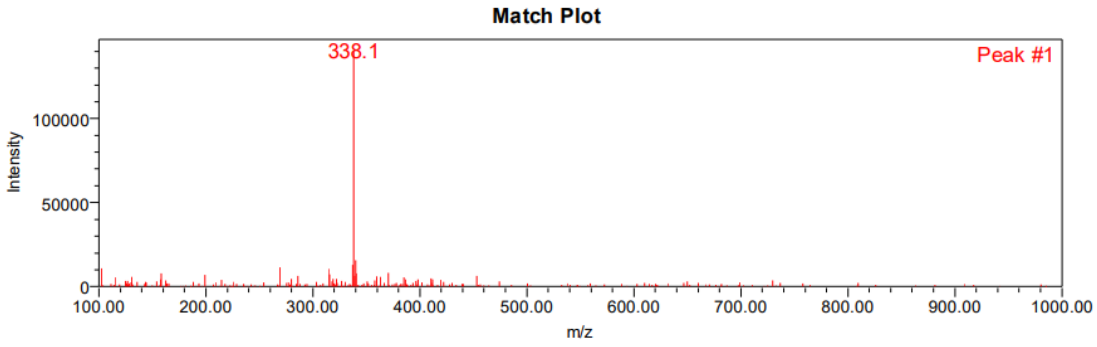

Figure 9: Representative mass spectrum of compound 8a

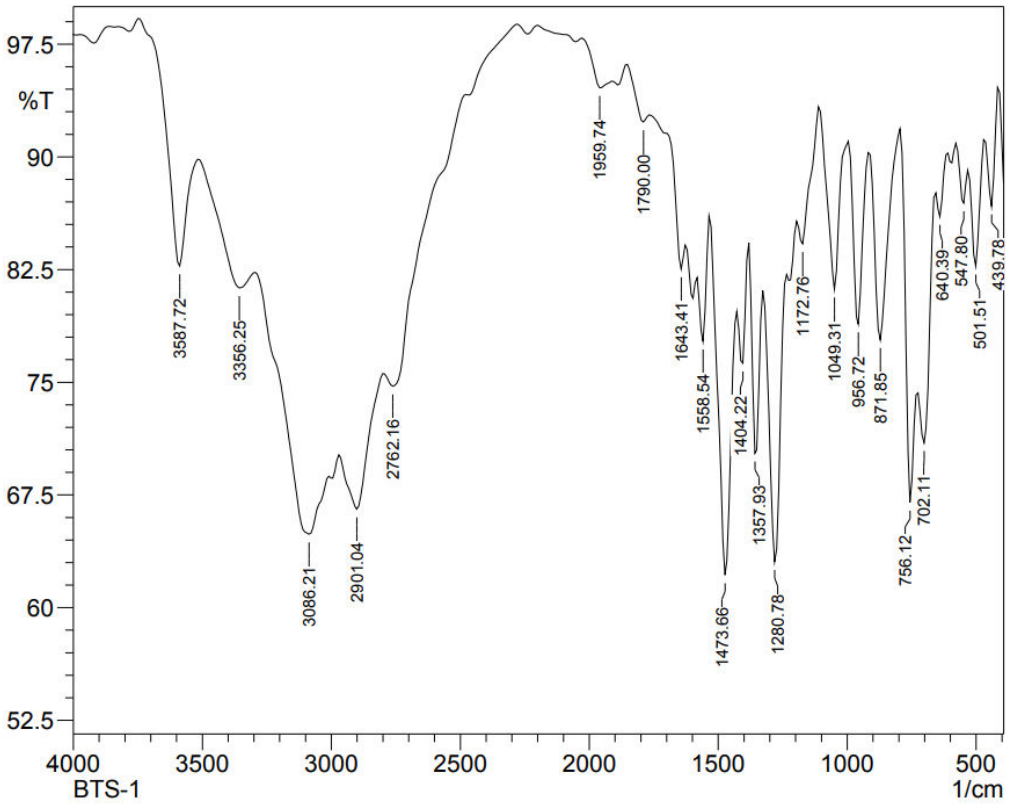

Figure 10: Representative FT-IR spectrum of compound 8a

- **Spectral data of compound 8b**

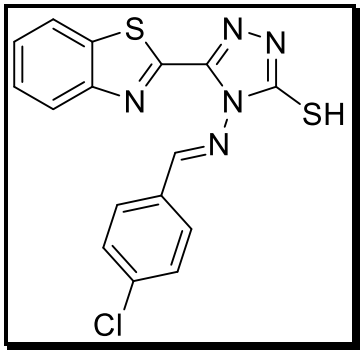

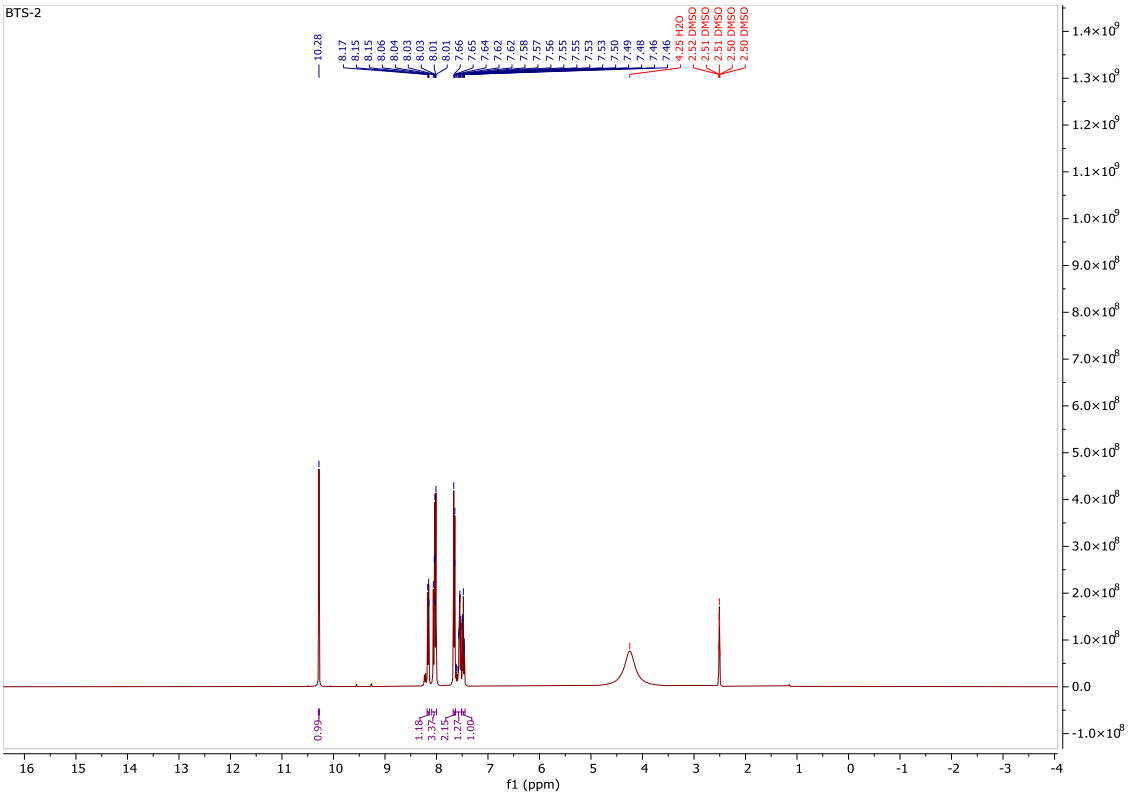

Figure 11: Representative ^{1}H NMR spectrum of compound 8b

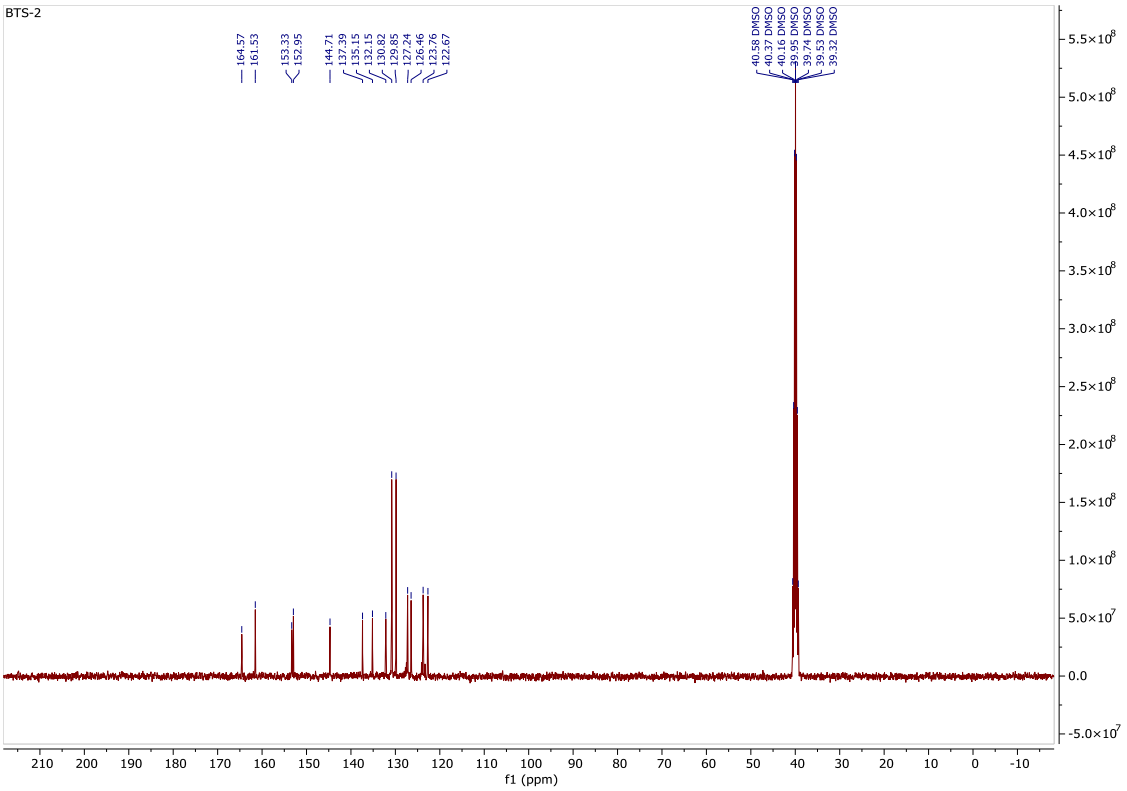

Figure 12: Representative 13C NMR spectrum of compound 8b

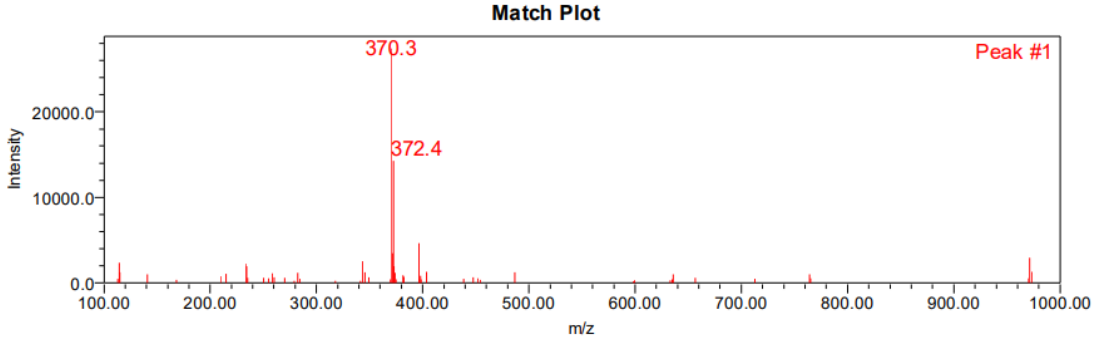

Figure 13: Representative mass spectrum of compound 8b

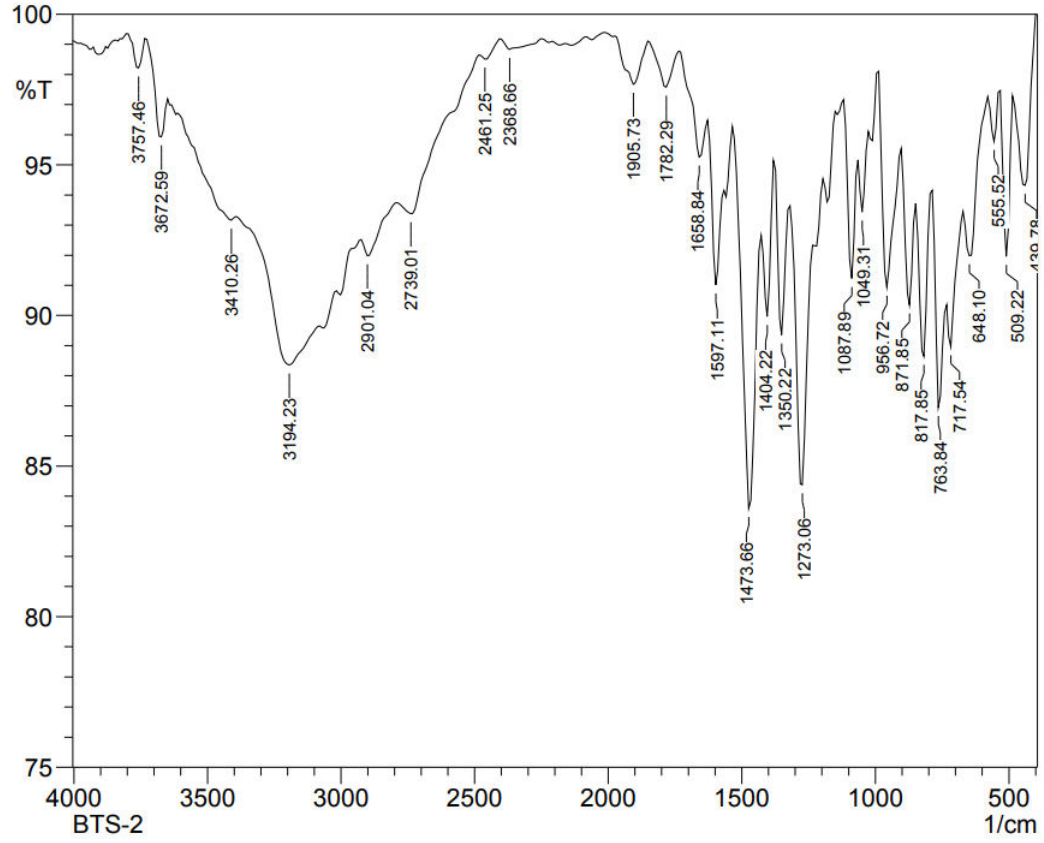

Figure 14: Representative FT-IR spectrum of compound 8b

- **Spectral data of compound 8c**

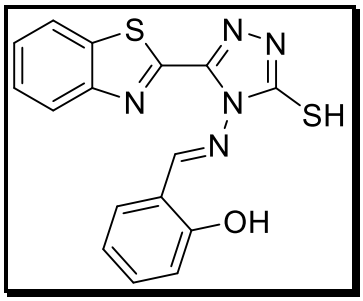

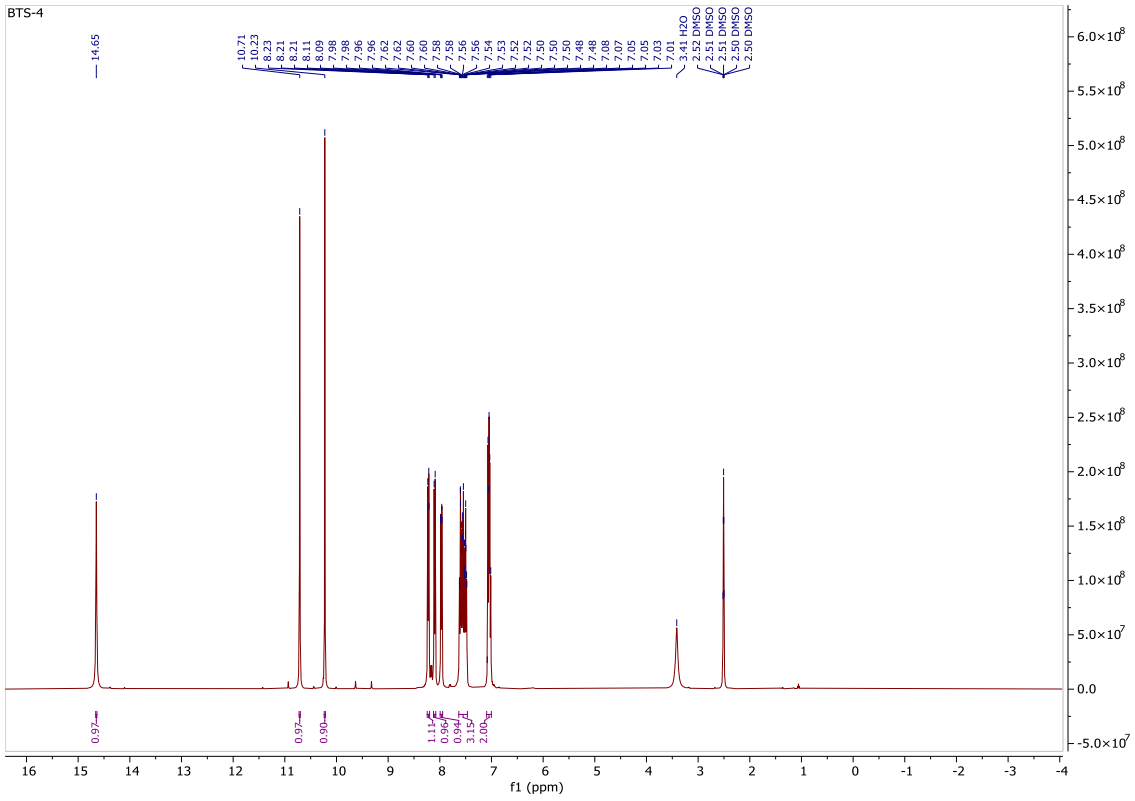

Figure 15: Representative 1H NMR spectrum of compound 8c

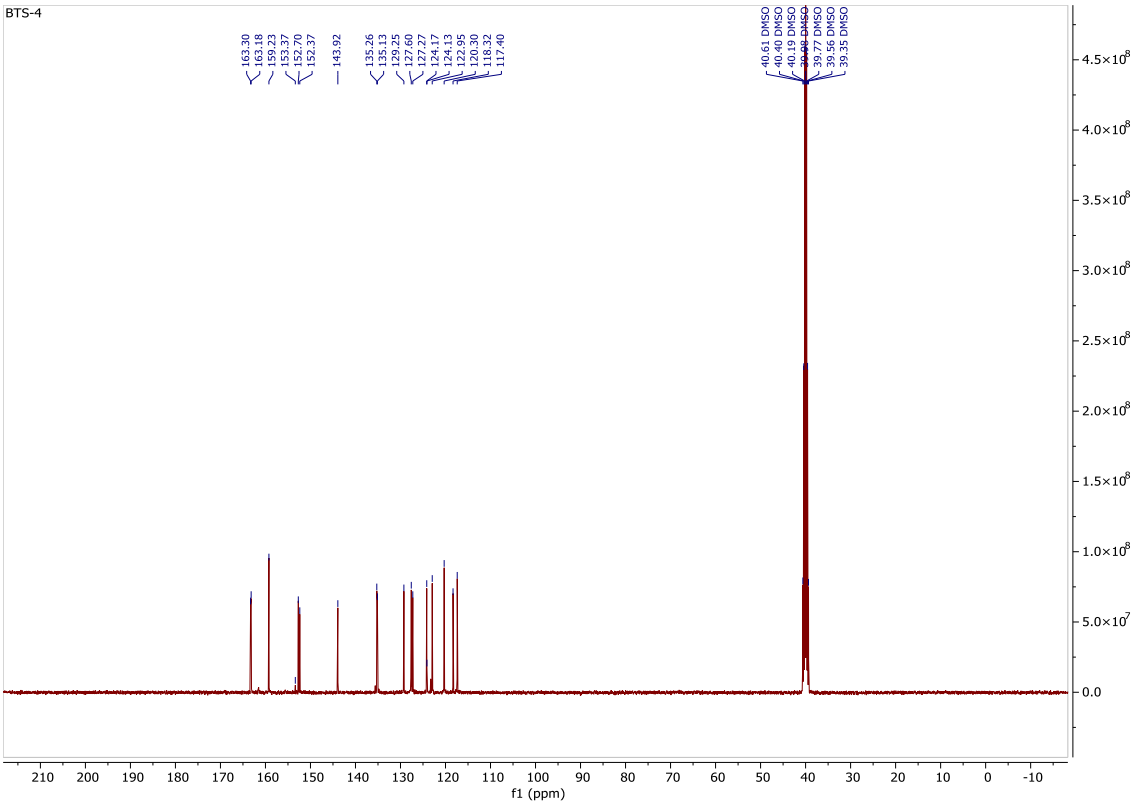

Figure 16: Representative ^{13}C NMR spectrum of compound 8c

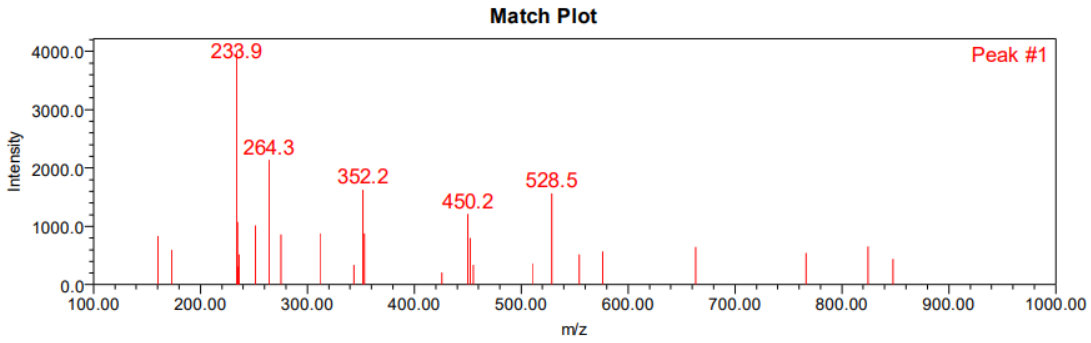

Figure 17: Representative mass spectrum of compound 8c

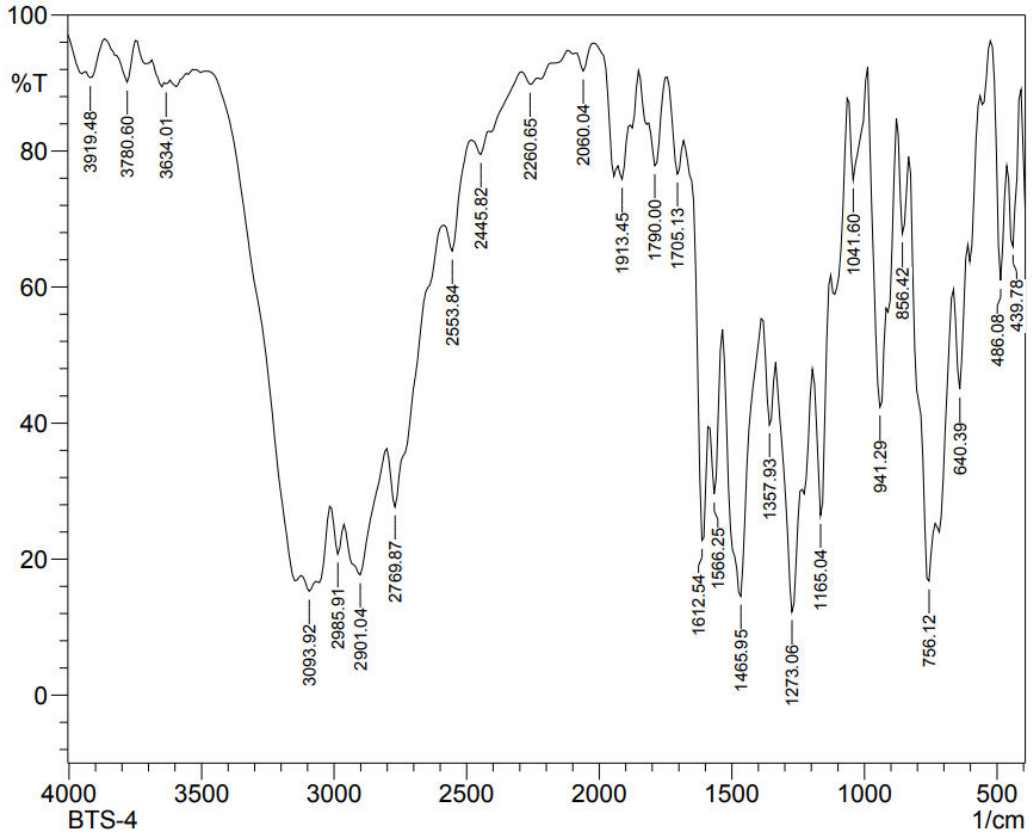

Figure 18: Representative FT-IR spectrum of compound 8c

- **Spectral data of compound 8d**

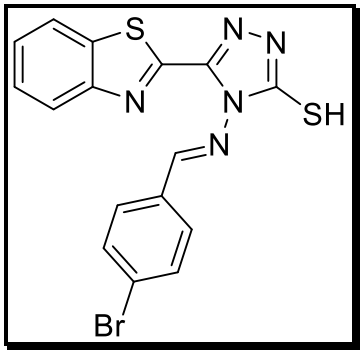

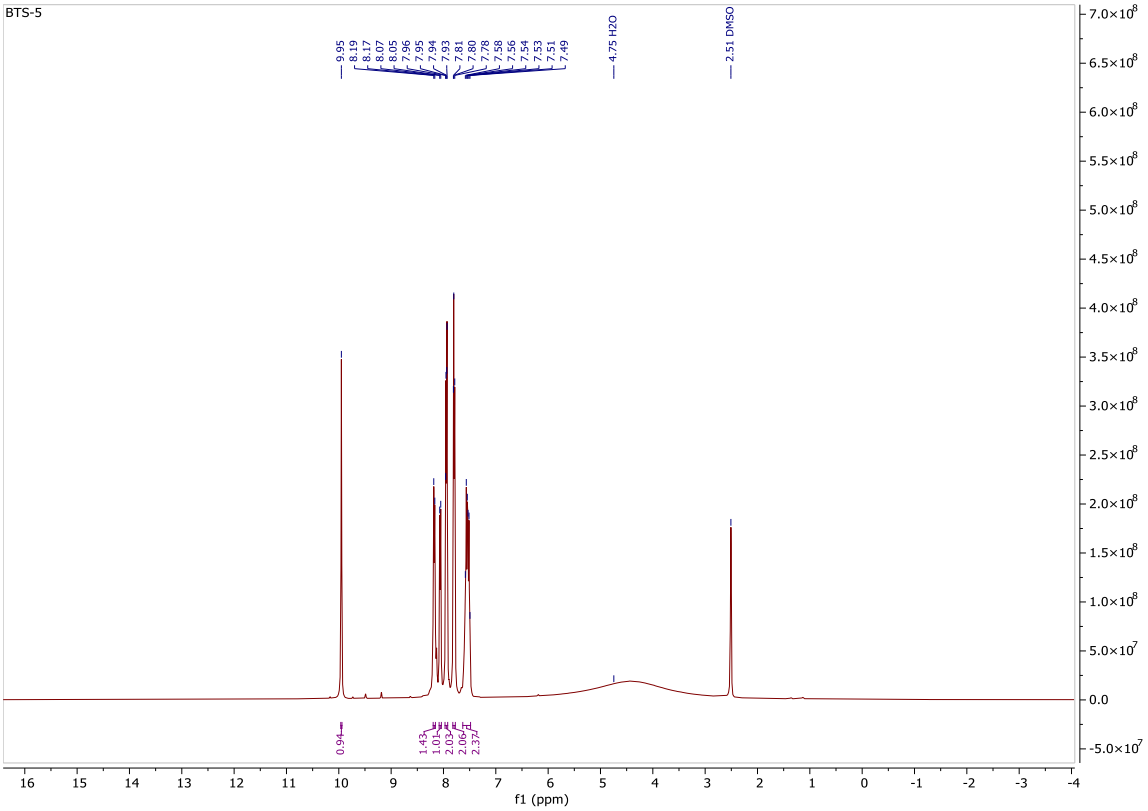

Figure 19: Representative ^{1}H NMR spectrum of compound 8d

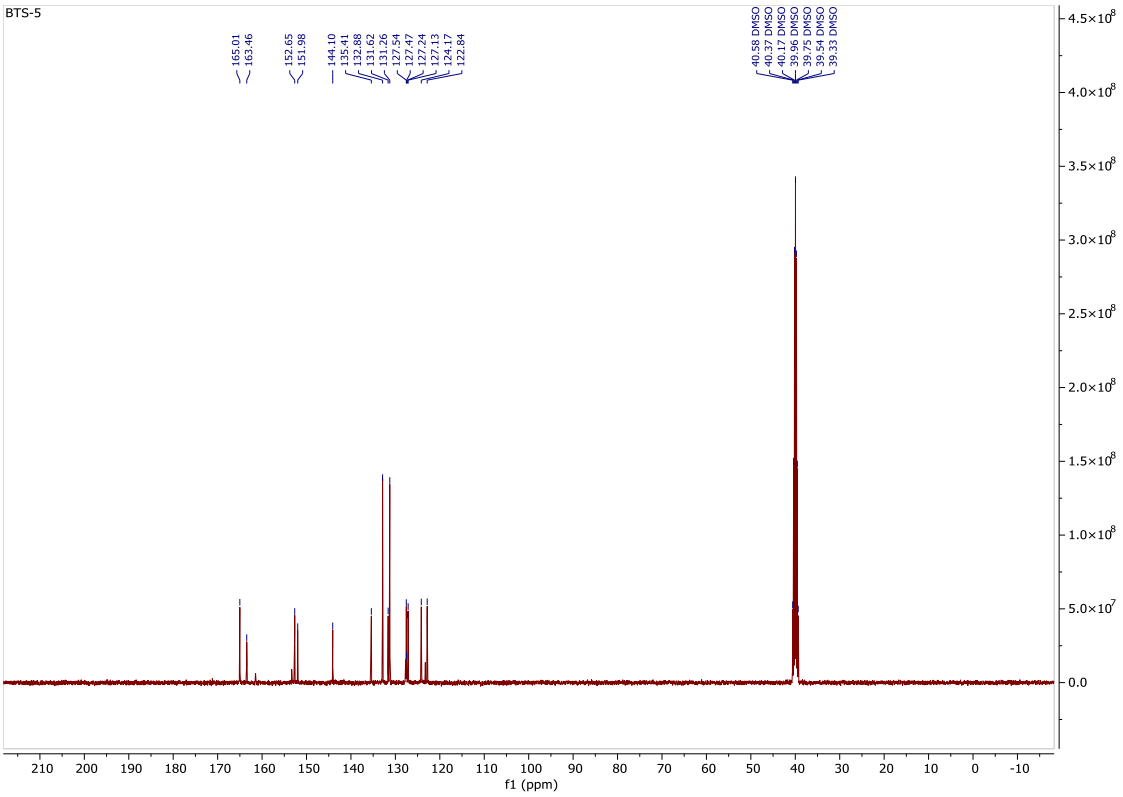

Figure 20: Representative ^{13}C NMR spectrum of compound 8d

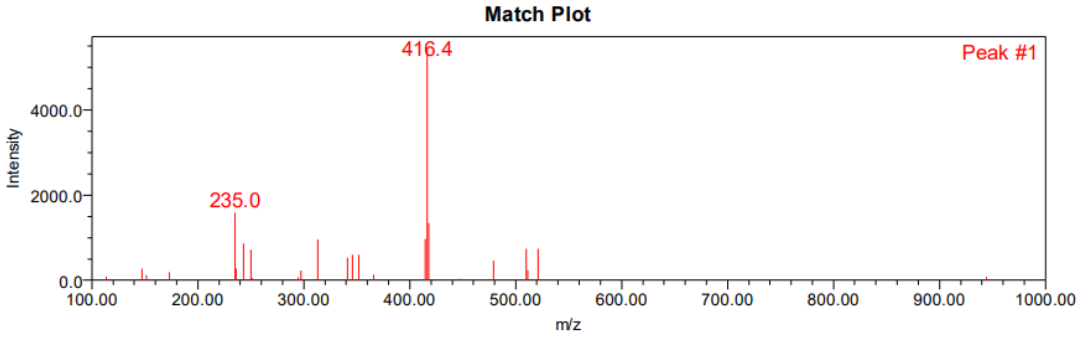

Figure 21: Representative mass spectrum of compound 8d

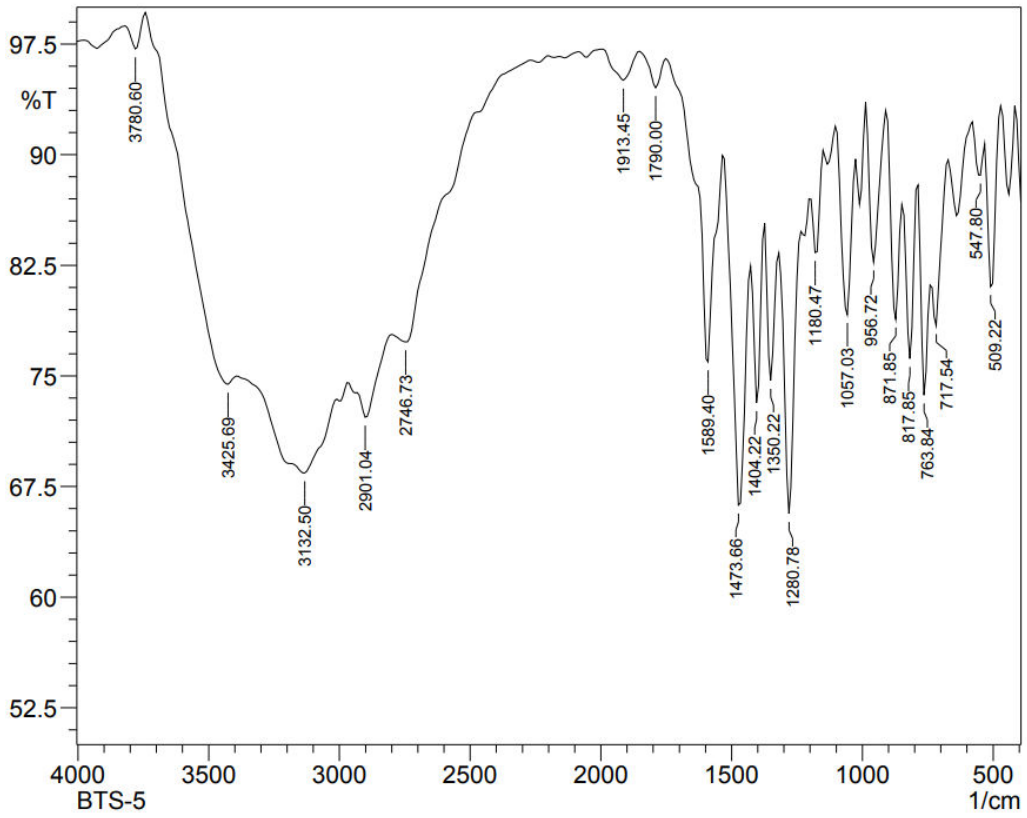

Figure 22: Representative FTIR spectrum of compound 8d

- **Spectral data of compound 8e**

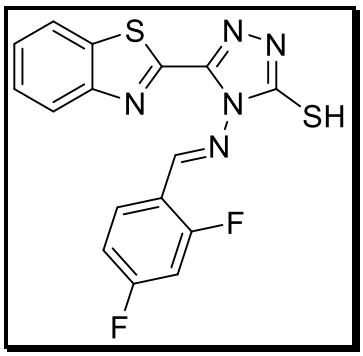

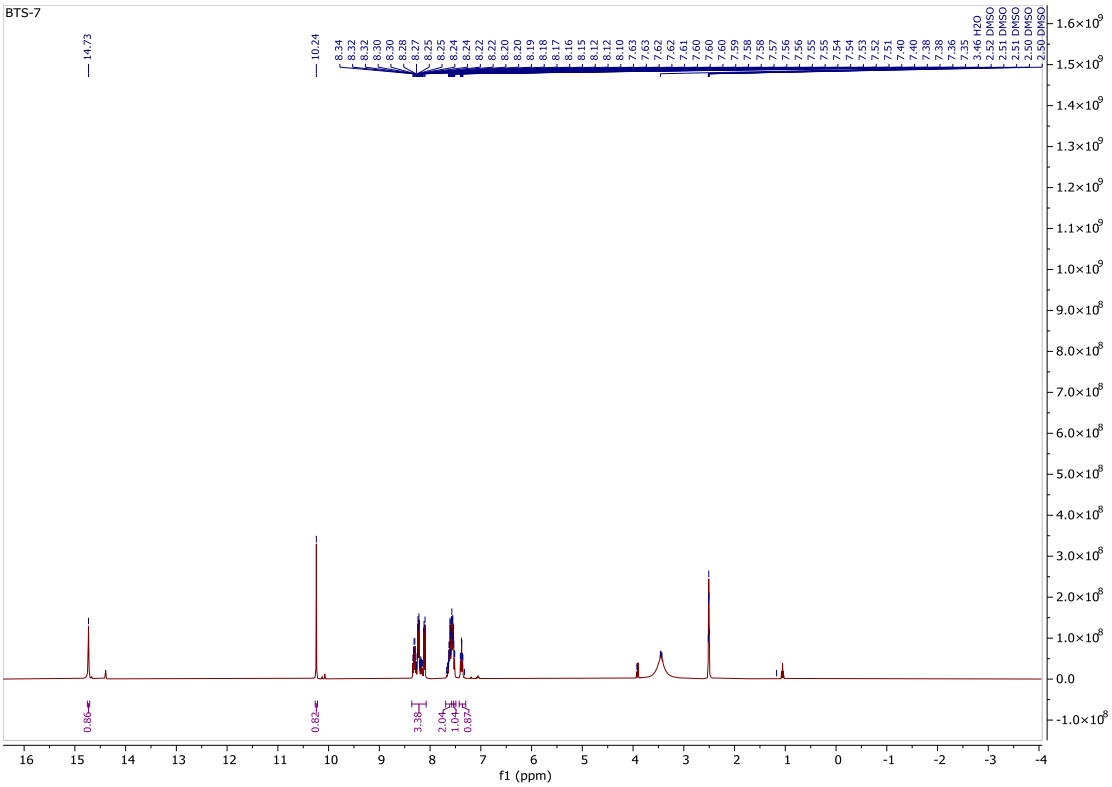

Figure 23: Representative ^{1}H NMR spectrum of compound 8e

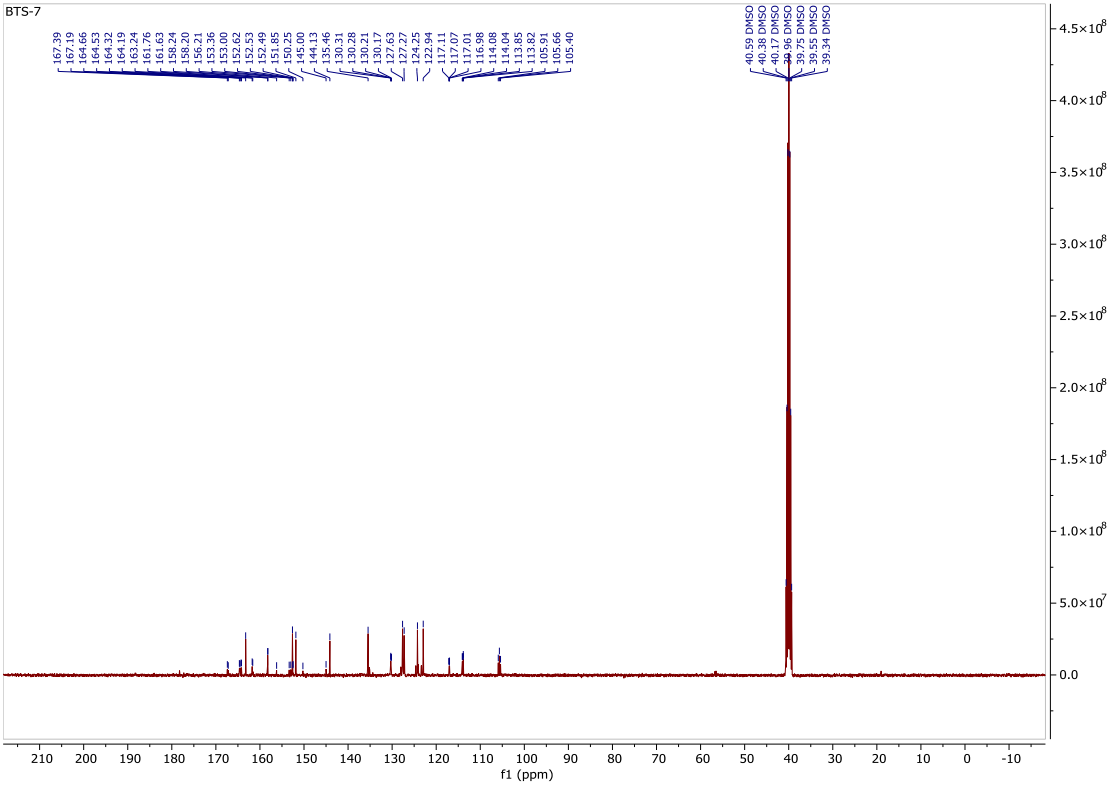

Figure 24: Representative ^{13}C NMR spectrum of compound 8e

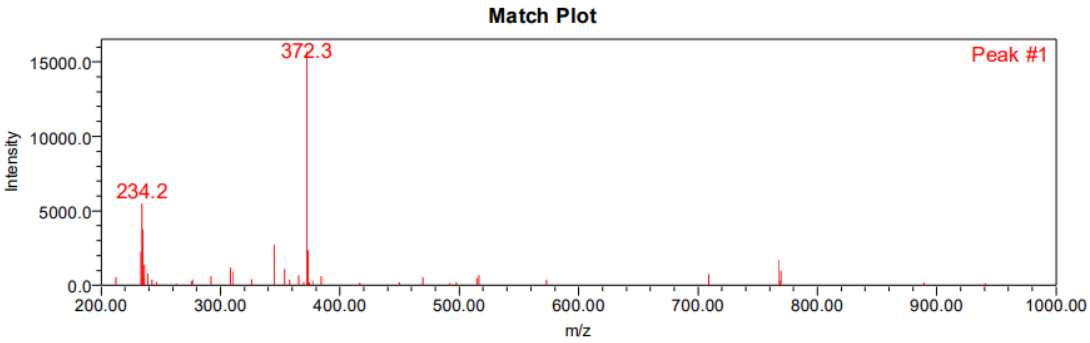

Figure 25: Representative mass spectrum of compound 8e

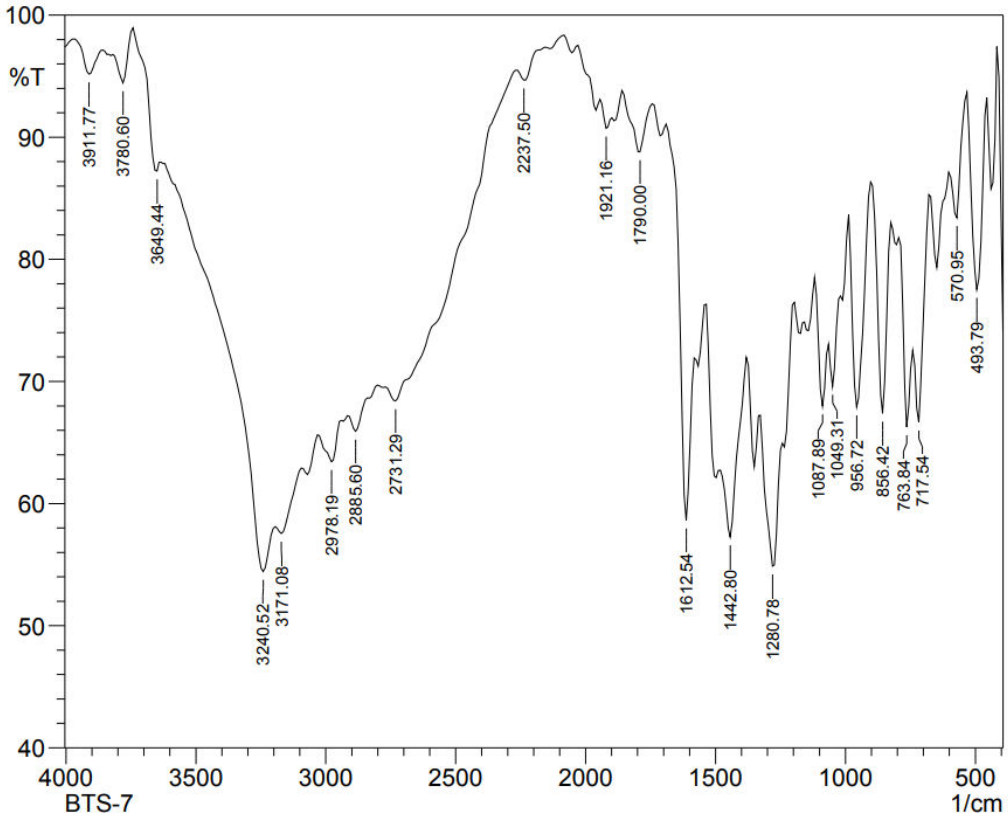

Figure 26: Representative FT-IR spectrum of compound 8e

- **Spectral data of compound 8f**

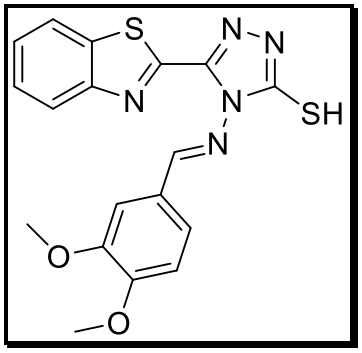

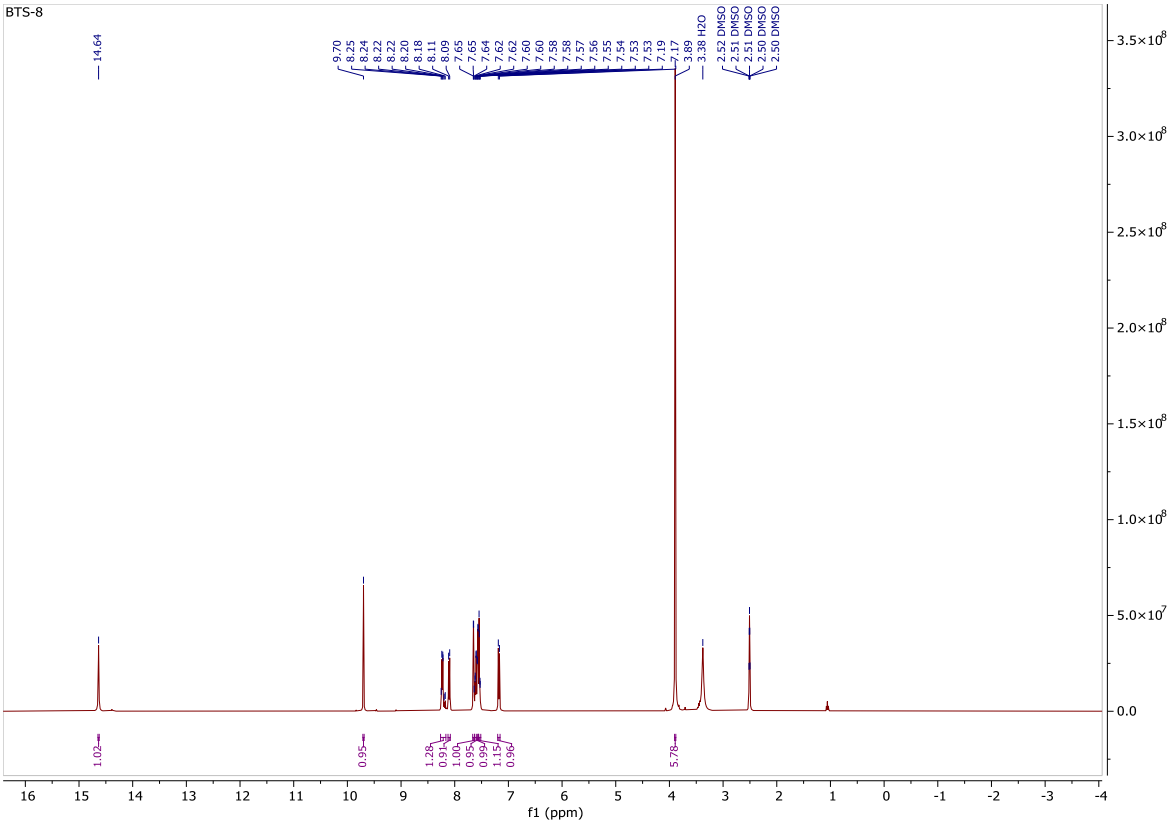

Figure 27: Representative ^{1}H NMR spectrum of compound 8f

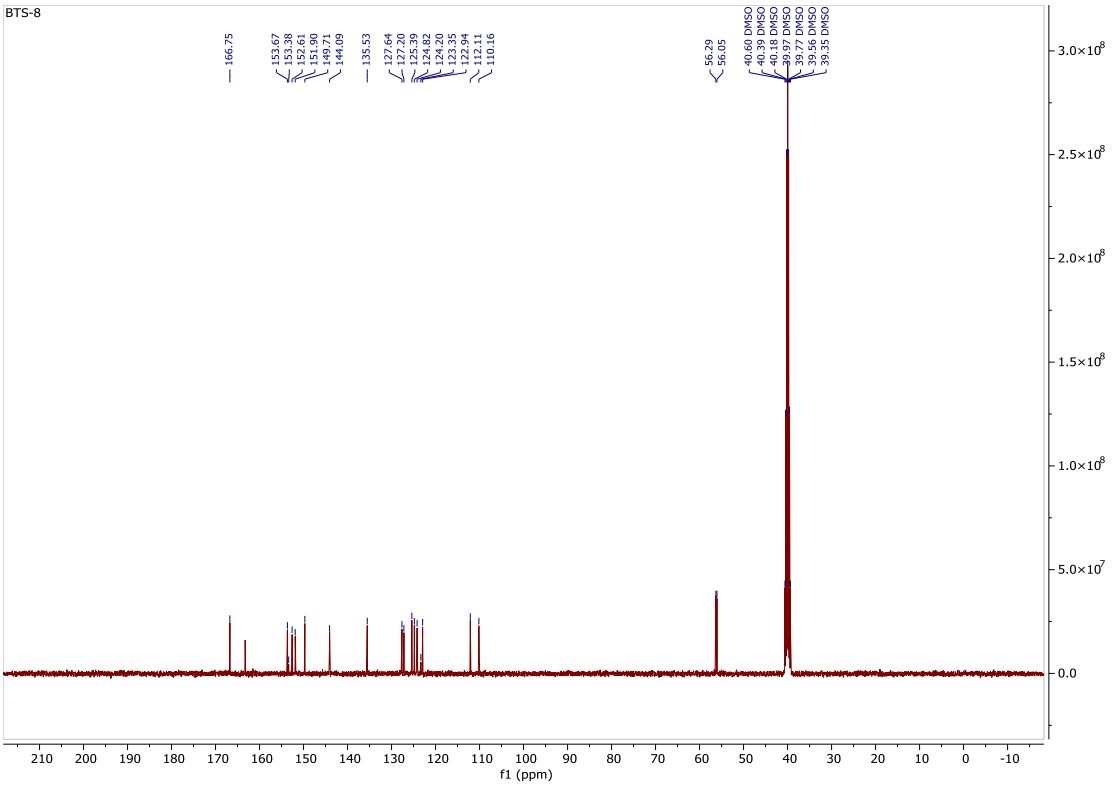

Figure 28: Representative ^{13}C NMR spectrum of compound 8f

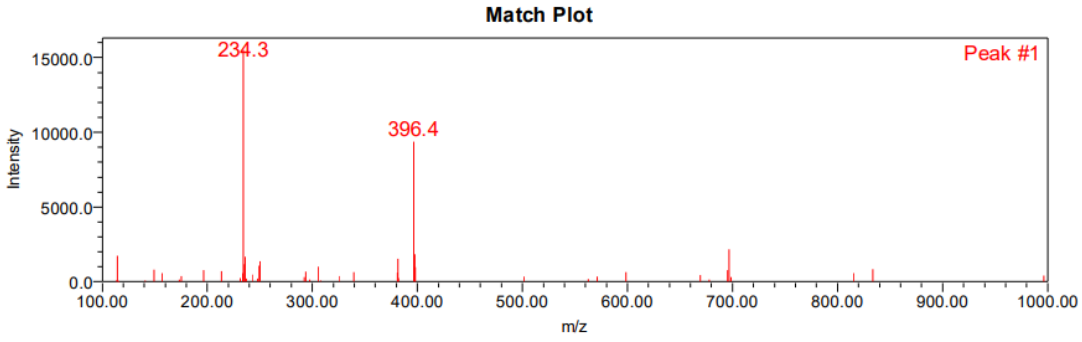

Figure 29: Representative mass spectrum of compound 8f

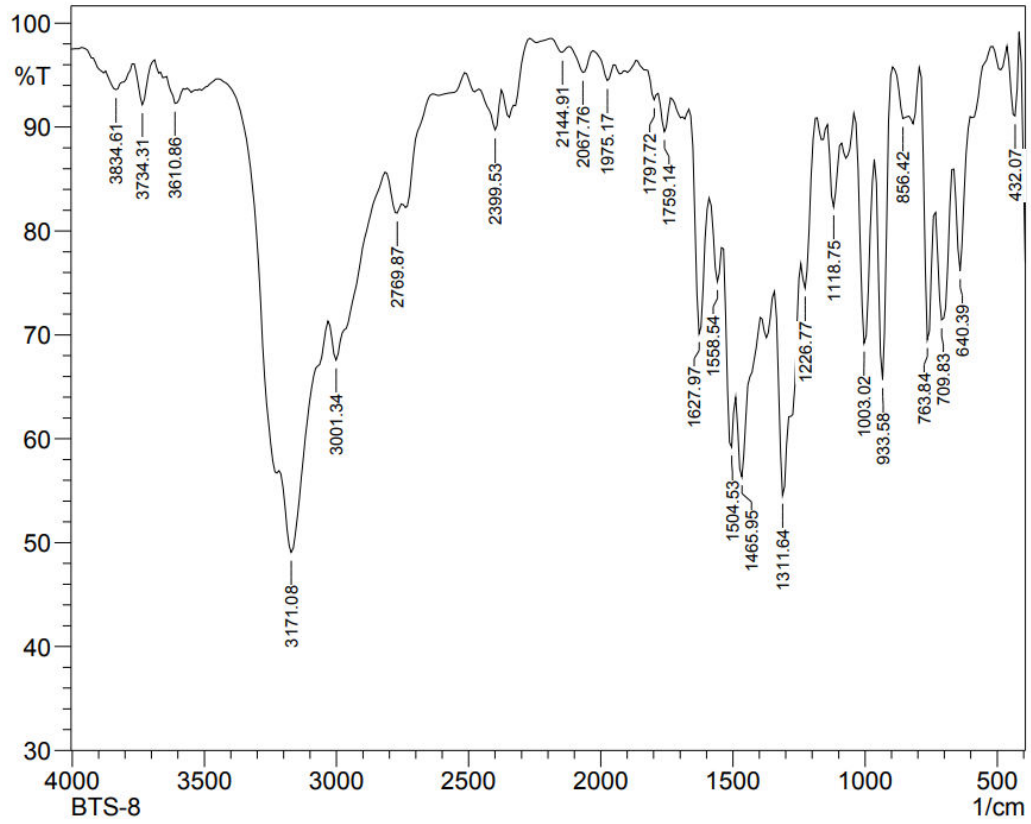

Figure 30: Representative FT-IR spectrum of compound 8f

- **Spectral data of compound 8g**

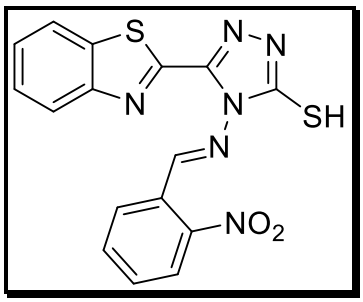

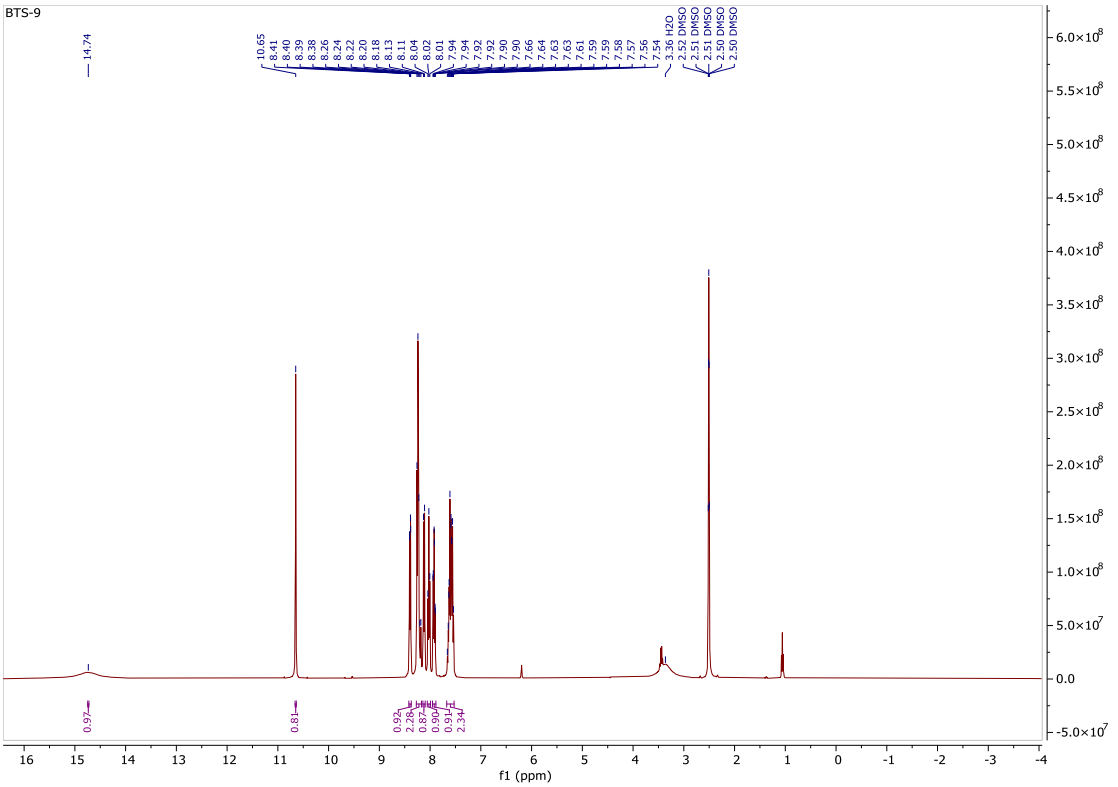

Figure 31: Representative ^{1}H NMR spectrum of compound 8g

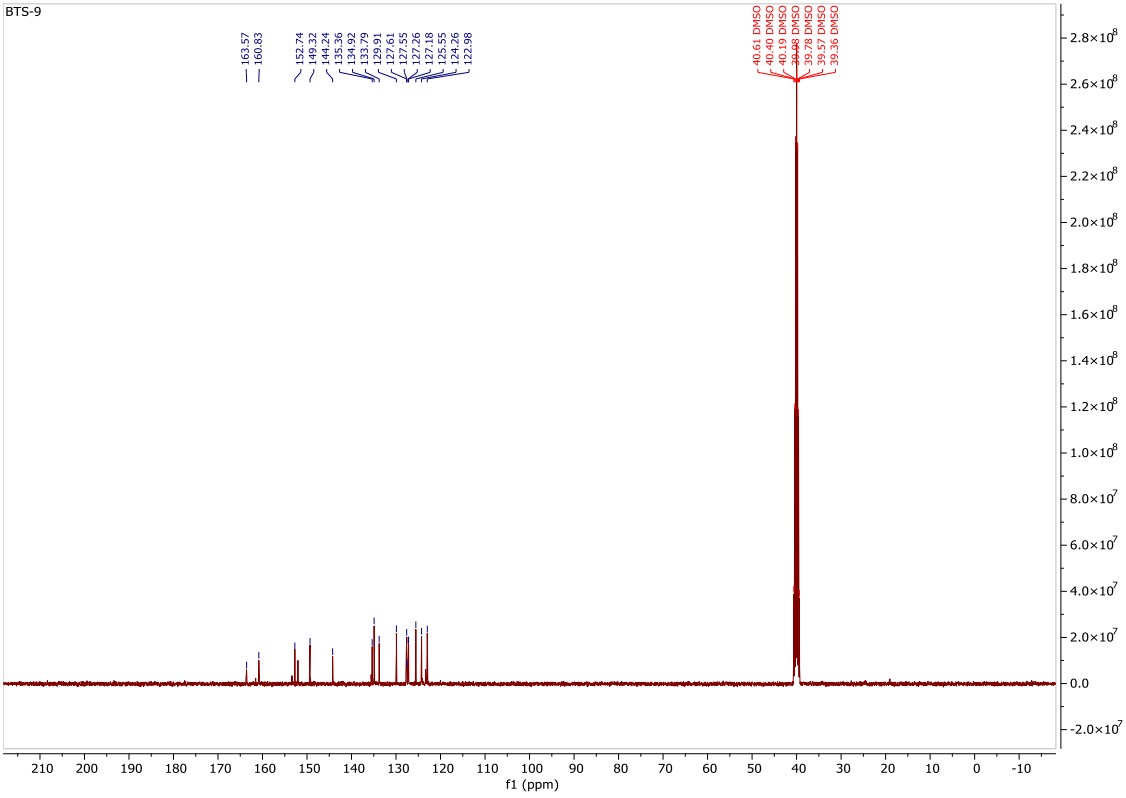

Figure 32: Representative 13C NMR spectrum of compound 8g

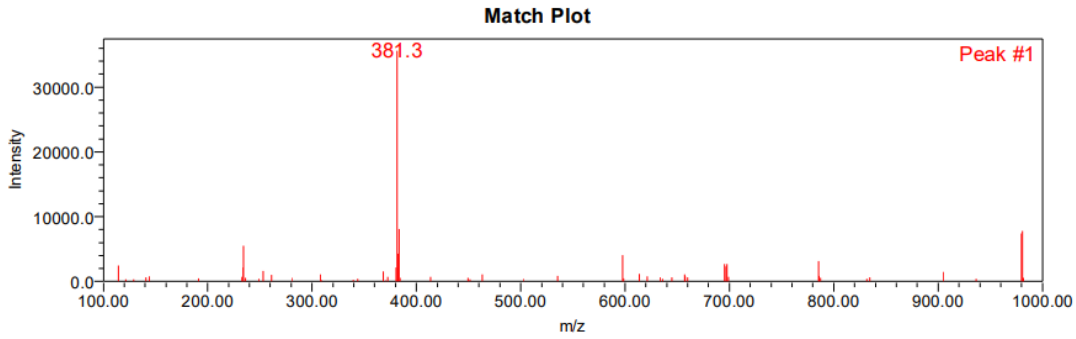

Figure 33: Representative mass spectrum of compound 8g

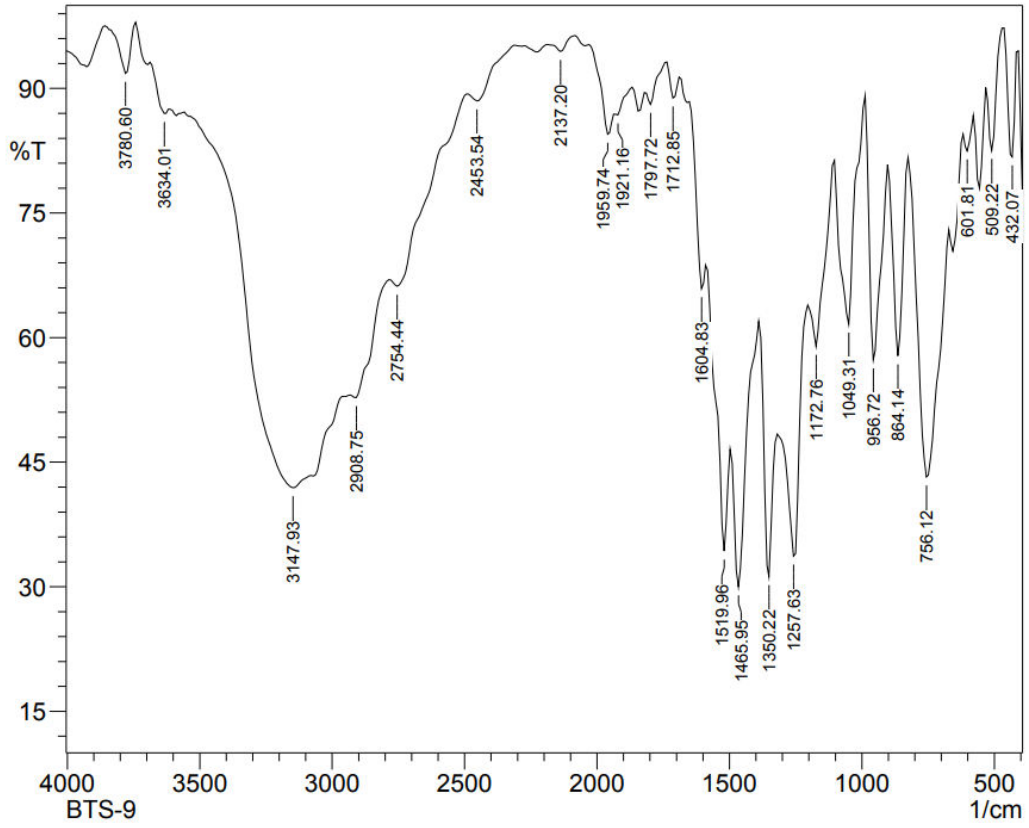

Figure 34: Representative FT-IR spectrum of compound 8g

- **Spectral data of compound 8h**

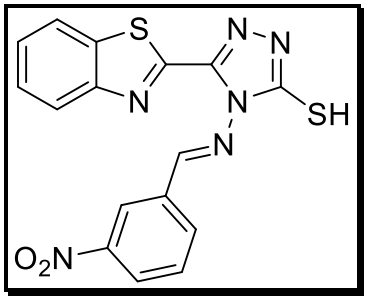

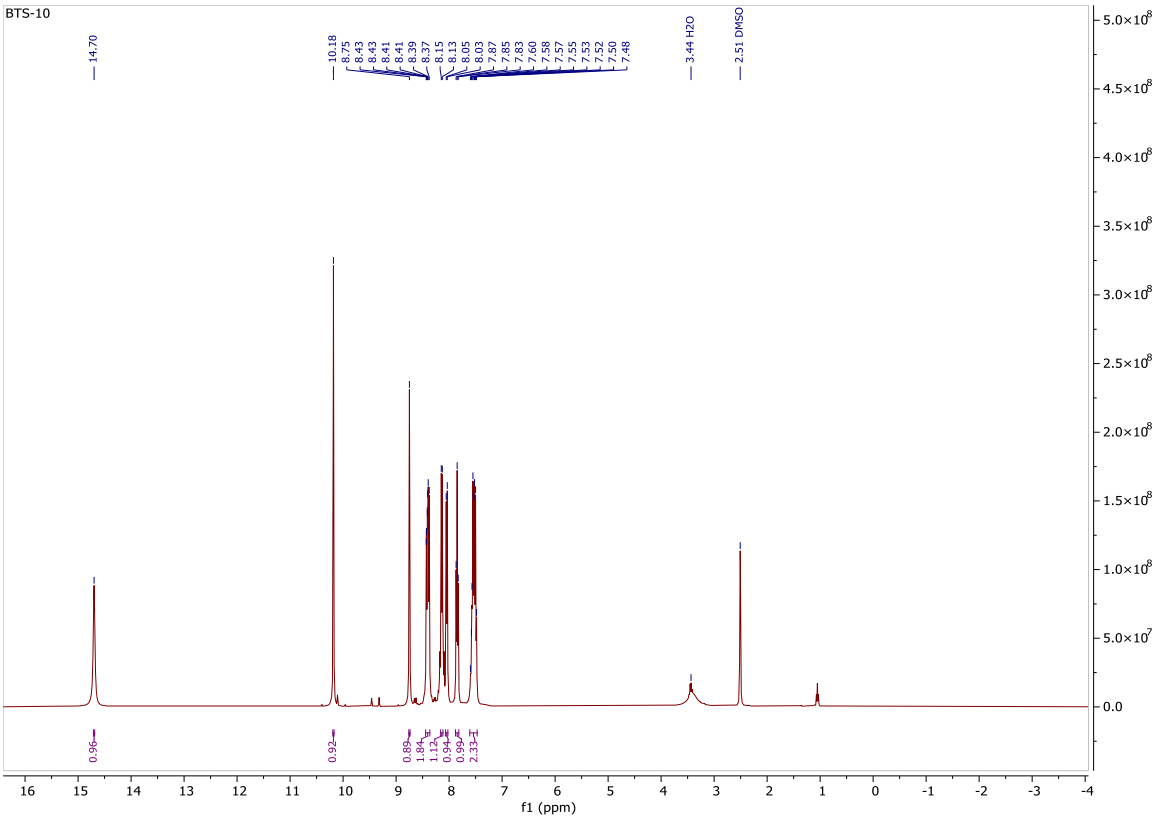

Figure 35: Representative ^{1}H NMR spectrum of compound 8h

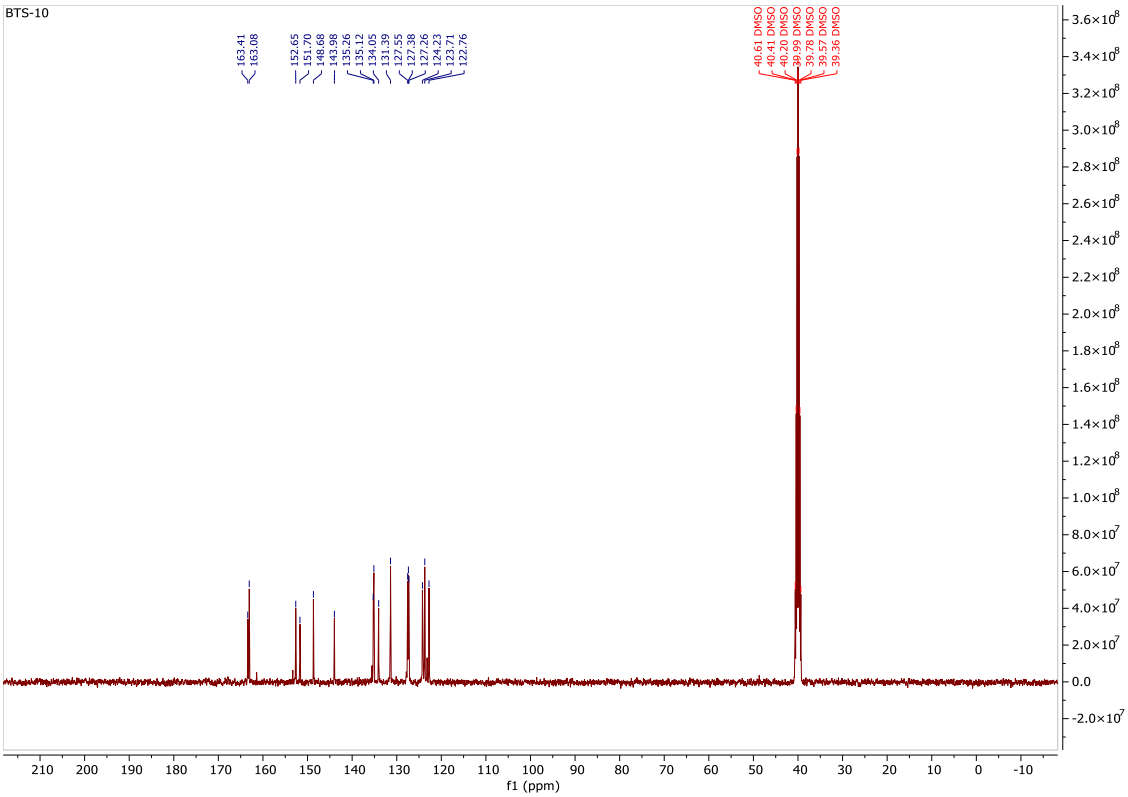

Figure 36: Representative ^{13}C NMR spectrum of compound 8h

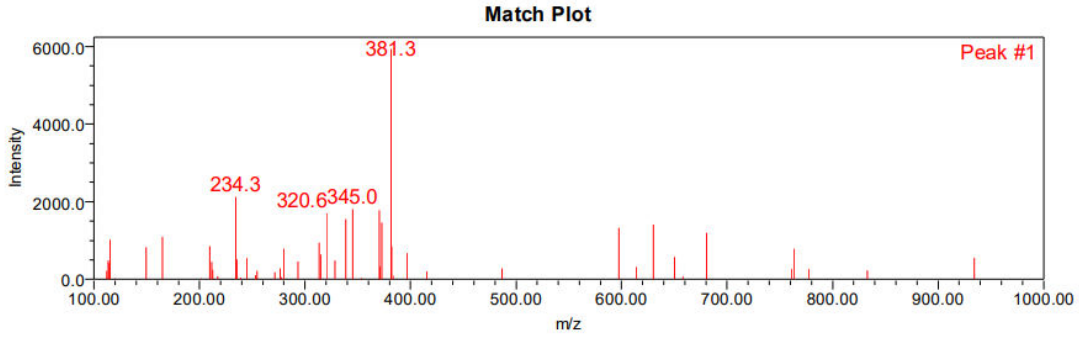

Figure 37: Representative mass spectrum of compound 8h

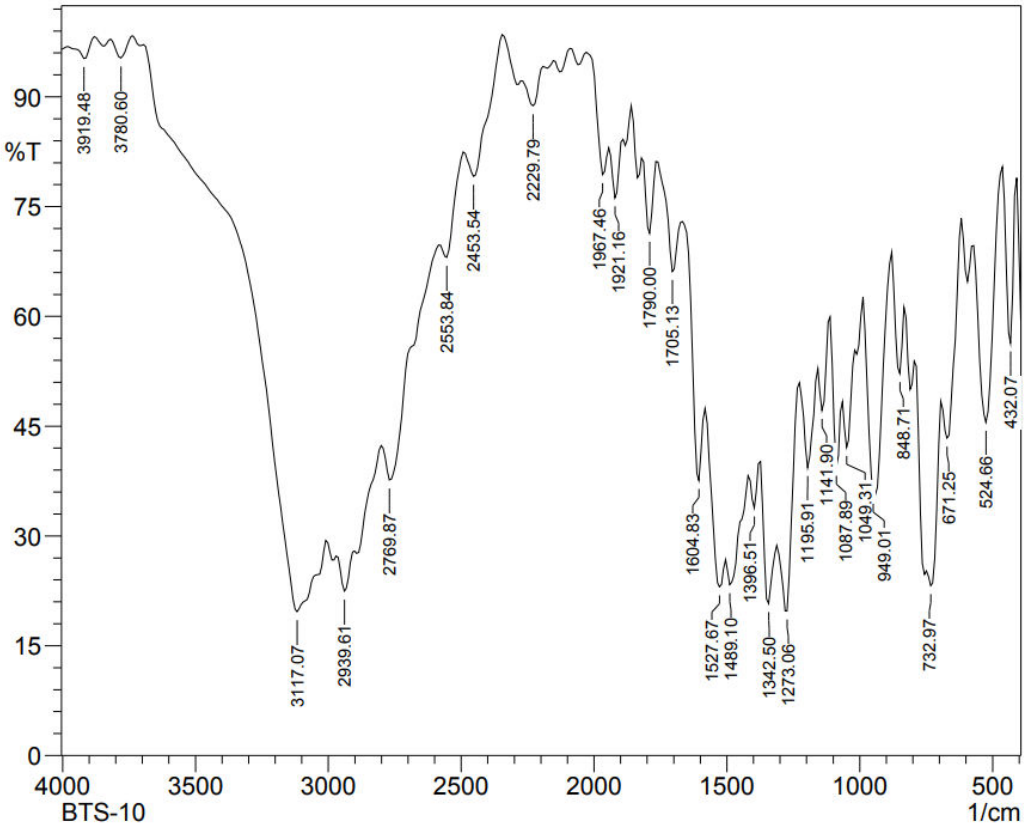

Figure 38: Representative FT-IR spectrum of compound 8h

- **Spectral data of compound 8i**

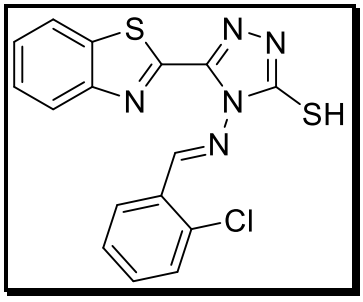

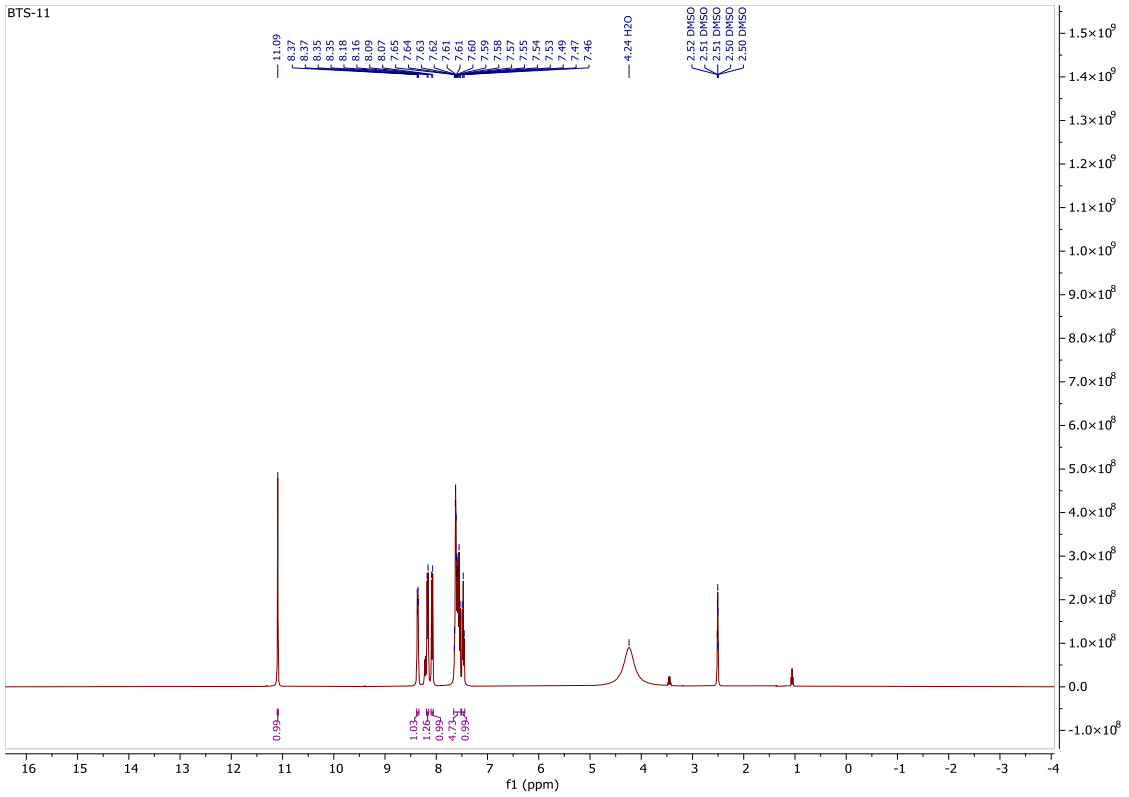

Figure 39: Representative ^{1}H NMR spectrum of compound 8i

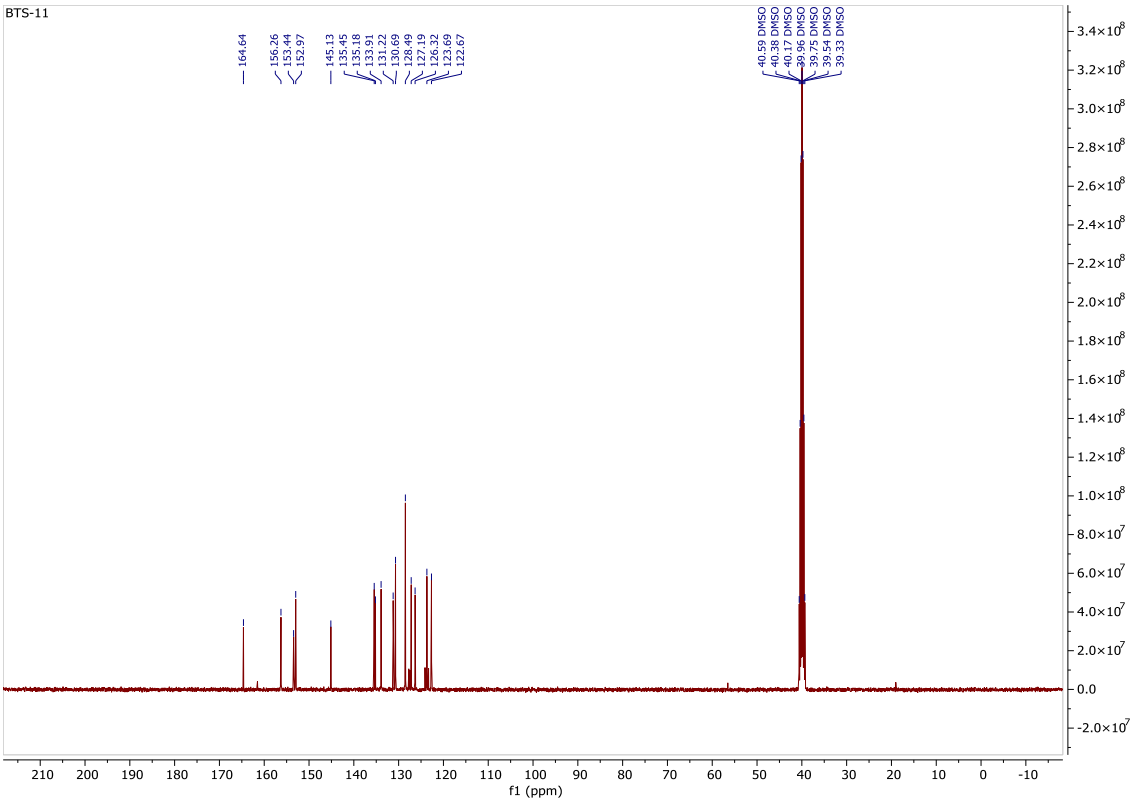

Figure 40: Representative ^{13}C NMR spectrum of compound 8i

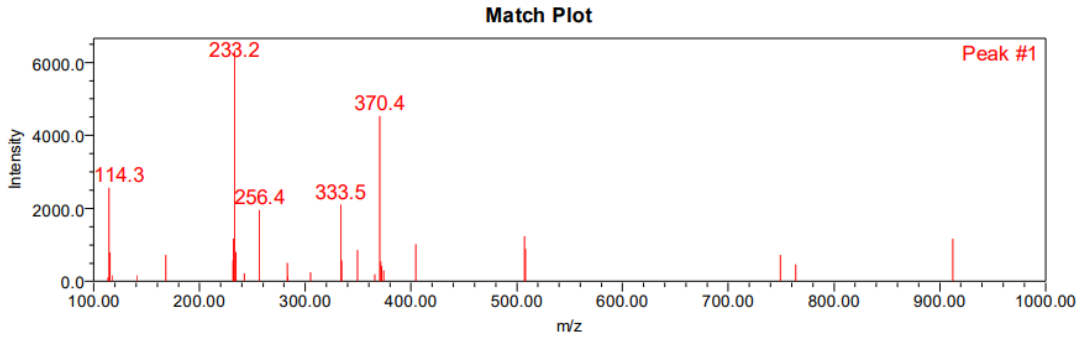

Figure 41: Representative mass spectrum of compound 8i

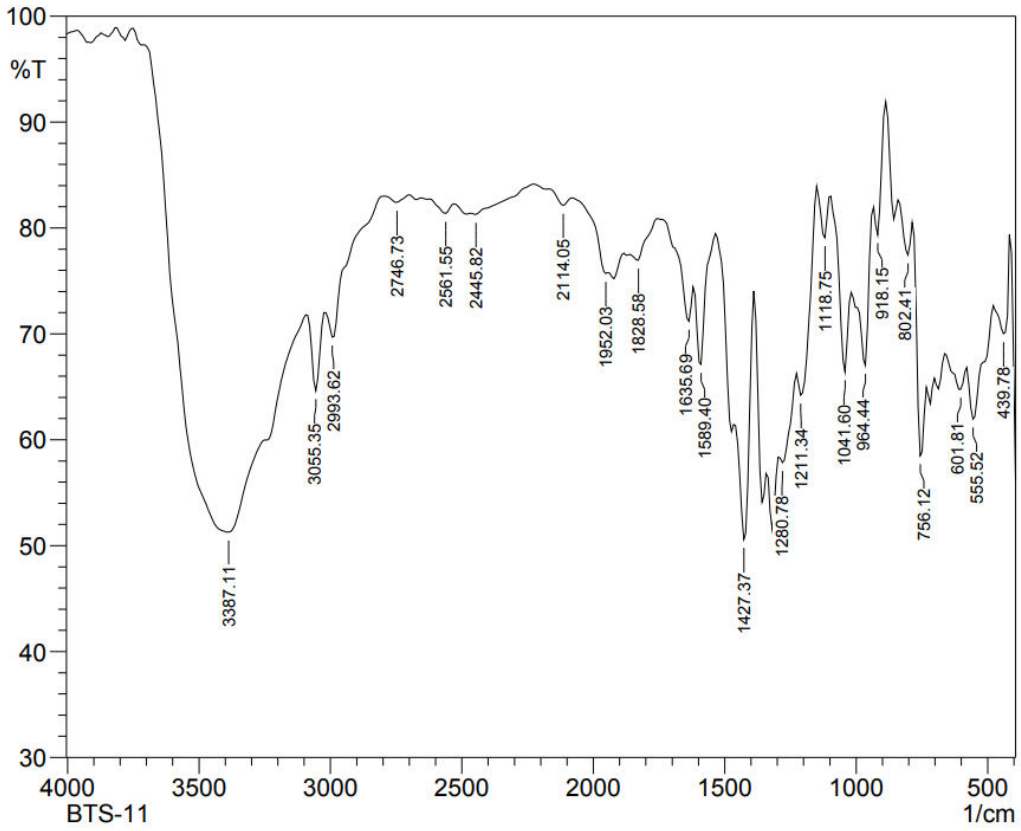

Figure 42: Representative FT-IR spectrum of compound 8i

- **Spectral data of compound 8j**

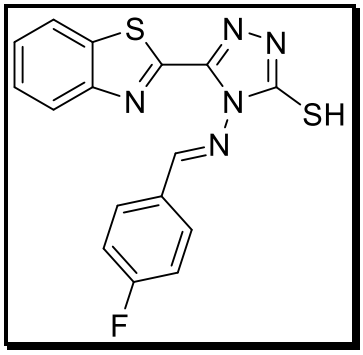

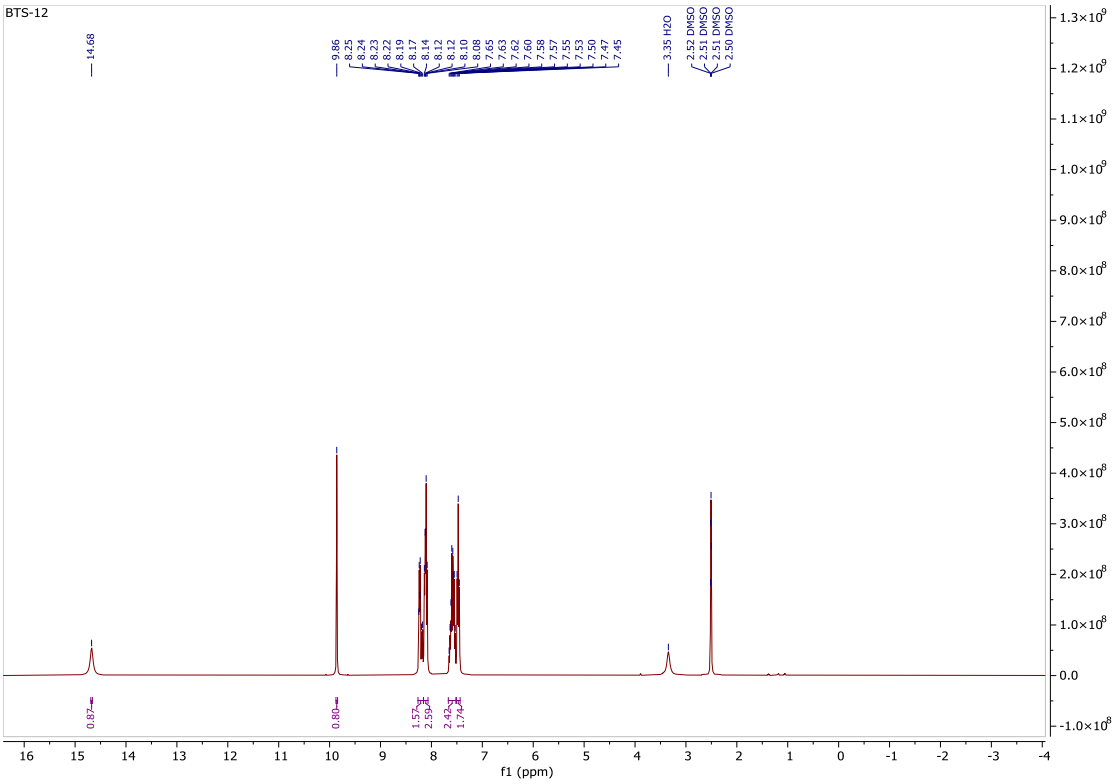

Figure 43: Representative ^{1}H NMR spectrum of compound 8j

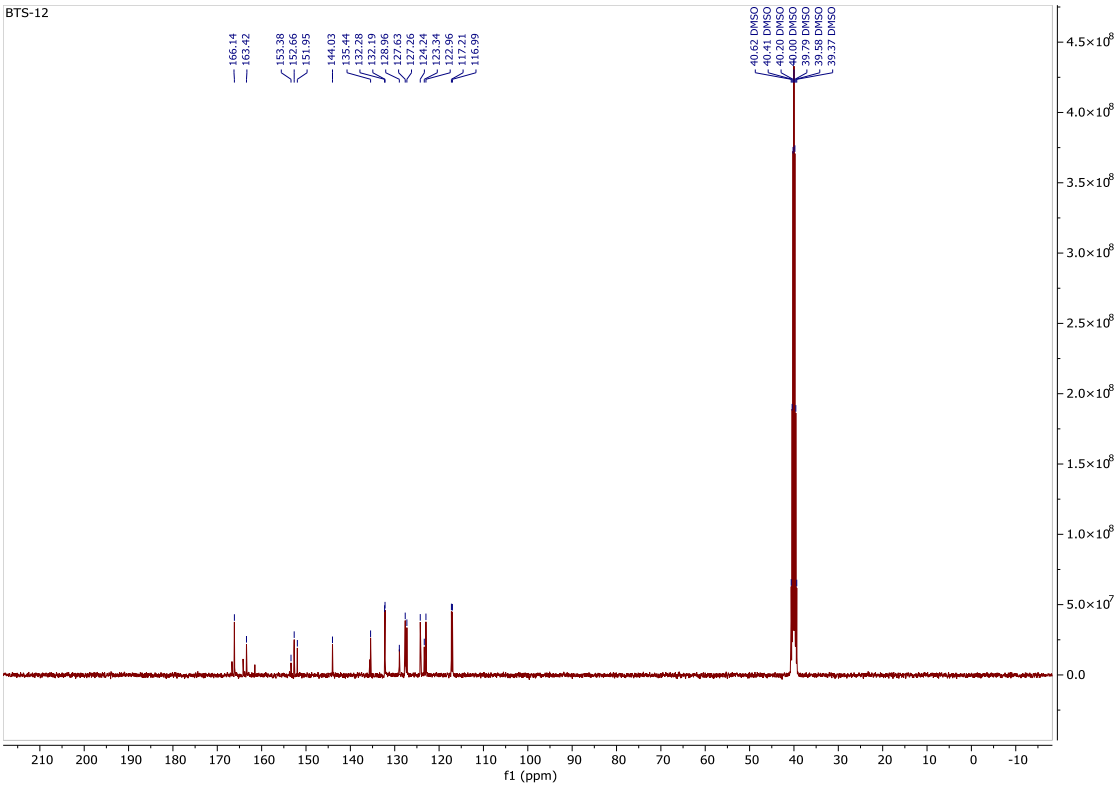

Figure 44: Representative ^{13}C NMR spectrum of compound 8j

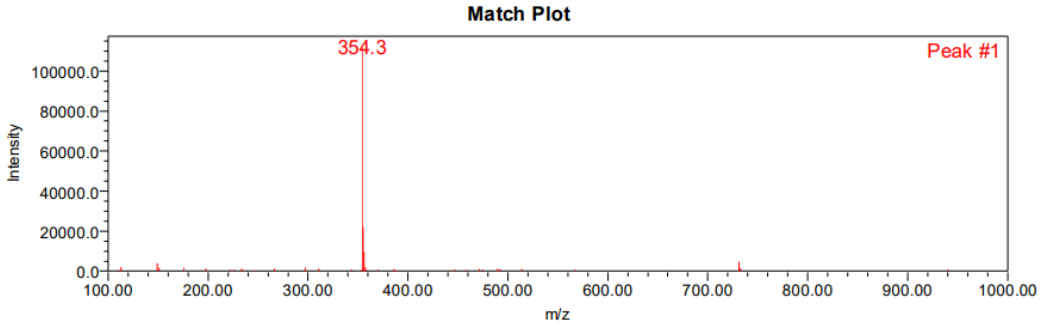

Figure 45: Representative mass spectrum of compound 8j

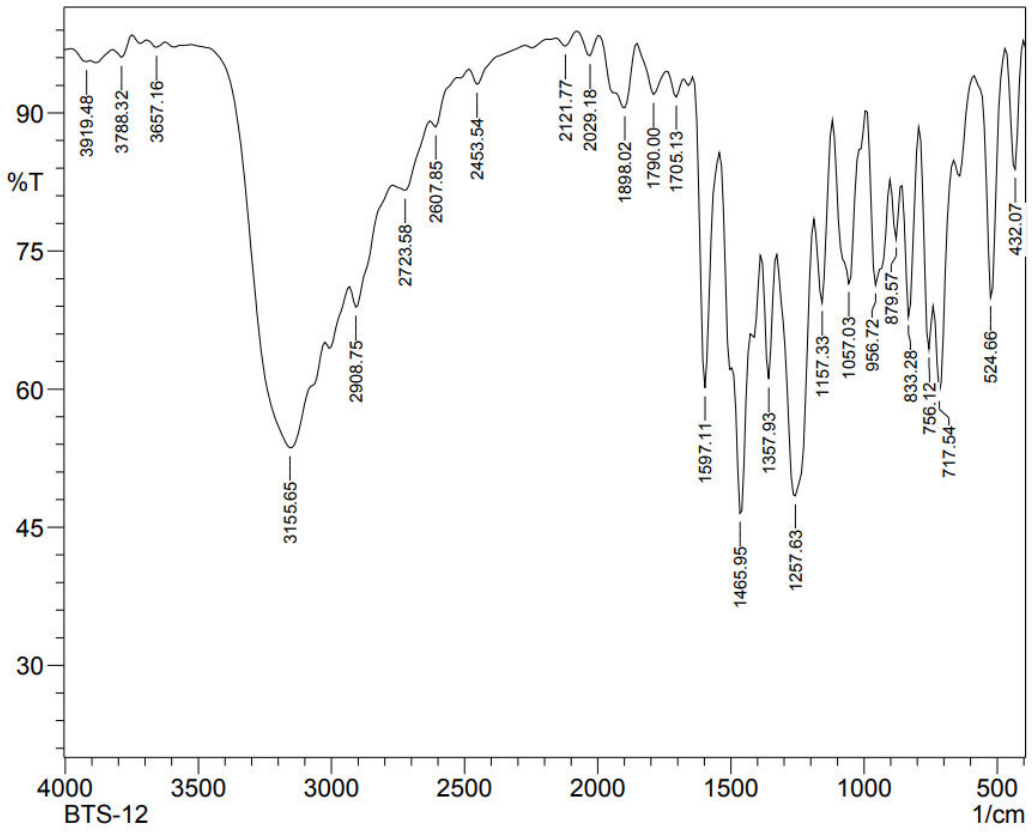

Figure 46: Representative FT-IR spectrum of compound 8j

- **Spectral data of compound 8k**

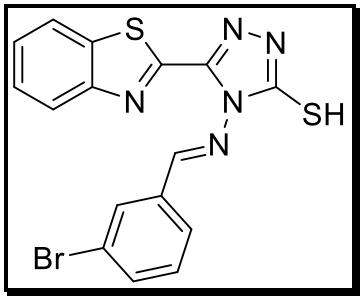

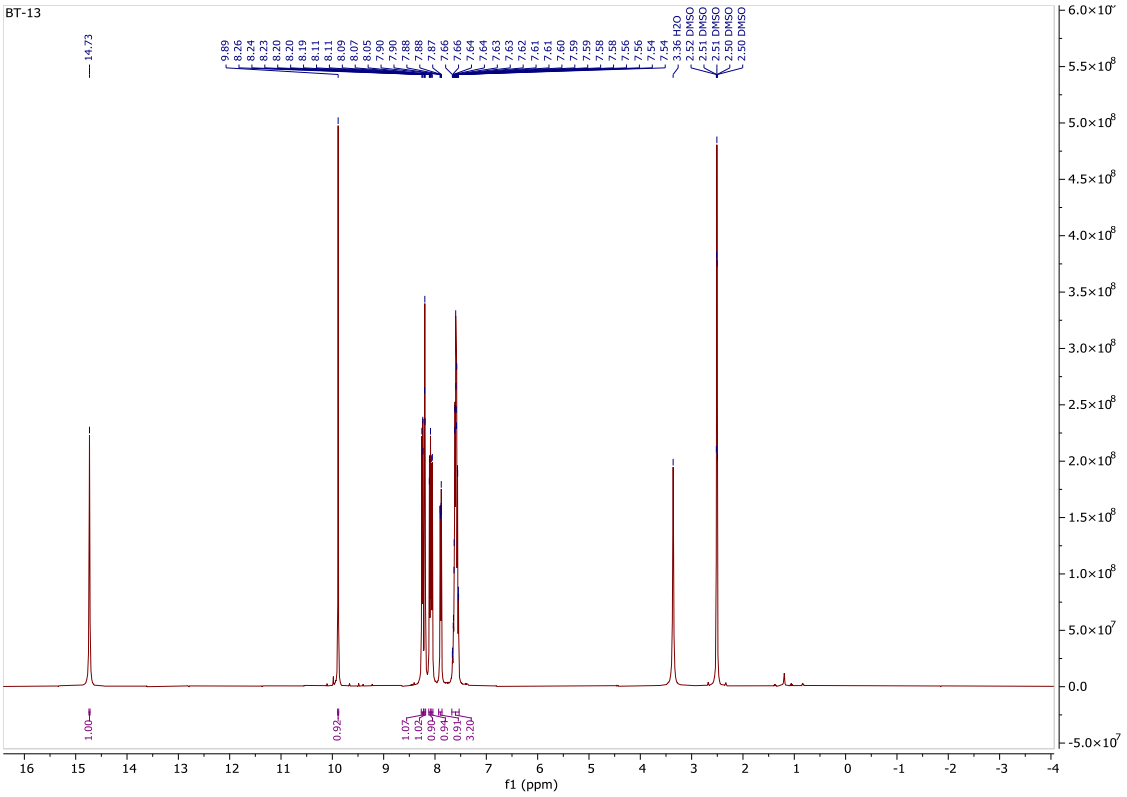

Figure 47: Representative ^{1}H NMR spectrum of compound 8k

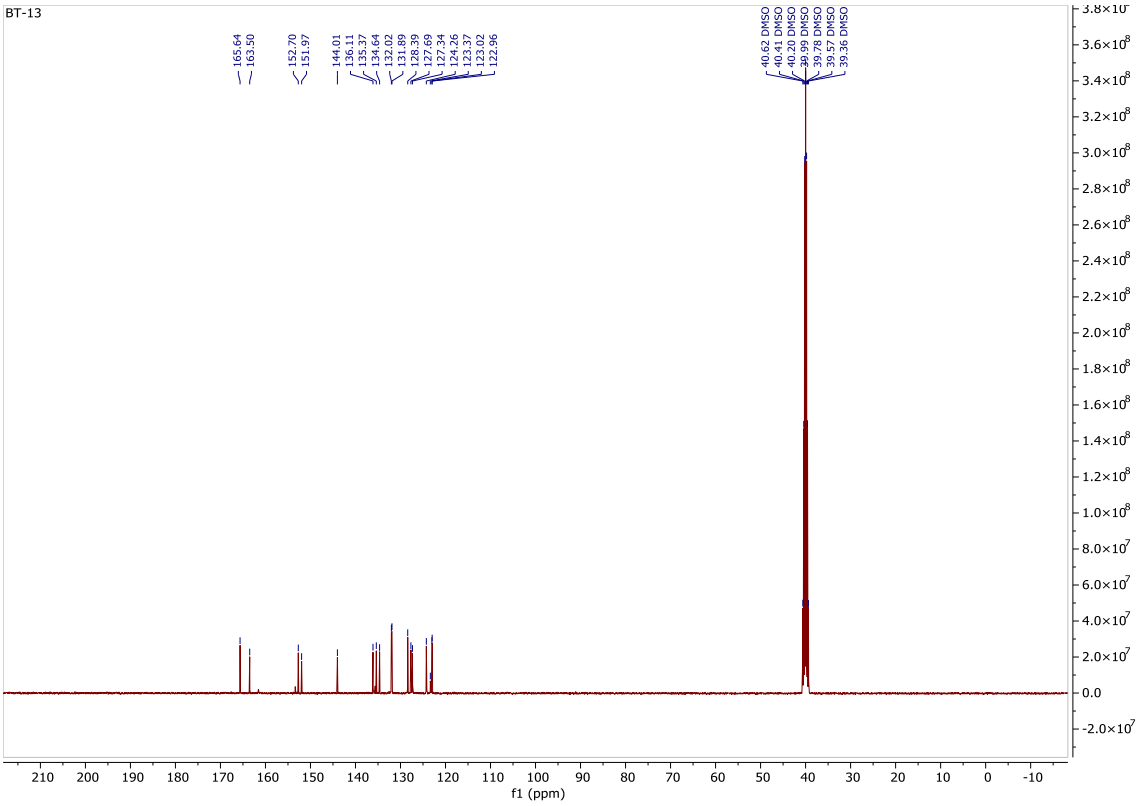

Figure 48: Representative ^{13}C NMR spectrum of compound 8k

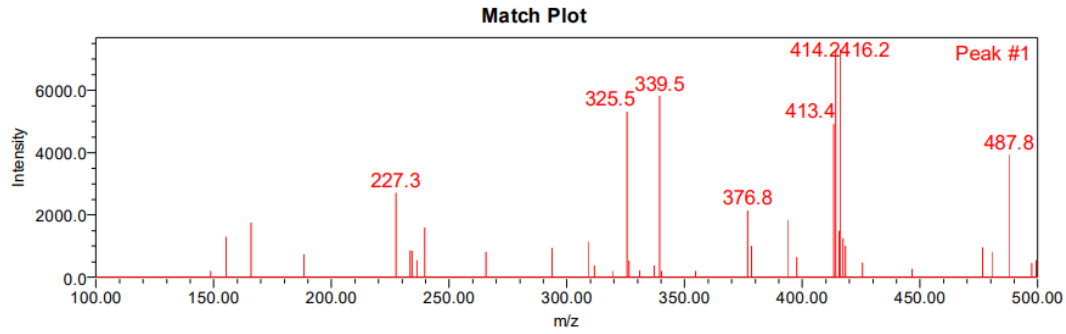

Figure 49: Representative mass spectrum of compound 8k

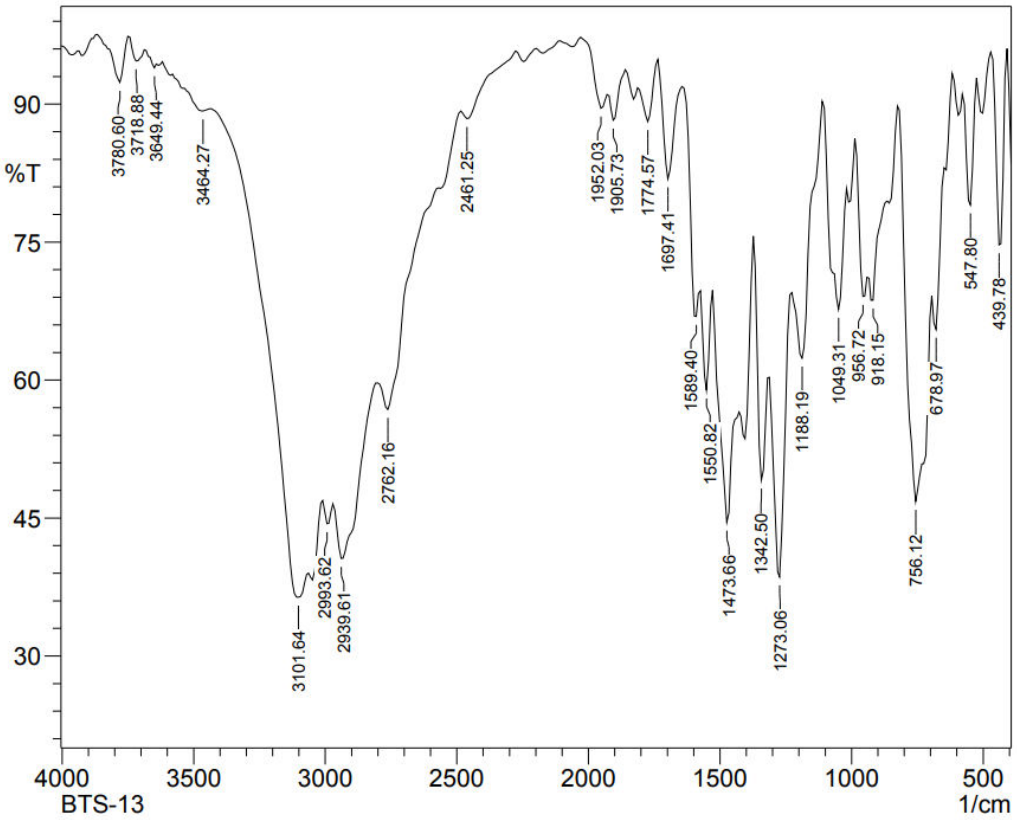

Figure 50: Representative FT-IR spectrum of compound 8k

- **Spectral data of compound 8l**

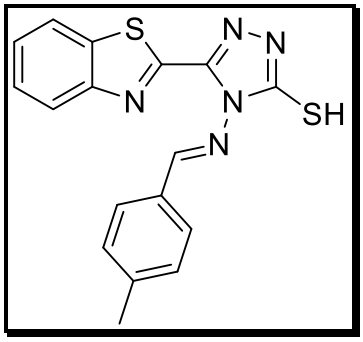

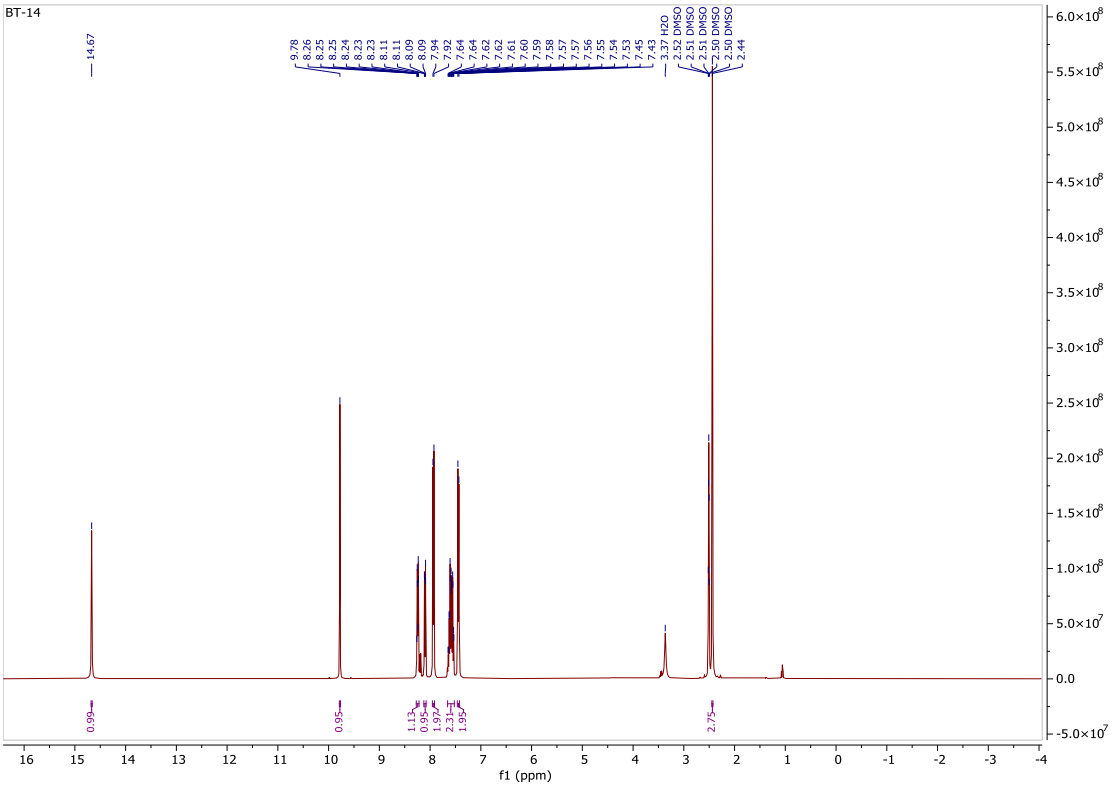

Figure 51: Representative ^{1}H NMR spectrum of compound 8l

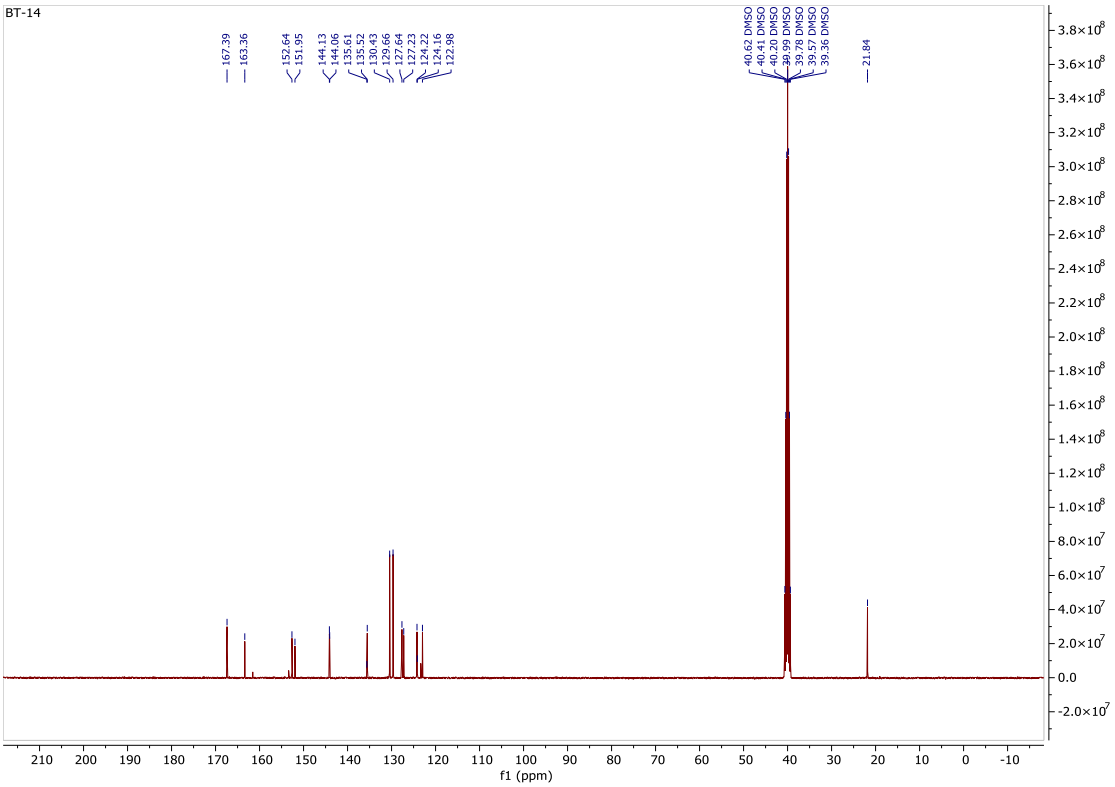

Figure 52: Representative ^{13}C NMR spectrum of compound 8l

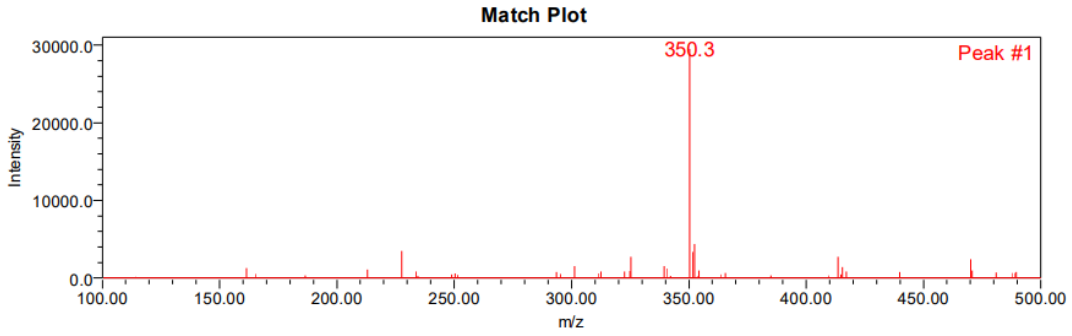

Figure 53: Representative mass spectrum of compound 8l

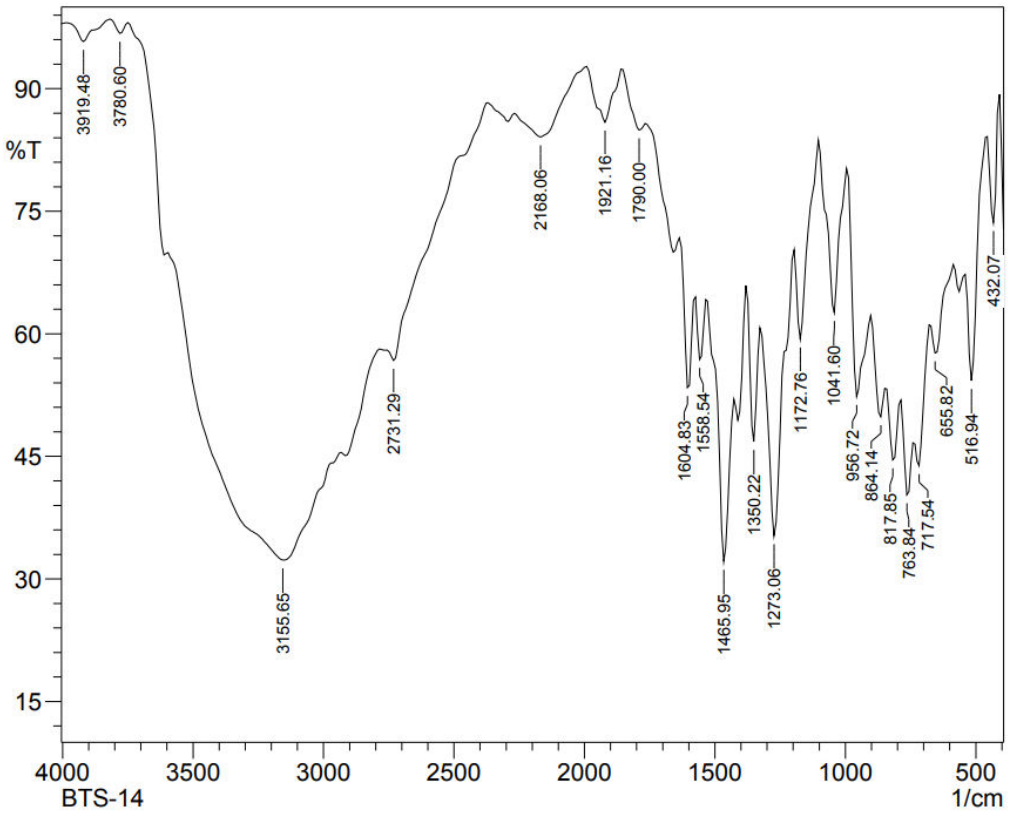

Figure 54: Representative FT-IR spectrum of compound 8l

- **Spectral data of compound 8m**

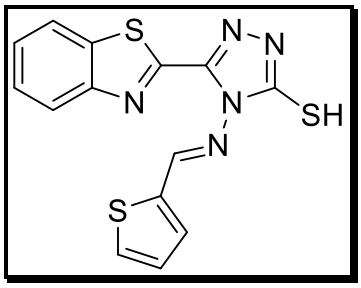

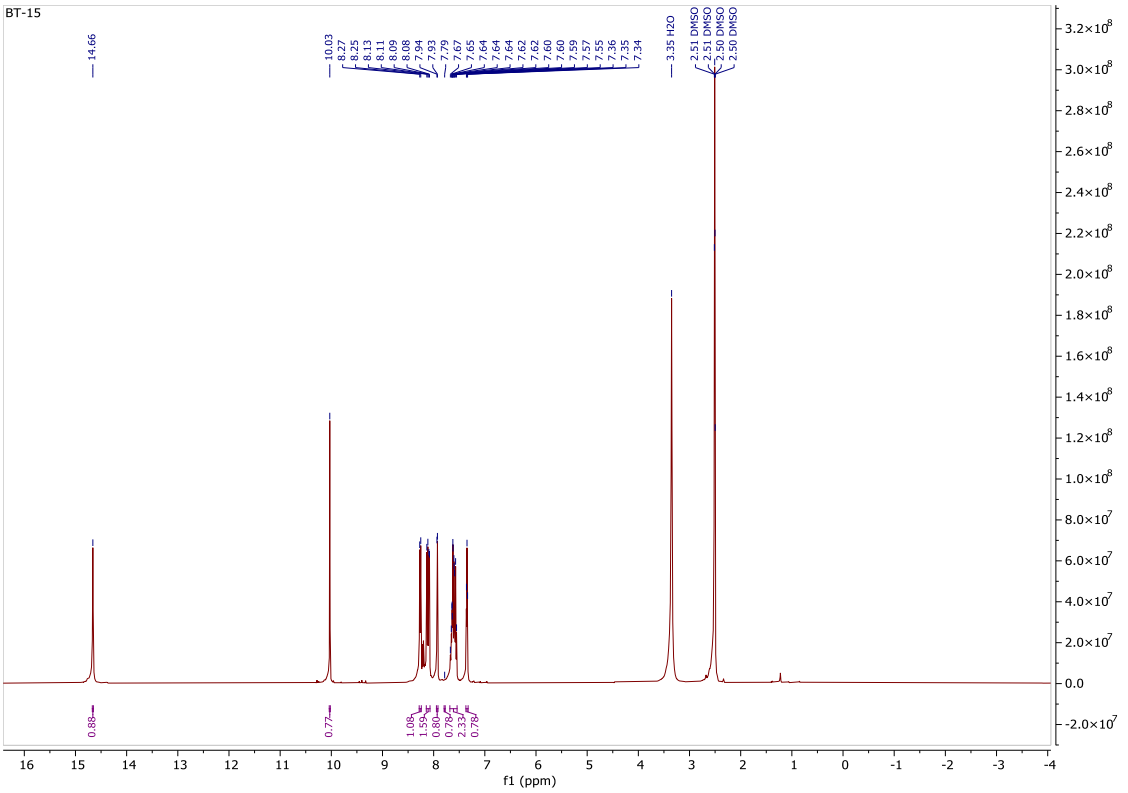

Figure 55: Representative ^{1}H NMR spectrum of compound 8m

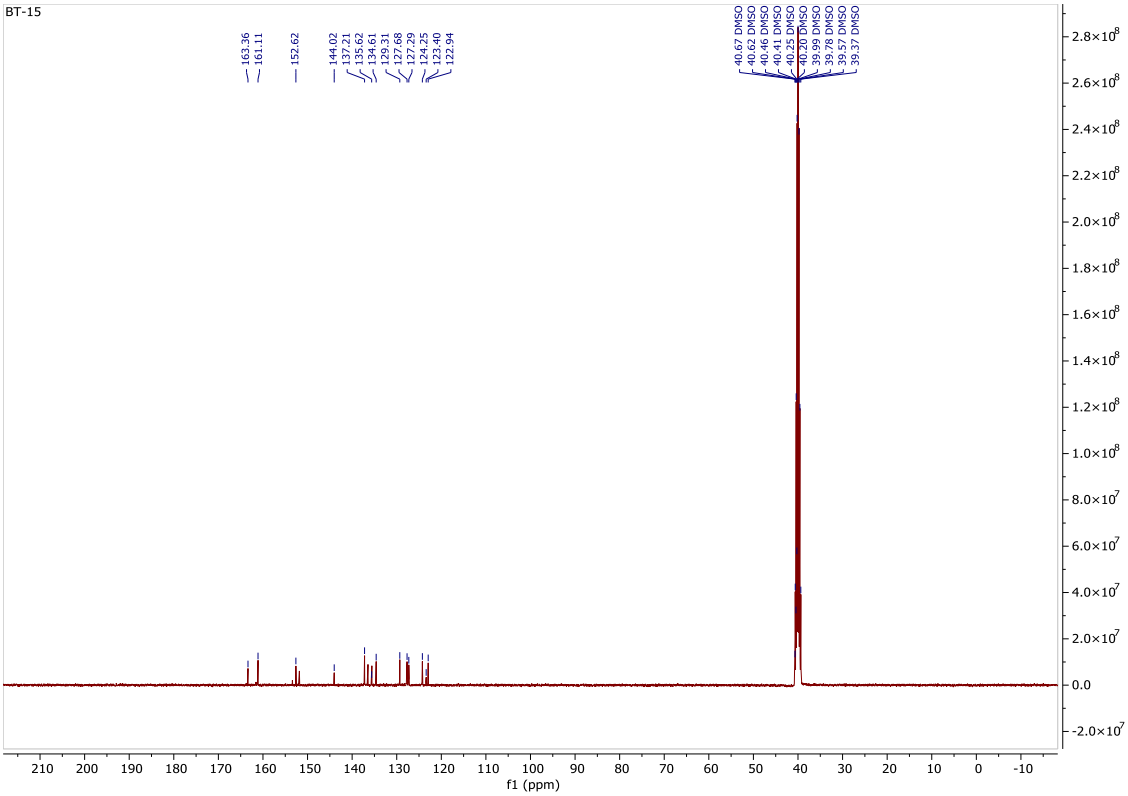

Figure 56: Representative ^{13}C NMR spectrum of compound 8m

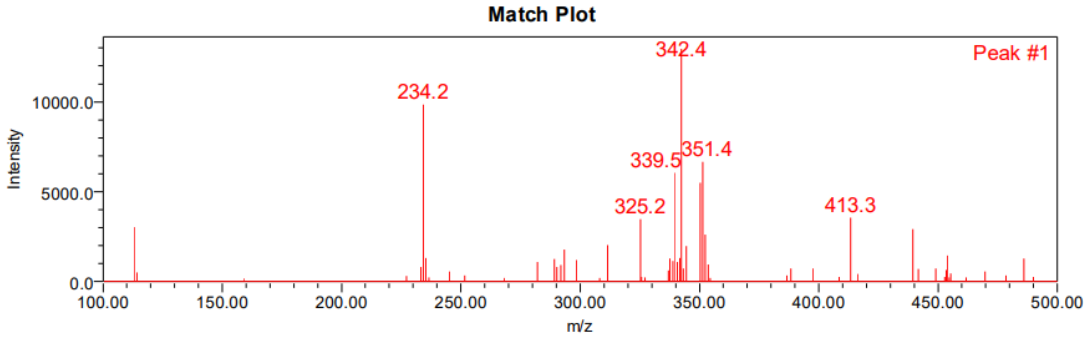

Figure 57: Representative mass spectrum of compound 8m

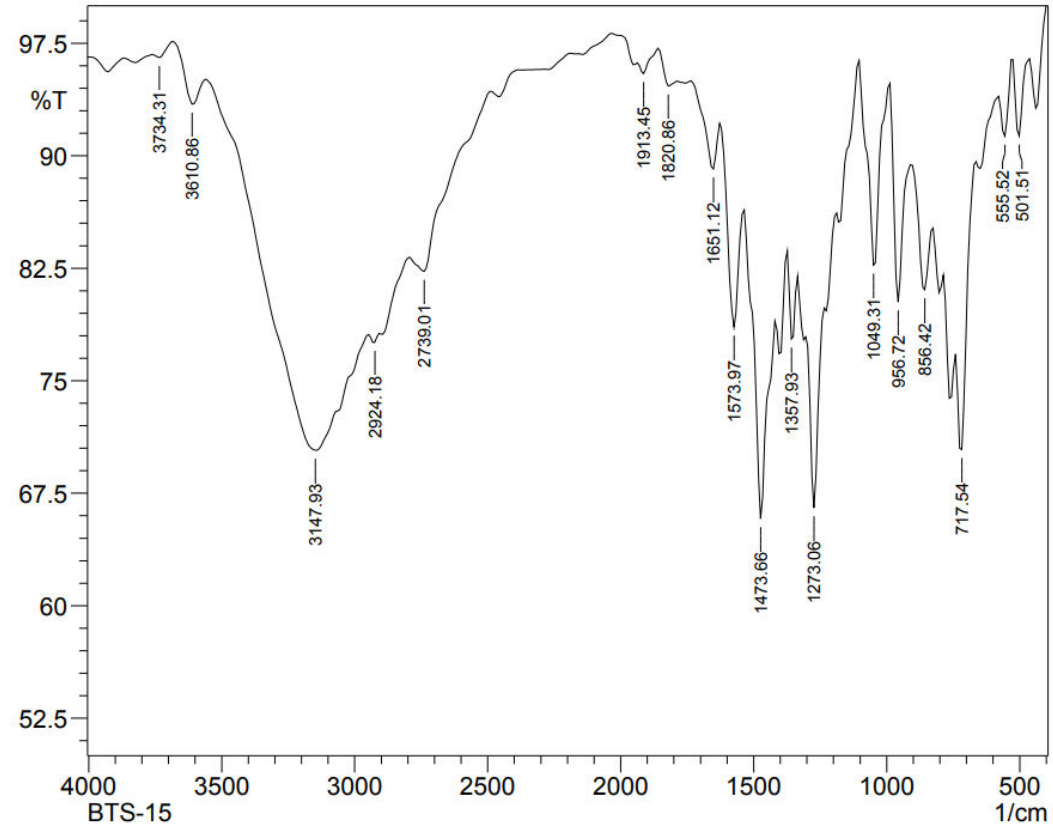

Figure 58: Representative FT-IR spectrum of compound 8m